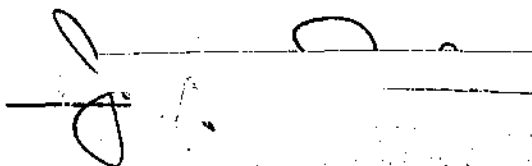


In presenting the dissertation as a partial fulfillment of the requirements for an advanced degree from the Georgia Institute of Technology, I agree that the Library of the Institute shall make it available for inspection and circulation in accordance with its regulations governing materials of this type. I agree that permission to copy from, or to publish from, this dissertation may be granted by the professor under whose direction it was written, or, in his absence, by the Dean of the Graduate Division when such copying or publication is solely for scholarly purposes and does not involve potential financial gain. It is understood that any copying from, or publication of, this dissertation which involves potential financial gain will not be allowed without written permission.

A handwritten signature, possibly "J. O.", is written over a rectangular stamp. The stamp contains some illegible text and a date, likely "3/17/65".

3/17/65  
b

AN INVESTIGATION OF SOLIDIFICATION RATES FOR MERCURY AND CERTAIN  
N-PARAFFINS USING THE ULTRASONIC PULSE-ECHO TECHNIQUE

A THESIS

Presented to

The Faculty of the Graduate Division

by

Joaquin R. Davila

In Partial Fulfillment

of the Requirements for the Degree

Master of Science in Mechanical Engineering

Georgia Institute of Technology

July, 1967

AN INVESTIGATION OF SOLIDIFICATION RATES FOR MERCURY AND CERTAIN  
N-PARAFFINS USING THE ULTRASONIC PULSE-ECHO TECHNIQUE

Approved:

  
Chairman

  
  
Date approved by Chairman: 24<sup>th</sup> July 1967

## ACKNOWLEDGMENTS

The author wishes to express his sincere appreciation to all those individuals who made this work possible. Special thanks are extended to Dr. John A. Bailey who introduced the author to the problem and kindly offered many hours of guidance and encouragement during all phases of the investigation. Appreciation is extended to Dr. J. E. Sunderland and Dr. J. H. Murphy for their review of this work.

In addition the author wishes to thank his relatives and friends for their many words and acts of encouragement.

Finally the author wishes to express appreciation for the financial support of this work provided by NASA Grant NSG-657.

## TABLE OF CONTENTS

	Page
ACKNOWLEDGMENTS . . . . .	ii
LIST OF TABLES . . . . .	v
LIST OF ILLUSTRATIONS . . . . .	vii
SUMMARY . . . . .	x
CHAPTER	
I. INTRODUCTION . . . . .	1
Statement of Intent	
Purpose	
II. REVIEW OF LITERATURE . . . . .	4
Introduction	
Metallic Systems	
Non-Metallic Systems	
Theoretical Studies	
Ultrasonic Studies	
III. INSTRUMENTATION AND EQUIPMENT . . . . .	21
Materials Selected for Study	
Mold and Heat Sink	
Insulation	
Thermocouples	
Temperature Recorder	
Ultrasonoscope	
Ancillary Equipment	
IV. PROCEDURE . . . . .	27
Calibration of Instruments	
Ultrasonoscope	
Thermocouples and Temperature Recorder	
Initial Set-Up	
Solidification Rate and Front Profile Measurements	
V. PRESENTATION AND DISCUSSION OF RESULTS . . . . .	36
VI. CONCLUSIONS AND RECOMMENDATIONS . . . . .	77

## APPENDIX

A. SOLIDIFICATION RATE DATA . . . . .	79
B. SOLIDIFICATION FRONT PROFILE DATA . . . . .	87
C. NUMERICAL SOLUTION OF THE SOLIDIFICATION PROBLEM . . .	94
Derivation of Numerical Approximations	
Boundary Conditions	
Initial Conditions	
Other Information	
D. NUMERICAL SOLUTION CONSTANTS . . . . .	104
E. SAMPLE COMPUTER PROGRAM . . . . .	111
F. SAMPLE COMPUTER OUTPUT . . . . .	115
G. NOMENCLATURE . . . . .	116
LITERATURE CITED . . . . .	118

LIST OF TABLES

Table	Page
1. Solidification Rate Data for Mercury at 75°F (Run No. 1) . . . . .	79
2. Solidification Rate Data for Mercury at 75°F (Run No. 2) . . . . .	80
3. Solidification Rate Data for N-Hexadecane at 70°F . . .	81
4. Solidification Rate Data for N-Hexadecane at 90°F . . .	82
5. Solidification Rate Data for N-Hexadecane at 120°F . . .	83
6. Solidification Rate Data for N-Octadecane at 90°F . . .	84
7. Solidification Rate Data for N-Octadecane at 100°F . . .	85
8. Solidification Rate Data for N-Octadecane at 120°F . . .	86
9. Solidification Front Profile Data for Mercury at 75°F . . . . .	87
10. Solidification Front Profile Data for N-Hexadecane at 70°F . . . . .	88
11. Solidification Front Profile Data for N-Hexadecane at 90°F . . . . .	89
12. Solidification Front Profile Data for N-Hexadecane at 120°F . . . . .	90
13. Solidification Front Profile Data for N-Octadecane at 90°F . . . . .	91
14. Solidification Front Profile Data for N-Octadecane at 100°F . . . . .	92
15. Solidification Front Profile Data for N-Octadecane at 120°F . . . . .	93
16. Numerical Solution Constants for Mercury at 75°F . . . .	104
17. Numerical Solution Constants for N-Hexadecane at 70°F . . . . .	105

	Page
18. Numerical Solution Constants for N-Hexadecane at 90°F . . . . .	106
19. Numerical Solution Constants for N-Hexadecane at 120°F . . . . .	107
20. Numerical Solution Constants for N-Octadecane at 90°F . . . . .	108
21. Numerical Solution Constants for N-Octadecane at 100°F . . . . .	109
22. Numerical Solution Constants for N-Octadecane at 120°F . . . . .	110



## LIST OF ILLUSTRATIONS

Figure	Page
1. Mold and Heat Sink Assembly . . . . .	22
2. Thermocouple Installation . . . . .	25
3. Ultrasonoscope Calibration Curve . . . . .	29
4. Correction Factor for Ultrasonoscope Measurements . . . . .	30
5. Ultrasonoscope Trace Patterns . . . . .	32
6. Solidification of Mercury at 75°F . . . . .	43
7. Solidification of N-Octadecane at 90°F . . . . .	44
8. Solidification of N-Octadecane at 100°F . . . . .	45
9. Solidification of N-Octadecane at 120°F . . . . .	46
10. Solidification of N-Hexadecane at 70°F . . . . .	47
11. Solidification of N-Hexadecane at 90°F . . . . .	48
12. Solidification of N-Hexadecane at 120°F . . . . .	49
13. Rate of Solidification for Mercury at 75°F . . . . .	50
14. Rate of Solidification for N-Octadecane at 120°F . . . . .	51
15. Rate of Solidification for N-Hexadecane at 120°F . . . . .	52
16. Solid Thickness versus $\sqrt{\text{Time}}$ for Mercury at 75°F . . . . .	53
17. Solid Thickness versus $\sqrt{\text{Time}}$ for N-Octadecane at 90°F . . . . .	54
18. Solid Thickness versus $\sqrt{\text{Time}}$ for N-Octadecane at 100°F . . . . .	55
19. Solid Thickness versus $\sqrt{\text{Time}}$ for N-Octadecane at 120°F . . . . .	56

20.	Solid Thickness versus $\sqrt{\text{Time}}$ for N-Hexadecane at 70°F . . . . .	57
21.	Solid Thickness versus $\sqrt{\text{Time}}$ for N-Hexadecane at 90°F . . . . .	58
22.	Solid Thickness versus $\sqrt{\text{Time}}$ for N-Hexadecane at 120°F . . . . .	59
23.	Solidification Front Profile for Mercury at 75°F . . . . .	60
24.	Solidification Front Profile for N-Octadecane at 90°F . . . . .	61
25.	Solidification Front Profile for N-Octadecane at 100°F . . . . .	62
26.	Solidification Front Profile for N-Octadecane at 120°F . . . . .	63
27.	Solidification Front Profile for N-Hexadecane at 70°F . . . . .	64
28.	Solidification Front Profile for N-Hexadecane at 90°F . . . . .	65
29.	Solidification Front Profile for N-Hexadecane at 120°F . . . . .	66
30.	Experimental Temperature Profile. Solidification of Mercury at 75°F . . . . .	67
31.	Experimental Temperature Profile. Solidification of N-Octadecane at 90°F . . . . .	68
32.	Experimental Temperature Profile. Solidification of N-Octadecane at 100°F . . . . .	69
33.	Experimental Temperature Profile. Solidification of N-Octadecane at 120°F . . . . .	70
34.	Experimental Temperature Profile. Solidification of N-Hexadecane at 70°F . . . . .	71
35.	Experimental Temperature Profile. Solidification of N-Hexadecane at 90°F . . . . .	72
36.	Experimental Temperature Profile. Solidification of N-Hexadecane at 120°F . . . . .	73

37.	Temperature Distribution at $D = 1\frac{1}{2}$ inches. Solidification of Mercury at $75^{\circ}\text{F}$ . . . . .	74
38.	Temperature Distribution at $D = 1\frac{1}{2}$ inches. Solidification of N-Octadecane at $120^{\circ}\text{F}$ . . . . .	75
39.	Temperature Distribution at $D = 1\frac{1}{2}$ inches. Solidification of N-Hexadecane at $120^{\circ}\text{F}$ . . . . .	76
40.	Description of Variables . . . . .	95

## SUMMARY

The principal objective of this work was the investigation of solidification rates for several materials by a direct application of the ultrasonic pulse-echo technique. Data were obtained from a study of mercury, n-octadecane and n-hexadecane paraffins solidifying under conditions of one-dimensional heat flow using a Magnaflux Model PS-810B Pulse Ultrasonoscope and a ceramic type piezoelectric transducer. In an extension of the basic technique, studies of the solidification front profile were also conducted. Initial temperatures above the freezing point of the test materials provided information on the effects of superheat during solidification.

Measurements were made in a specially constructed glass mold. Acetone and dry ice provided the cooling source from a heat sink adjacent to the mold area. The mold and heat sink assembly was insulated to assure conditions of one-dimensional heat flow. Thermocouples placed in the mold cavity recorded the temperature distribution in the mold and indicated the progress of solidification.

To record the movement of the solidification front, a beam of ultrasonic energy from the transducer was sent into the mold. Upon reaching the solid-liquid interface, the sound waves were reflected back to the transducer. The time interval between the sending and receiving of the beam was transformed by the ultrasonoscope into cathode ray tube trace patterns which continuously gave a picture of the interface position. By scanning the interface with the transducer, the

solidification front profile could be determined.

Results are presented in the form of solid thickness and freezing front velocity versus time curves for the solidification rate studies. The results of a numerical solution of the one-dimensional heat transfer equation are also included for comparison. Solidification front profile data are shown as the shape of the interface in inches of solid formation versus the position of the transducer at varying times during the solidification process. Thermocouple readings within the mold are presented as temperature versus time profiles. Experimental and theoretical temperature distribution curves are plotted as temperature versus distance from the heat sink at the instant when the freezing front had advanced half the distance across the mold.

The ultrasonic pulse-echo technique was found to give an accurate picture of the progress of solidification. The technique as applied in this investigation has the distinct advantage of being wholly external and having no noticeable effect on the solidification process.

## CHAPTER I

### INTRODUCTION

#### Statement of Intent

It is the purpose of this work to investigate the use of ultrasonics as a means of detecting the movement of the solidification front during the freezing of mercury, n-octadecane and n-hexadecane paraffins. The approach will be first to design and construct a mold where the test materials will be allowed to solidify under conditions of one-dimensional heat flow, then to use the ultrasonic pulse-echo method to detect the motion of the solidification front. The use of one-dimensional heat flow conditions will simplify interpretation of the data, and allow a comparison of experimental results with a numerical solution to the one-dimensional heat transfer equation. Initial temperatures above the freezing point of the test material will be used to evaluate the effects of various degrees of superheat on the solidification front profile.

#### Purpose

The solidification rate and direction are among the most important factors in determining the soundness of castings. A difficult problem which casting design engineers have to face today is the production of shrinkage-free casting designs. When the liquid metal solidifies in the mold the first solid to form undergoes shrinkage, but voids do not remain in it because molten metal flows in and compensates for the contraction. In vertical molds if the transverse solidification

rate exceeds the vertical rate, then a pool of molten metal becomes entrapped inside the casting and when this portion solidifies there is no reservoir from which feeding of liquid metal can occur: a shrinkage cavity results, leaving the casting with an internal defect. In the design of castings it is very important, therefore, to determine the solidification rate and direction so as to control the solidification process such that it proceeds toward the feeder head where shrinkage can be concentrated. Excessively fast solidification rates, while producing fine grain structures, may cause undesirable segregation patterns. Slow solidification rates generally result in coarse grain structures with acceptable segregation patterns. The yield strength, ductility and other mechanical properties of a casting are thus directly dependent on the rate and direction of solidification.

Existing methods of study of solidification rates, briefly summarized in Chapter II, either destroy the casting, introduce foreign materials into the melt or are ineffective under conditions of actual production. There is therefore a definite need for a method by which the progress of solidification in a casting may be determined accurately under production conditions without rendering the casting useless for further processing. Such a method would be particularly welcome in the growing field of continuous casting where control of the solidification rate determines the maximum casting speed at which sound products can be produced. At present, the control in this or any area of production casting is largely based on trial and error procedures.

Ultrasonic techniques, while finding wide acceptance in the area of non-destructive testing, have just recently begun to be applied to the

study of solidification rates. It is hoped that the ultrasonic pulse-echo technique as used in this work will promote continued research aimed at further improving this method so that possible applications may be found in the area of production casting.



CHAPTER II

REVIEW OF LITERATURE

Introduction

The solidification of metals and non-metals is a very complex phenomenon. The mechanisms of solidification need to be further clarified and the techniques available for the investigation of solidification rates need improvement and development. Numerous studies in this field have been promoted in the past, and especially in recent years. In the following an attempt will be made to give a very brief summary of the research conducted in the past concerning solidification rates, with particular emphasis on the experimental techniques.

A review of the history of solidification has recently been given by Winegard (1), with an interesting description of the contributions to the field since the sixteenth century. The work carried out since 1900 is summarized in decades, as most of the contributions have occurred since that time. A brief comment on what to expect from future research is also given. A review of the experimental methods that have been used in the past and which are currently used at the present time to study solidification rates has also been given (37) recently. Some of the most widely used methods are the pour-out method, the temperature measurement method, the dip stick method, and the use of tracers.

The pour-out or bleeding method consists of casting a number of identical ingots and overturning the molds individually at different

elapse times so as to bleed off the remaining liquid metal. Solidification rates are obtained by comparing the shell or skin thickness versus the time of bleeding for each of the molds. The greatest disadvantage of this method is encountered in the study of alloys, as some of the liquid metal becomes entrapped in a "mushy" zone that exists between the solidus and liquidus. Upon overturning the mold some of this entrapped liquid escapes, leaving the casting slightly porous so that an accurate determination of the shell thickness is not possible.

The disadvantages of the pour-out method led to the development of the temperature measurement technique. This technique consists of placing thermocouples in the mold cavity so as to record temperature changes during the process of solidification. The passage of the solidification front is revealed by observing the time at which each thermocouple location indicates that the temperature of the metal has dropped below its melting point. This method has the advantage of following the beginning and end of solidification very accurately. An obvious disadvantage is that the final casting cannot be processed further because of the embedded thermocouples.

The dip stick method consists of inserting a rod or stick into the mold cavity until the solidification front is reached. Measurement of the depth of the rod in the molten pool indicates the position of the front at that point. This method appears to be widely used in foundry control practices.

The use of tracers consists of adding a small amount of material to the liquid metal which will diffuse throughout the liquid. This material is chosen such that it freezes at the solid-liquid interface

and reveals the shape of the solidification front upon sectioning of the finished casting.

Most of the experimental results obtained by the previously described methods can be expressed mathematically by an equation for the solidification rate of the form

$$D = q\sqrt{t} + C$$

where  $D$  represents the solidified shell thickness,  $t$  is the time interval, and  $q$  and  $C$  are constants determined from the experimental data. The numerical value of  $C$  is thought to represent the period during which the superheat is dissipated before solidification begins, and  $q$  gives an indication of the rate of solidification.

Most of the research that has been carried out recently is concerned with the development of theories of the mechanism of solidification. The investigators attempt to explain solidification in terms of nucleation and growth processes. An attempt will be made in the following sections to give a review of the work that has been done recently along these lines for both metallic and non-metallic systems. A brief review of recent theoretical and ultrasonic studies on solidification rates will also be presented.

#### Metallic Systems

The basic principles which govern the solidification of cast metals have been presented by Oostdijk (18). The subjects discussed were the formation of nuclei and their growth, homogeneous and heterogeneuous nuclei formation and the use of formulas and constitu-

tion diagrams to study various aspects of the growth of nuclei.

Chalmers (19) has outlined the basic principles of solidification in order to examine the origin of the chill, columnar, and equiaxed zones in ingots. Some experimental data were presented on the effects of pouring temperature on the length of the columnar zone and the equiaxed grain size. It was shown that the currently accepted explanation of the termination of the columnar zone and the origin of the equiaxed zone is unable to account for the experimental facts obtained. An alternative theory was proposed, in which nucleation of the equiaxed grains was considered to take place during the initial chilling on contact with the cold mold.

Theoretical studies on nucleation have recently been reported by Uhlmann and Chalmers (32). A general theory appropriate to a physical understanding of the nucleation process was presented, and some of the difficulties inherent in the formalism noted. Some of the salient features of the alternative transformation of spinoidal decomposition were described. Further studies on the mechanism of nucleation from the melt have been presented by Jackson (33).

Laukonis (20) has reported on the nucleation phenomena associated with the growth of iron whiskers by the hydrogen reduction of ferrous chloride. Three stages of growth were discussed: first, nucleation and the initial growth of iron whiskers; second, subsequent nucleation and transport processes which lead to the thickening of a whisker crystal and finally, the general behavior of impurities in the system. It was noted that certain combinations of impurities promote whisker growth, while others inhibit or poison growth.

Biloni and Chalmers (2) have performed a metallographic study of microsegregation in regions of solidifying metal where crystal nuclei transform into a dendritic pattern. They reported that dendritic growth is preceded by a predendritic region, and its morphology and composition change according to the conditions under which the nucleation and subsequent growth take place. With a high degree of undercooling growth was found to be dominated by a diffusionless process, most of the structure being composed of predendritic regions. At intermediate degrees of undercooling the inner predendritic particles had a composition similar to the liquid. At small degrees of undercooling, as is the case for the growth of the grains in the equiaxed region of ingots, the predendritic region consisted of an irregular region that grew by a diffusion process.

Kattamis and Flemings (3) have studied the changes in dendrite morphology and grain size as a function of the increase in undercooling on bulk samples of iron and nickel base alloys. Their results indicated that dendrite morphology gradually changes with increasing undercooling from the usual dendritic structure to a structure composed of cylindrical dendrite arms. At a critical undercooling of  $170^{\circ}\text{C}$  in these alloys there was an abrupt transition to a fine-grained structure of spherical morphology. The conclusion was reached that structure coarsening, with a reduction of surface area as the driving force, is the principal mechanism determining final dendrite-arm spacing in melts nucleated at small undercoolings and grain size in melts nucleated at large undercoolings.

Bower and others (4) have conducted a series of experiments with

Al-Cu alloys which showed that the usual assumptions for the analysis of solute redistribution for the solidification of castings and ingots were reasonable. These assumptions were: negligible undercooling before nucleation of solid phases, negligible increase of solute in advance of the tips of growing dendrites, complete diffusion within the liquid over distances the order of dendrite arm spacings and platelike dendrite morphology.

Glicksman and Schaefer (5) have observed the dendritic profiles during the solidification of pure tin by an optical method permitting high resolution of the surface. They described specimen preparation, measurements of tip profiles and speed of advance, and measurements of side branching. In a previous study Glicksman (6) developed a relationship between interphase mass transfer and mechanical behavior of bounded systems undergoing rapid solidification from an analysis of the kinematics and dynamics of dendritic freezing. He presented a unified approach to solidification dynamics and discussed some effects of rapid solidification.

Courtland and Elliot (7) have investigated the transition from cellular interface structure to dendritic structure during solidification of Pb and Sn base alloys. Measurements were made of cell size as a function of the temperature gradient in the liquid ( $G$ ), rate of solidification ( $R$ ), and solute concentration ( $C_0$ ). The results obtained were in agreement with the theory that on an interface of constant orientation, cell width varies inversely with the product " $GR$ " and directly with " $C_0$ ."

During the past few years there have been a number of reviews

concerning eutectic solidification (8, 9, 10). The most recent review in this area has been carried out by Kerr and Winegard (11). Here an attempt was made to review the history, and to present a simplified interpretation of the most recent research and theories of eutectic freezing up to 1965, relating these when possible to earlier work. It was shown that there is serious doubt about the existence of globular eutectics, and that the definition of anomalous eutectics must be clarified.

An interesting approach to eutectic freezing has been taken by Davies (12), who solidified eutectic alloys between glass plates in such a way that the interface was always visible. The results led to the conclusion that it is possible to predict, by means of data derived from phase diagrams, in which group of eutectic microstructures any binary system will crystallize.

Experiments aimed at studying solid and liquid structures at interface zones of unidirectionally solidified Al-Al<sub>3</sub>Ni alloys with 5.7 per cent Ni have been described by Gosh (13). Results were interpreted to show that the concept of the formation of segregated zones in the liquid as proposed in earlier papers can be meaningfully applied to controlled as well as uncontrolled eutectic structure formation.

A method to improve the accuracy of decanting experiments when the detailed shape of the growing solid-liquid interface in eutectic alloys is studied has been proposed by Hunt and Chilton (14, 15). A precise technique for determining the position of the interface at any given instant of time was developed. A schematic diagram of the apparatus is given and results obtained on the Zn-Mg<sub>2</sub>Zn<sub>11</sub> eutectic alloy were

reported.

An experimental investigation of single crystals of zone refined tin which had been decanted near the onset of constitutional supercooling has been reported by Biloni et al (16). Results, together with a reexamination of recent literature, point to inconsistencies between experimental observations and the idea that the formation of a projection is a causal step in the development of a cellular substructure. An argument is presented to show instead how it is plausible for substantial depressions to form in the presence of constitutional supercooling at dislocations threading the solid-liquid interface.

A study of the solidification mechanism of melts of monotectic composition has been reported by Chadwick (17). It was shown that important microstructural differences can arise as a result of changes in the relative magnitudes of the interfacial energies between two liquids and a solid substrate. Conflicting results from previous publications are rationalized by the proposed theory.

The effect of fluid flow during solidification on the structure of as-cast metals was investigated on four Pb-Sb alloys at superheats of 40°C and 100°C by Cole and Bolling (21). Forced fluid flow in the same sense as natural convection was introduced by applications of interacting magnetic and electrical fields. The method was found to produce an equiaxed structure in the castings.

The determination of the time of solidification in castings by means of temperature measurements has been recently carried out by Beckhoven (35). Results of an analog test showed that the assumption that the end of solidification is reached at the last bending point in



the temperature-time curve is wrong. The conclusion was reached that the end of solidification can be established only by determining the time at which the solidus temperature is reached.

### Non-Metallic Systems

Studies on the rate of growth of crystals and on the morphology of the crystal surfaces of organic compounds have been made by Jackson and Hunt (22). These authors showed that the roughness on an atomic scale of the solid-liquid interface plays an important role in the solidification process, and that the diffuseness of an interface is inversely proportional to a parameter  $\gamma$  which is equal to the entropy of melting times a factor  $\xi$ . The numerical value of  $\xi$ , which depends on the crystallography of the interface, was between  $1/2$  and  $1$  for the closest packed face of a crystal and decreased for higher index planes. On closed-packed planes growth was extremely slow and usually aided by a screw dislocation as proposed by Frank (23).

Materials can be classified in terms of their freezing behavior according to the factor  $\gamma$ . All materials that have  $\gamma$  less than  $1$ , as is the case for most metals, can grow, if they are pure enough, with a planar "non-crystallographic" interface which is planar to an isotherm, but are likely to grow dendritically into undercooled melts. The interface in this case is rough and growth would not require nucleation of new layers in the normal sense. Materials which have  $1 < \gamma < 2$  present little difficulty in forming new atomic layers during growth from the melt. The solid-liquid interface for these materials will also be rough. Materials with  $\gamma$  greater than  $2$  present some difficulty in forming new

atomic layers. A crystal growing from these liquids is bounded by smooth faces. Materials under this category grow in a faceted manner, frequently by a twin mechanism.

Most organic compounds usually exhibit high entropies of melting. There are some, however, which have high symmetry crystal structures near their melting points and at lower temperatures transform to a lower symmetry structure in which the molecules are oriented as in the solid state. During this transformation, the crystal loses the rest of the entropy which a normal compound would lose on freezing, and as a result has a small entropy of melting. Materials with a small entropy of melting have small  $\gamma$  factors with numerical values very close to those of metals. Consequently these organic compounds exhibit the same freezing characteristics as metals. By studying these organic compounds, which are transparent in the liquid state, it is possible to investigate through visual means many of the phenomena which determine the structure of cast metals.

Solidification rate experiments using n-octadecane as the test substance have been reported by Thomas and Westwater (38). The material was allowed to freeze unidirectionally and the shape of the interface observed with a microscope. Results showed the interface to be populated with microscopic peaks and valleys which increased the heat transfer characteristics of the interface. Actual results on the rate of solidification were found to be as much as 100 per cent higher than those predicted mathematically.

Experiments on the crystal nucleation behavior of some normal alkane liquids was investigated by the droplet technique by Turnbull and Cormia (24). They concluded that the relative undercooling in the

n-alkanes studied was very small. It is to be expected that in any linear polymer the relative undercooling required for appreciable crystal nucleation should be quite small. A comparison of experimental results with theoretical values was also included.

Jackson and others (25) have conducted microscopic observations on alloys of organic materials which showed that dendrite arms can melt off under normal conditions of growth. It was postulated that this remelting phenomenon occurred in metal alloys, giving rise to the equiaxed region in castings. Experiments performed on castings of transparent materials support remelting as a primary source of detached crystals.

A new classification of eutectics based on the entropies of melting of the two eutectic phases has been proposed by Hunt and Jackson (26). The classification was used to predict suitable transparent analogs of metallic systems. Experimental confirmation was obtained for the theoretical shape of the lamellar solid-liquid interface, for the fault mechanism of lamellar spacing changes, and for the development of low-energy solid-solid boundaries between the lamellae. A general theory for the growth of lamellar and rod eutectics has been presented in a later work (30).

#### Theoretical Studies

Mathematical methods for the analysis of solidification problems have become quite extensive and useful in the past few years. These methods include analytical, graphical, numerical approximations, and analog and digital computer techniques.

Analytical techniques attempt to study the thermal aspects of

solidification by analyzing exact heat transfer equations describing the phenomena. The complexity of most practical applications is such that an exact solution could only be obtained with extreme difficulty. The usual approach is to make simplifying assumptions in order to solve the equations. Some of these are: one-dimensional heat flow, semi-infinite mold material, constant interface temperature, and thermal properties which do not vary with temperature.

Graphical and numerical techniques have more general application than analytical methods. They can solve similar problems but in addition can also handle composite solids, mold-casting interface resistance, two dimensional heat flow, and a variation in thermal properties with temperature. The most widely used of all mathematical approaches today is a combination of the principles of numerical techniques with the digital computer. This combination offers greater versatility, speed, and accuracy than any other method.

Analog computer techniques simulate the flow of heat during solidification by appropriate substitution of equivalent electrical characteristics: heat flow is substituted by current flow, and temperature difference by voltage difference.

Previous work with analytical, graphical, and computer techniques applicable to solutions of solidification problems has been reviewed recently by Muehlbauer and Sunderland (27). An attempt will be made here to update that review.

Modern computer methods have been used by Kohn and Morillon (28) to study the solidification of 12-ton ingots of low and medium carbon content. Results showed that the movement of the fusion front at the

beginning of solidification was a function of the square root of time only in the zone near the ingot surface. The solidification rate was constant for the greater part of the process, and accelerated in the final stage.

The solidification pattern of a 20,000 lb. production steel turbine inner shell casting having wall sections from 2 to  $11\frac{1}{4}$  inches was calculated by Henzel and Keverian (29) using a new numerical technique and the digital computer. The results obtained compared favorably with experimental data.

A mathematical study of the solution of the heat transfer problem involving a change of phase has recently been carried out by Tien (31). The "heat balance integral" was employed to obtain a solution to the temperature distribution as well as the position of the solidification front for the case of the freezing of a semi-infinite slab with time-dependent surface temperature. Numerical solutions for the case of linear variations and exponential decay for the surface temperature were also given.

Work with the electrical analog has recently been carried out by Jackson et al (34). A consistent solution was obtained for the shape of a lamellar interface and the diffusion field by an iterative process. The results showed that the shape of the interface was independent of growth velocity and lamellar spacing, but depended on the relative values of the interfacial free energies at the phase boundaries.

#### Ultrasonic Studies

The use of ultrasonic methods as a means of studying solidifica-

tion rates has a great potential. Methods which have been used in the past to determine rates of solidification, as discussed in Chapter II and by Dula (37), either destroy the casting or render it useless.

Ultrasonic techniques have the unique advantage of preserving the casting and of being the fastest of all the methods now used in this field.

Application of an ultrasonic field to a solidifying material may alter some of its mechanical properties, change somewhat the mechanism of solidification, or in most cases accelerate the rate of solidification. The effects of ultrasound on the kinetics of crystallization have been reviewed and studied by Kapustin (36). Experimental work was carried out using several transparent substances of low melting point. These substances were allowed to crystallize with and without the application of an ultrasonic field. Microscopic observations were made on the solidified substances, and the rate of growth during solidification was noted. The results obtained from the experiments showed that the continuous action of ultrasonic energy has a very pronounced effect on the growth kinetics of the crystalline phase at many different frequencies, intensities, and degrees of supercooling.

It was observed that when crystals are made to grow slowly upon the introduction of a seed crystal into a supercooled drop of thymol and ultrasonic energy applied a vigorous production of new centers of growth results at the solid-liquid interfaces: the number of crystals increases rapidly, and the whole preparation becomes crystalline in a few seconds. Freezing of a bulk sample of thymol under normal conditions gave a growth rate of 0.15 mm/sec, but with the application of a strong ultrasonic field (2 KV/mm) the growth rate was increased to 25 mm/sec. It was found that

the rate of crystallization was governed by the intensity; the minimum electric field that produced organized movement of the interface was 0.6 KV/mm. The rate of crystallization was found proportional to the intensity of the electric field.

Kinetic studies have shown that an ultrasonic field affects the nucleation rate in a supercooled medium. For a pure material the application of ultrasound can accelerate the production of the first crystallization center if the melt is near the limit of metastability. Nucleation at impurities does not occur in response to ultrasound if the impurities have not previously been in contact with the crystalline material; but there may be an acceleration of nucleation if the impurities have been in contact with the solid.

The growth and dissolution of monocrystals is affected by variations in the frequency of the ultrasonic field. Measurements on the linear growth rate of the octahedron faces of potash alum monocrystals indicate that high frequency ultrasound (2 Mc) accelerated dissolution when the temperature of the solution was above the saturation point, and doubled the mean linear rate of displacement of the faces. When the solution was supersaturated, the ultrasound increased the mean linear growth rate by a factor of two to three. For a low frequency ultrasonic field the linear rate of growth of the faces was increased by a factor of three. The rate of growth was found to be inversely proportional to the ultrasonic frequency.

The effect of ultrasound on the final grain size is worth noting. Ultrasound renders the crystalline phase more homogeneous and of smaller grain size over a wide frequency range. The process is described in two

stages: first the ultrasonic field produces a large number of fresh nuclei, then the resulting crystals coalesce. The final homogeneous fine-grained product is a result of the lack of space for free growth. The ultrasonic field breaks off microcrystals from the growth front, and these cannot become very large for they themselves are soon broken up to form fresh nuclei. The stronger the electric field the more crystals break off, and the resulting grain size will be finer. Low frequencies give a more homogeneous structure and a smaller grain size than high frequencies.

Other effects of ultrasound include raising of the elastic limit and the rupture stress for organic material as well as for metal castings, partial or total elimination of the columnar zone, acceleration of the onset of eutectic crystallization, and production of zoned structures.

Recent work on the use of the ultrasonic pulse-echo technique as a means of locating the solid-liquid interface in solidifying metals has been reported by Kurz and Lux (39). Experiments were carried out with Woods Metal, a complex alloy of eutectic composition, a lead alloy, and an unalloyed steel with 0.1 per cent carbon. These last two materials show a freezing range of approximately 100 degrees centigrade. Echoes from the solid-liquid interface were received by the transducer in all three cases. The intensity of the reflected echoes, however, was highest for the Woods metal and lowest for steel.

The degree of reflection for a given substance at a constant temperature is a maximum when the solid-liquid interface is smooth and perpendicular to the incoming signal. As the angle formed between the interface and the incoming signal decreases from 90 degrees, the reflected



signal becomes weaker and weaker, until a critical angle is reached when the sound waves no longer return to the transducer, and no signal is received. The smoothness of the interface is also important, as crystals which extend into the melt result in diffused reflection losses. Other factors which reduce the intensity of the received impulses are the damping by the material structure and high temperatures. A low frequency ultrasound is recommended for maximum intensity of the transmitted signal.

The travel time of sound waves in a given direction is inversely proportional to the velocity of sound in the material. The velocity of sound in most metals is inversely proportional to the temperature. So it follows that travel time of sound waves increases with increasing temperature. Measurements of the velocity of sound in liquid metals (40) confirm this relation.

Further work using the ultrasonic pulse-echo technique for studying solidification rates in water has been carried out by Dula (37). Experimental results obtained during the freezing of water at 32, 70, and 110 degrees Fahrenheit compare favorably with actual and theoretical values.

## CHAPTER III

### INSTRUMENTATION AND EQUIPMENT

The instrumentation and equipment used in the present work consisted of an ultrasonoscope, transducer, temperature recorder, insulated mold with thermocouples and associated components. The individual components and materials tested will now be described in detail in the sections that follow.

#### Materials Selected for Study

The test materials used in this work were mercury, n-octadecane and n-hexadecane paraffins. The corresponding freezing temperature of these materials are respectively  $-38^{\circ}\text{F}$ ,  $83^{\circ}\text{F}$ , and  $62^{\circ}\text{F}$ . The paraffins offer the unique advantage of being transparent in the liquid phase so that visual observations as solidification progressed were possible. Mercury, being a metal, permitted a more direct evaluation of the ultrasonic technique as it would be applied to the studies of solidification of metal castings.

#### Mold and Heat Sink

The mold and heat sink were constructed of  $3/32$  inch thick glass so that visual observations of the solidification process could be made through the front glass panel. A common partition divided the  $4\frac{1}{2}$  inch deep by 4 inch wide by 4 inch high unit into two chambers of 3 inches and  $1\frac{1}{2}$  inches deep as shown in Figure 1. The small chamber served as the heat

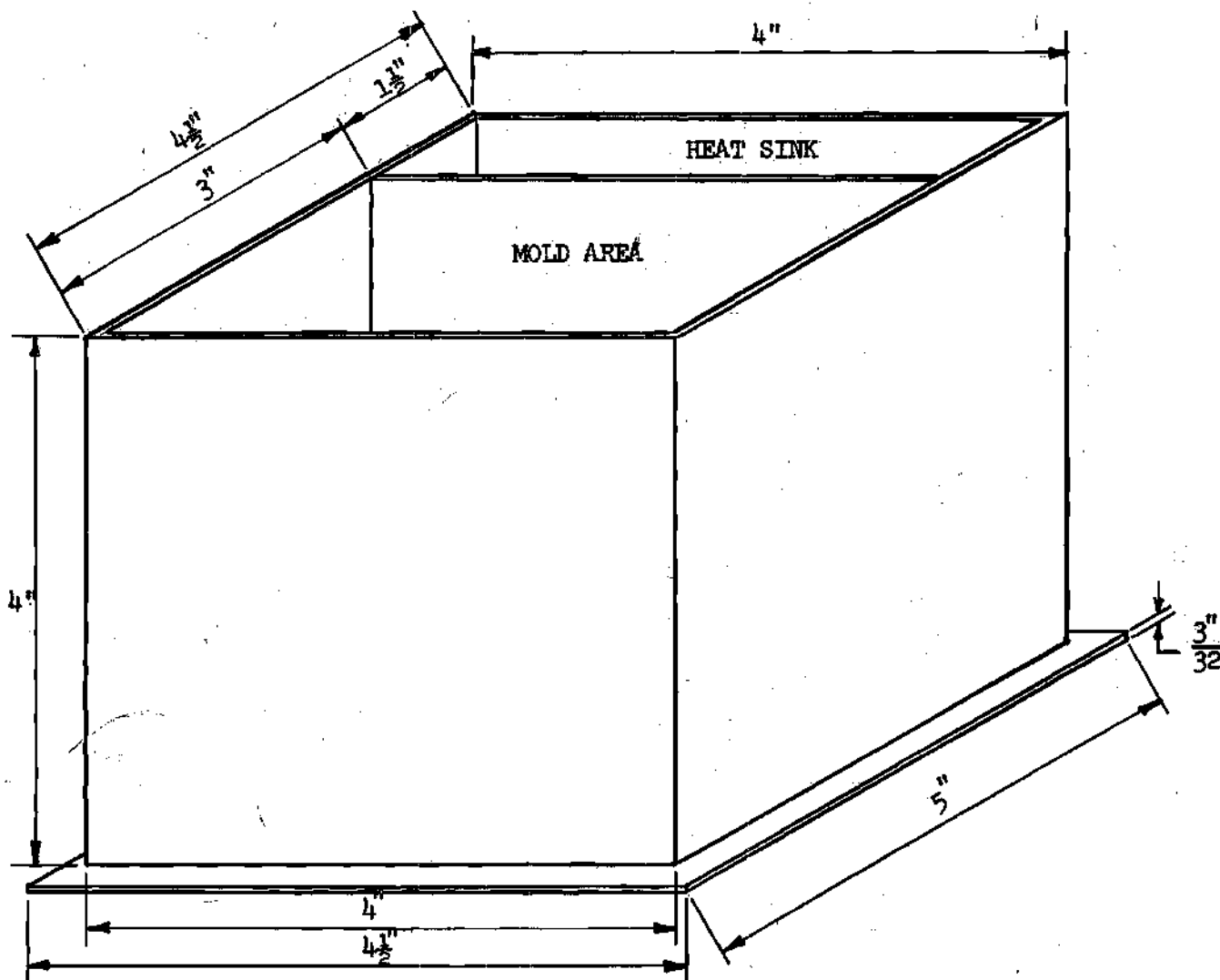


Figure 1. Mold and Heat Sink Assembly

sink and the large chamber as the mold area. Dow Corning ceramic cement was used as the adhesive in the assembly of the glass sections. This method of construction provided a unit of uniform heat transfer properties.

#### Insulation

To assure that the heat flow would approach one-dimensional conditions, it was necessary to insulate the mold. Two inch thick blocks of polyurethane insulation were placed adjacent to the mold and heat sink on all sides with the exception of the top of the heat sink and the glass section forming the front of the mold. The polyurethane block covering the top of the mold was constructed so as to achieve a tight fit. This arrangement assured minimum heat transfer through this section and facilitated the loading of materials into the mold. The entire system was enclosed in a plywood container.

#### Thermocouples

Eight 10 gage iron-constantan thermocouples were used in this work. Seven of the thermocouples were placed in the mold cavity to record temperatures of the solidifying material with respect to time, the eighth thermocouple was placed in the heat sink to record the temperature of the acetone-dry ice mixture. The first seven thermocouples were held in place by stretching the wire leads between two parallel glass rods cemented as close to the side walls of the mold as possible and one inch from the bottom. The eighth thermocouple was installed such that it could be removed from the heat sink and placed against the glass panel in the mold area in order to determine the temperature at the solid-mold interface. The thermocouple leads were brought outside the mold and attached to

junction boxes on either side of the plywood container where connections were made to the multichannel temperature recorder. Figure 2 shows the positions of the thermocouples.

#### Temperature Recorder

A 24 channel Honeywell Brown Electric Recorder, Model No. SY153X89-(C)-II-III-16, was used to record temperatures during solidification. Only eight of the channels were used and the temperature measurements were recorded in sequence according to the numbered positions of the thermocouple junctions as shown in Figure 2. The elapsed time between each reading was five seconds and the chart speed 0.20 inches per minute.

#### Ultrasonoscope

A Magnaflux Model PS-810B Pulse Ultrasonoscope was used to determine the position of the freezing front at any time during solidification. The instrument was applicable to pulse-echo, through transmission, immersion and contact methods of flaw detection and had a test range of 1.6 to 320 inches in steel and a frequency range of 0.5 Mc to 15 Mc. Readings were displayed on a five inch, flat faced cathode ray tube. The gain of the ultrasonoscope could be set so that the readings on the graduated scale corresponded to the pulse-echo distance.

A Magnaflux 2.25 Mc - 3/8 inch miniature ceramic type transducer was used for all tests. Piezoelectric transducers of this type can be used at temperatures up to 140°F.

#### Ancillary Equipment

To assure that the glass section forming the front wall of the mold

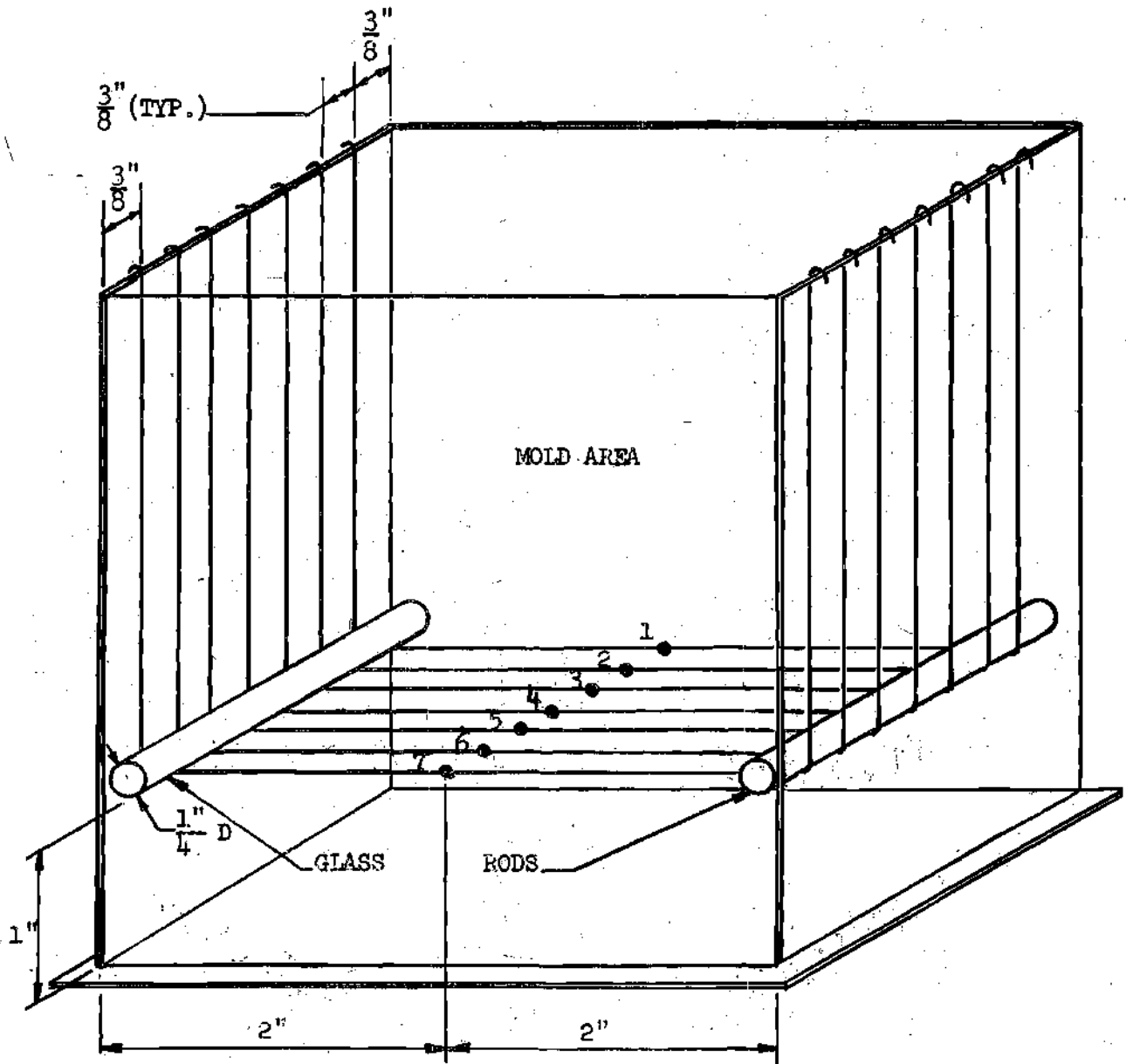


Figure 2. Thermocouple Installation

was always kept above the freezing temperature of the material, two flat faced 400 ohm resistances 3 inches high by 1 5/8 inches wide were placed 1/8 inch from the glass surface in slots made of wood that provided support for the heating assembly. To facilitate scanning of the solid-liquid interface the heating elements were arranged such that the entire front glass section up to the level of the liquid material was covered except for a 3/4 inch vertical gap at the middle portion. The resistances were connected across a type 500B Staco variable voltage instrument having a range of 0 to 140 volts. The heating elements were removable, and were used only for the n-octadecane runs, as this was the only material whose melting point is above room temperature.

A Tektronix Oscilloscope Camera, Type C-12, fitted with 3000 Speed, Type 47 Polaroid Film was used to record the cathode ray tube patterns. Heat sink temperatures and additional mold temperatures were checked with standard mercury or alcohol in glass thermometers. A Leeds and Northrup Millivolt Potentiometer was used to standardize the Honeywell temperature recorder.

## CHAPTER IV

## PROCEDURE

Calibration of Instruments

Adjustment of the ultrasonoscope and standardization of the temperature recorder was required before each experimental run to assure accuracy in the measurements. The standard calibration procedures are described in the following sections.

Ultrasonoscope

For all tests, the pulse-echo technique was used. In this technique a pulse of ultrasonic energy is sent out by a single transducer through the glass mold and into the liquid portion of material under study. Upon reaching the solid-liquid interface the sound waves are reflected back to the transducer through the liquid medium. The travel time of the signal is then transformed by the ultrasonoscope into a cathode ray tube trace pattern which continuously gives a measure of the distance from the phase boundary to the transducer.

The travel time of sound waves in a medium is inversely proportional to the velocity of sound in the medium. For the materials studied in this investigation: mercury, n-octadecane and n-hexadecane, it was found that travel time increased with increasing temperatures. As a result the ultrasonoscope registered a change in the distance recorded proportional to the change in temperature of the liquid medium.

To illustrate this phenomenon, liquid material at a temperature



equal to its freezing point was placed in the mold and the ultrasonoscope set to record the actual mold width of 3 inches. The liquid material was then heated and the ultrasonoscope readings recorded to obtain the curve shown in Figure 3. The relationship between temperature and sound velocity is clearly demonstrated. In the present work, this relationship had to be considered during each experimental run if accurate readings were to be obtained. In all tests the ultrasonoscope was calibrated so that it gave an accurate measure of the mold cavity width at the melting point of the material.

Studies of the solidification behavior of n-hexadecane and n-octadecane showed that when the initial liquid temperature was above the freezing point, freezing started as soon as the mold cavity was filled and the superheat dissipated during solidification. In this case the data had to be corrected to account for the variation in the speed of sound with temperature. With mercury as the test substance direct readings were obtained at all times as solidification in this case did not start until all the superheat was dissipated.

In order to correct the readings during the early moments of solidification when the liquid was superheated, a correction factor based on 3 inches was calculated directly from Figure 3 and plotted as in Figure 4. This curve gives a correlation between temperature and the correction factor by which the actual readings must be multiplied to give true readings. Therefore by noting the temperature of the liquid at any given time and obtaining the corresponding correction factor from Figure 4 an accurate measurement of the position of the solid-liquid interface was achieved at all times. This procedure assumes a uniform

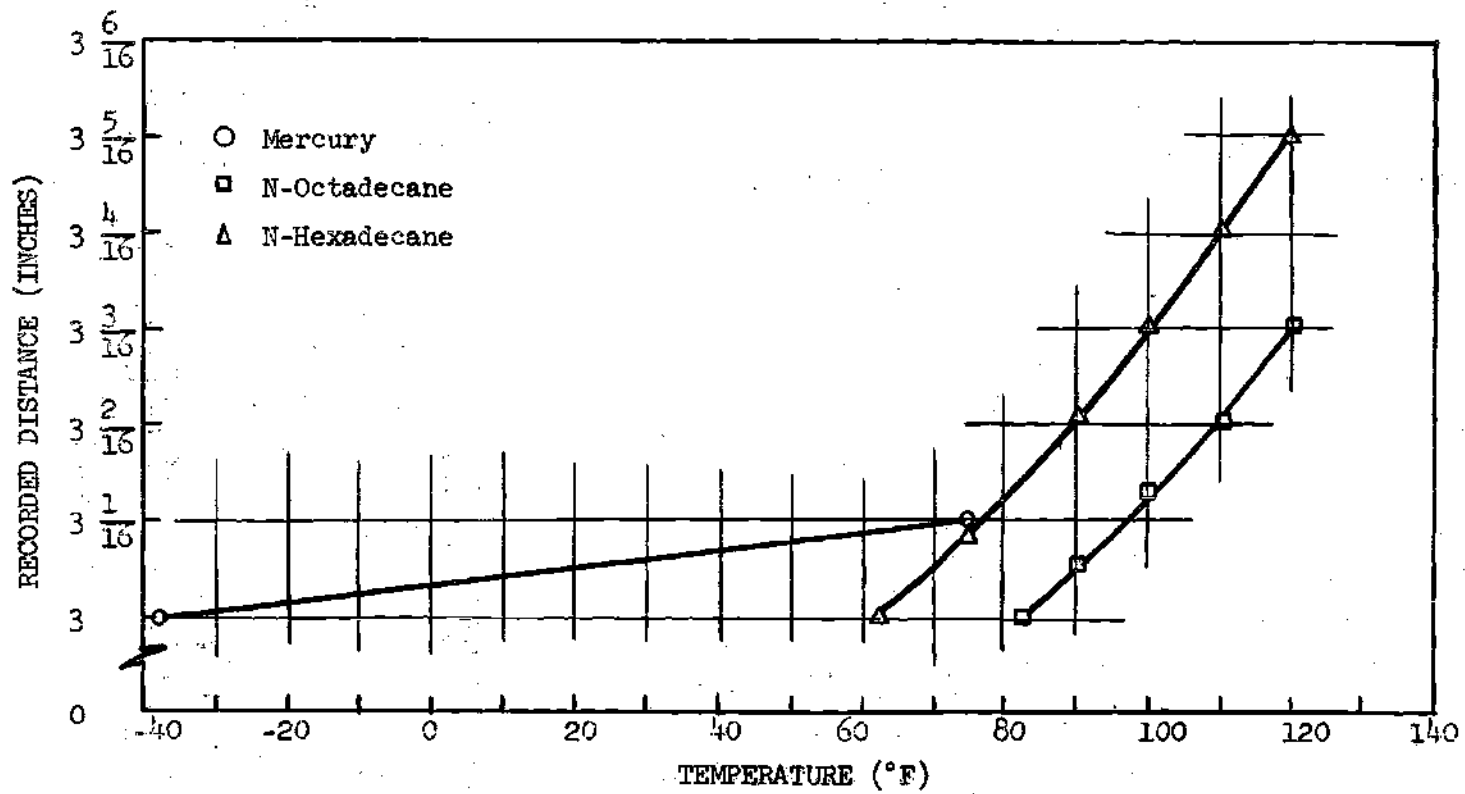


Figure 3. Ultrasonoscope Calibration Curve

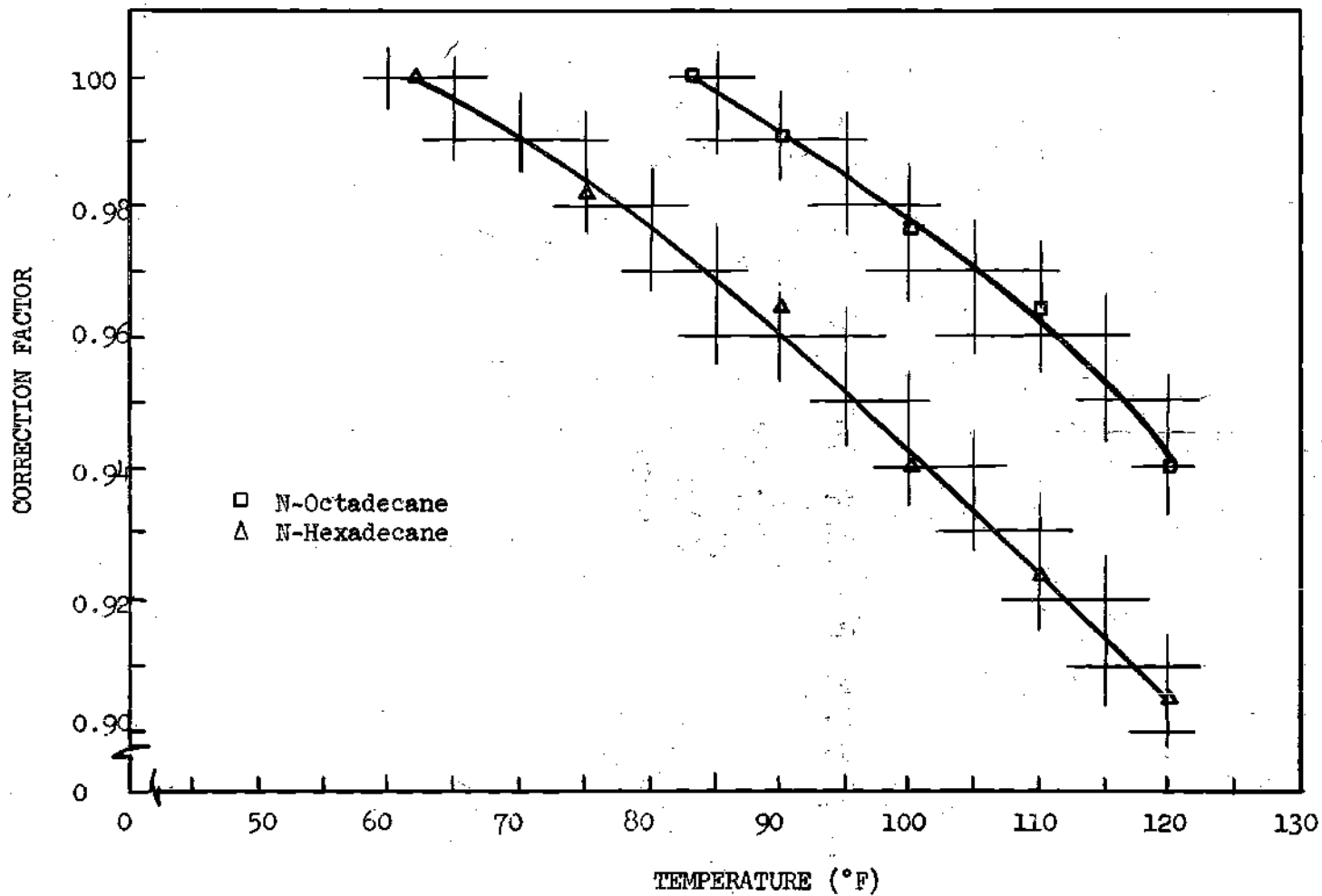


Figure 4. Correction Factor for Ultrasonoscope Measurements.

temperature throughout the liquid.

Figure 5 shows actual ultrasonoscope trace patterns obtained during solidification of mercury. The bottom pattern is for mercury at 75°F before the start of solidification as indicated by the set point of 3 1/16 inches as obtained from Figure 3. The top pattern indicates that solidification has proceeded to the point such that two inches of liquid mercury path remain. All readings were made at the point where the first discontinuity appeared in the horizontal trace of the ultrasonoscope pattern.

#### Thermocouples and Temperature Recorder

Before each experiment, the temperature recording system was checked for accuracy. The Honeywell temperature recorder was first standardized by using the Leeds and Northrup Millivolt Potentiometer. The response of the system was then checked by placing liquid material, at a known temperature, in the mold and observing the readings of the thermocouples.

#### Initial Set-Up

After the temperature measurement system had been checked according to the procedure outlined in the preceding section, the temperature recorder was maintained at the "on" position and the strip chart set at the zero time position.

If n-octadecane was the material to be solidified then the heating elements were placed in the slots which provided support and the voltage was set at 20 volts. This maintained the temperature of the air in the immediate vicinity of the glass panel at 85°F, two degrees above the freezing temperature of n-octadecane. The heating elements were not used during the mercury and n-hexadecane runs.

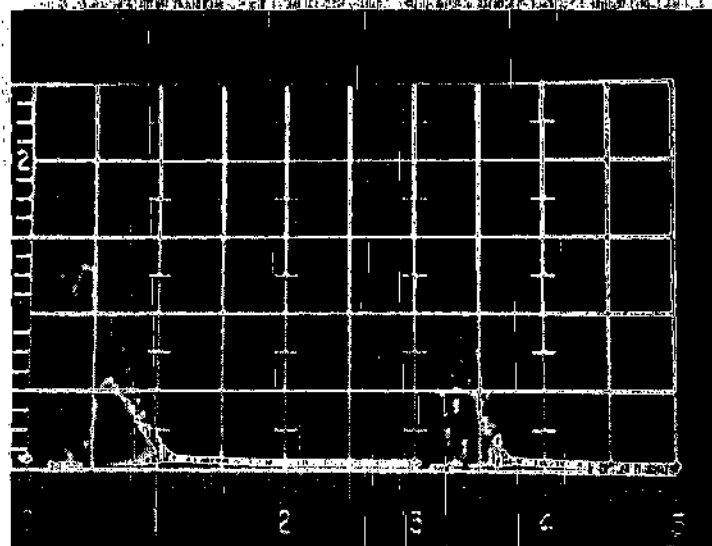
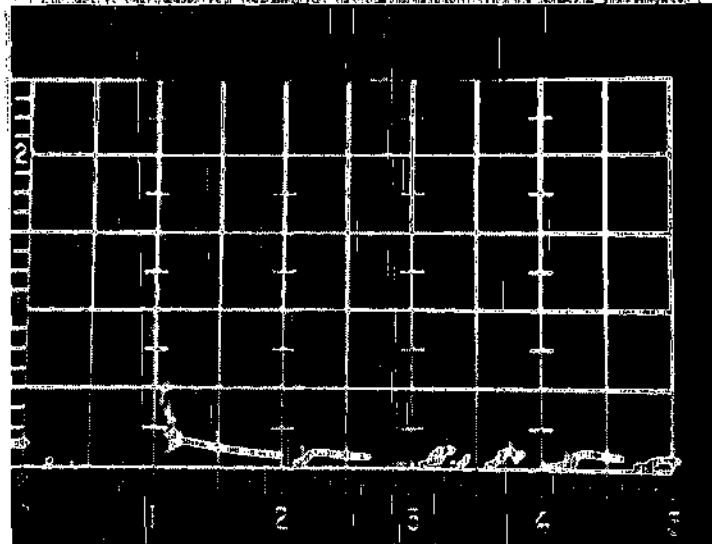


Figure 5. Ultrascope Trace Patterns.

The transducer was positioned on the front glass panel of the mold approximately  $1/4$  of an inch from the bottom and centered with respect to the width of the mold. A thin film of light machine oil was applied to insure good contact between the glass and transducer. The ultrasonoscope was set according to the instruction manual for operation with the pulse-echo technique.

To prepare the heat sink, a mixture of acetone and dry ice was placed in a beaker and brought to its equilibrium temperature ( $-107^{\circ}\text{F}$ ). Small blocks of dry ice were then placed in the heat sink chamber but not allowed to touch the partition separating the heat sink from the mold at this stage in order to minimize the possibility of uneven cooling. The test material was then brought to the desired initial temperature by external heating and placed in the mold chamber to a depth of three inches. As quickly as possible, the cathode ray tube trace pattern was set to correspond to the liquid material at its freezing point as outlined in the first section of this chapter. Introduction of the acetone and dry ice mixture followed the ultrasonoscope calibration steps. The level of the acetone in the heat sink was always maintained at a level above that of the material in the mold. A low temperature thermometer was then placed in the heat sink in order to check the accuracy of the temperature recorder. Experimental data on the solidification rate and front profile development could now be recorded.

#### Solidification Rate and Front Profile Measurements

Readings from the ultrasonoscope were recorded along with time. Continuous readings of the temperatures inside the mold and heat sink

were noted by the temperature recorder. Occasional checks of these temperatures were made with mercury or alcohol in glass thermometers. Once solidification began, an ultrasonoscope reading was taken at a point  $1/4$  of an inch above the bottom of the mold and centered with respect to the width of the mold. In rapid succession, similar readings were taken at points  $3/4$ ,  $1\ 1/4$ ,  $1\ 3/4$ , and  $2\ 1/4$  inches above the bottom of the mold and in a vertical line with the initial point. Readings were repeated every  $1/16$  or  $1/8$  of an inch of solid formation as indicated by the ultrasonoscope. The accuracy of the ultrasonoscope readings was checked by noting the time at which a sudden drop in temperature occurred at the thermocouple positions as indicated by the temperature recorder. Visual observations of the passage of the freezing front through each of the thermocouple positions were possible during the n-octadecane and n-hexadecane runs, as these substances are transparent in the liquid state, but not with mercury of course.

During any run, occasional adjustments to the sensitivity and power output controls of the ultrasonoscope were necessary in order to maintain a clear trace pattern. Adjustments of this nature were mainly required when the solidification front varied from the one-dimensional configuration and assumed a curve surface as viewed from the side of the mold. When the path of sound waves at the point of reflection is not perpendicular to the tangent plane to the curved surface at that point, then some of the sound waves are scattered and lost, and only a portion of the reflected waves are transmitted back to the transducer. This conditions results in a weak signal. It was found desirable to mount the transducer at the lower part of the mold cavity where the effect of front curvature would be a minimum.

One run for each initial temperature of 90°F, 100°F, and 120°F for n-octadecane, and 70°F, 90°F and 120°F for n-hexadecane was carried out in order to investigate the effect of various degrees of superheat on the solidification rate and solidification front profile. By performing two identical tests on mercury at 75°F it was established that data could be reproduced to  $\pm \frac{1}{32}$  inches. Readings were terminated when two inches of material had solidified.



## CHAPTER V

## PRESENTATION AND DISCUSSION OF RESULTS

The results obtained from the experimental investigation and the numerical solution to the one-dimensional heat transfer equation using a technique developed by William D. Murray (41) are shown in Figures 6 through 39. The solidification rate and front profile data obtained during the experimental runs are given in Appendices A and B. Appendices C, E and F give respectively a brief presentation of the approximations developed by Murray for the derivation of the mathematical expressions used in the numerical solution, a sample of the computer program used to solve the problem, and a sample of the computer output.

The experimental results of solid formation as a function of time are shown in Figures 6 through 12. All experimental runs were started at a temperature above the freezing point of the material. As discussed in Chapter IV an error proportional to the amount of superheat remaining in the liquid was present in the ultrasonoscope readings. These initial readings were corrected by multiplying the actual readings by the proper correction factor corresponding to the temperature of the liquid at that instant as obtained from Figure 4.

It can be seen that there are some differences in the results obtained experimentally and those given by the numerical solution. These differences arise from several causes. In the numerical solution, it is assumed that a perfectly insulated one-dimensional heat flow system exists. In practice, however, heat can flow into the mold particularly

through the front glass panel which would tend to reduce the actual rate of solidification. In an attempt to produce a closer agreement between the experimental data and the theoretical curves, the computer solution was modified to account for natural convection and conduction through the front glass panel. Even after this modification some differences in the data still remained.

Another source of error could arise from the fact that in the numerical solution the mold wall temperature at the solid-mold interface is assumed to be the same as that inside the heat sink, namely  $-107^{\circ}\text{F}$ . In practice it would be expected that a temperature gradient would exist in the glass mold wall separating the dry ice and acetone mixture from the solidified material. Because of this assumption a linear distribution of temperature in the solid between the solidification front and the solid-mold interface results in the numerical solution, which is clearly not the situation as can be seen from the experimental curves of Figures 37, 38 and 39.

For n-octadecane and n-hexadecane this temperature gradient would be expected to be small since these materials have a thermal conductivity comparable with that of the glass mold wall. Hence the reasonable good agreement between the temperature distributions assumed in the numerical solution and the experimental data as shown in Figures 38 and 39. A thermocouple placed adjacent to the mold wall showed the solid-mold interface temperature to be  $-107^{\circ}\text{F}$ .

The thermal conductivity for mercury is approximately two orders of magnitude greater than that for glass. This would result in a solid-mold interface temperature considerably higher than the heat sink tempera-

ture of  $-107^{\circ}\text{F}$ . A thermocouple placed at this interface showed that the temperature decreased with time, and in fact was  $-70^{\circ}\text{F}$  at the instant when  $1\frac{1}{2}$  inches of solid had formed. In the tests with mercury the computer solution was modified to account for the differences in thermal properties and temperature gradients for the mercury and glass. After this modification, reasonable agreement was obtained between the numerical computer solution and the experimental data as shown in Figure 37. Further, the numerical solution assumes a constant density for both the liquid and solid phases and neglects the effects of superheat and natural convection within the liquid. It was noted in the computer solution that a small change in the numerical value of the density of the material has a marked effect on the total solidification time. The thermal constants (see Appendix D) employed in the solution had to be assumed at an arbitrarily chosen temperature for both the solid and liquid phases which contributed additional errors.

Figure 6 shows a comparison of the experimental data with the numerical solution for the thickness of solid formed with respect to time for mercury at  $75^{\circ}\text{F}$ . It can be seen that there is reasonably good agreement between the experimental and theoretical results. Thickness of solid formation versus time curves for n-octadecane are shown in Figures 7, 8 and 9. The times for complete solidification as given by the numerical solution are seen to be about 200 per cent higher than those obtained experimentally. This tremendous difference between the experimental and numerical results is probably due to the shape of the solid-liquid interface which could be populated with microscopic peaks and valleys as observed in a previous study (38), and to natural convection in the liquid region.

The numerical solution used in this work assumed a flat solid-liquid interface and no natural convection within the liquid. The low thermal conductivity of n-octadecane indicates that the assumption of negligible natural convection through the liquid would give rise to appreciable errors in the numerical solution. The mechanism of solidification of n-octadecane is such that as this material freezes many crystals grow out of the main solid-liquid interface orienting themselves in such a manner that their axes of high thermal conductivity are more or less perpendicular to the interface. Heat would then be removed from the liquid laterally through these crystals as well as normally through their ends. Consequently the crystals at the interface increase in width at the expense of the neighboring liquid, while the continual appearance of new crystals helps to maintain an average crystal width. It is believed that the increase in the growth rate of crystals at the interface and the increase in the heat transferred through the liquid as a result of natural convection are the principal causes for the disagreement between theoretical and experimental results for n-octadecane. Although the shape of the solid-liquid interface during freezing of pure n-hexadecane has not been observed, it is suspected that the same mechanism of crystal growth described above governs the solidification of this material. Natural convection through the liquid would further decrease the actual time for complete solidification. Solid thickness versus time curves for n-hexadecane are shown in Figures 10, 11 and 12.

As opposed to n-octadecane and n-hexadecane the solid-liquid interface for mercury is known to be planar and non-crystallographic. Further, the high thermal conductivity of this material indicates that heat trans-

fer through the liquid region would occur mainly by conduction. This implies that no appreciable error would result in the numerical solution which assumes a flat interface and negligible effects of natural convection through the liquid region. Hence the good agreement between the experimental and theoretical solidification rates for mercury.

The velocity of the freezing front as a function of time is shown in Figures 13, 14 and 15. The experimental velocity was determined from the slope of the experimental curves in Figures 6, 9 and 12. The motion of the freezing front in all cases is such that it experiences a very rapid acceleration for a short time at the beginning of solidification, then a slow deceleration as solidification progresses. In both the experimental and theoretical curves the peaks of maximum velocity are observed to occur at the same time. Figures 14 and 15 show that the maximum velocity peak for n-hexadecane occurs at a later time than for n-octadecane. This is so because in these particular runs n-hexadecane had 58 degrees Fahrenheit of superheat at time zero compared with only 37 for n-octadecane. The dashed lines in the curves represent assumed values of the velocity near time zero, as accurate measurements during this small time interval could not be made. Agreement between numerical and experimental results for mercury as shown in Figure 13 is seen to be reasonably good. For n-octadecane and n-hexadecane the values of freezing front velocity as obtained from the experimental results are seen to be approximately 100 per cent higher than the values given by the numerical solution.

Figures 16 through 22 show solid thickness as a function of the square root of time for each of the initial temperatures. This form of presentation is of the type discussed in Chapter II where the mathemati-

cal expression

$$D = q\sqrt{t} + C$$

is used to predict solidification rates for various materials. The constants  $q$  and  $C$  have units of inches/minutes<sup>1/2</sup> and inches respectively. The variables  $D$  and  $t$  have units of inches and minutes respectively. The values of  $q$  and  $C$  for mercury were found to be 0.825 and -2.5 respectively. For n-octadecane and n-hexadecane  $q$  ranges from 0.19 to 0.21;  $C$  ranges from -0.11 to -0.25, and increases in absolute value for increasing degrees of superheat. A small time delay before the start of solidification is indicated by the small numerical value of  $C$  for n-octadecane and n-hexadecane. A large numerical value of  $C$  for mercury indicates that a considerable amount of time was spent during the dissipation of superheat, actually about 1/3 of the total time for complete solidification. It is noted also that solidification of mercury did not start until all the superheat was dissipated and the liquid metal was slightly undercooled.

Figures 23 through 29 show representative solidification front profiles for all runs. The presence of convection currents during the dissipation of superheat accounts for the curved profiles. The curves show that as solidification progresses, the profiles approach the ideal one-dimensional concept. The profiles for mercury as shown in Figure 23 are seen to be more curved than those for n-octadecane and n-hexadecane. This is so because a great deal more of superheat had to be dissipated during the mercury run. Figures 24, 25 and 26 for n-octadecane, and Figures 27, 28 and 29 for n-hexadecane show how the curvature of the

profiles increases with increasing amounts of superheat.

Figures 30 through 36 show representative experimental temperature profiles for all runs. Referring to the thermocouple positions shown in Figure 2 the temperature profiles show the time at which the solidification front passed each of the thermocouple positions by the sudden drop in temperature. Correlation between these times and those noted by the ultrasonoscope are good.

The temperature distribution in the solid and liquid portions for the case where solidification is half-way complete across the mold is shown in Figures 37, 38 and 39. The points plotted represent experimental and theoretical temperatures at each of the thermocouple positions. The dashed portion of the experimental curve represents the assumed temperature distribution from the seventh thermocouple to the mold wall. Agreement between experimental and theoretical results for all the materials is seen to be reasonably good. Differences in the experimental and theoretical temperature distributions in the solid region are probably due to the assumption of constant physical properties in the mathematical equations used in the numerical solution.

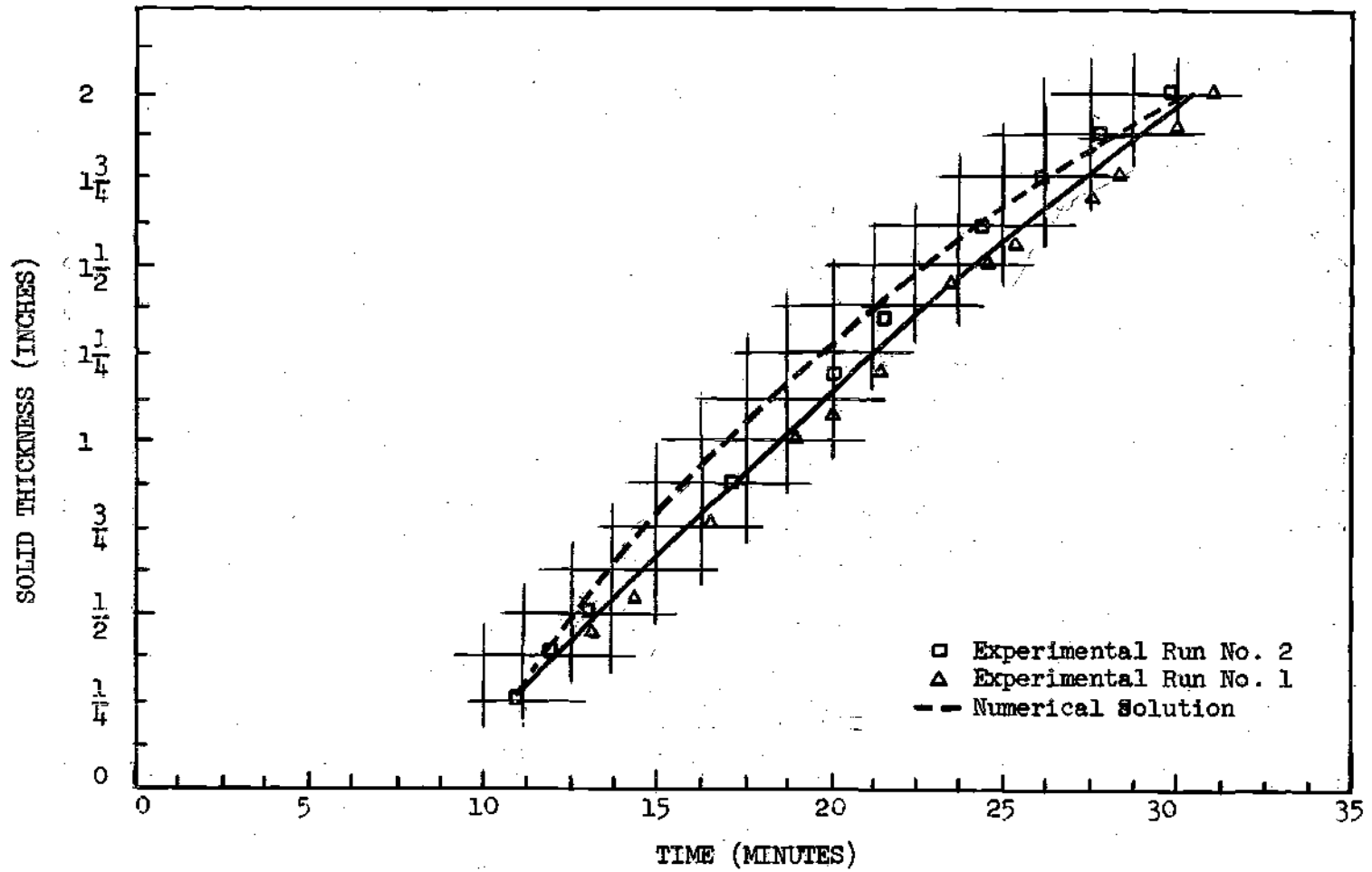


Figure 6. Solidification of Mercury at 75°F.



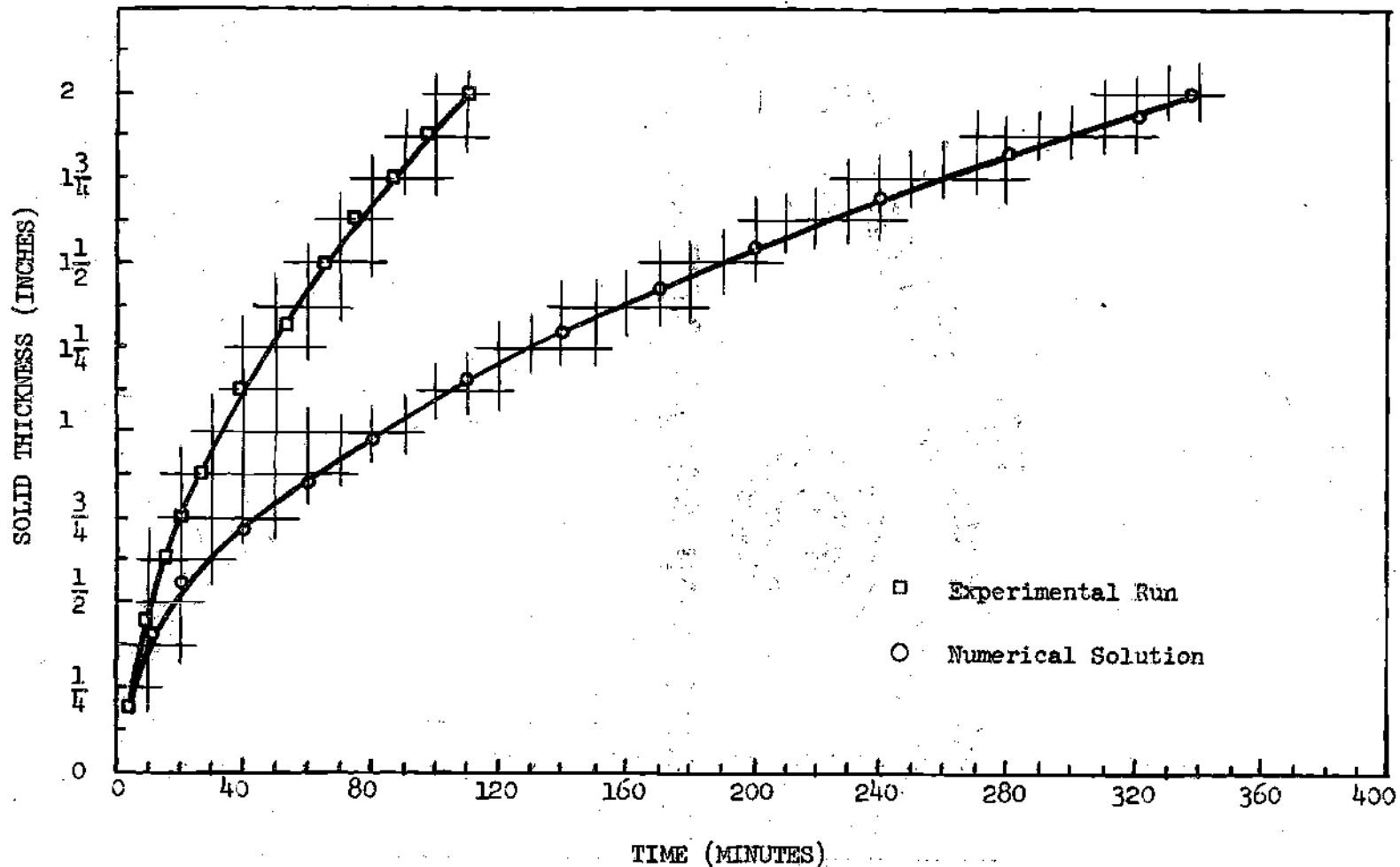


Figure 7. Solidification of N-Octadecane at 90°F.

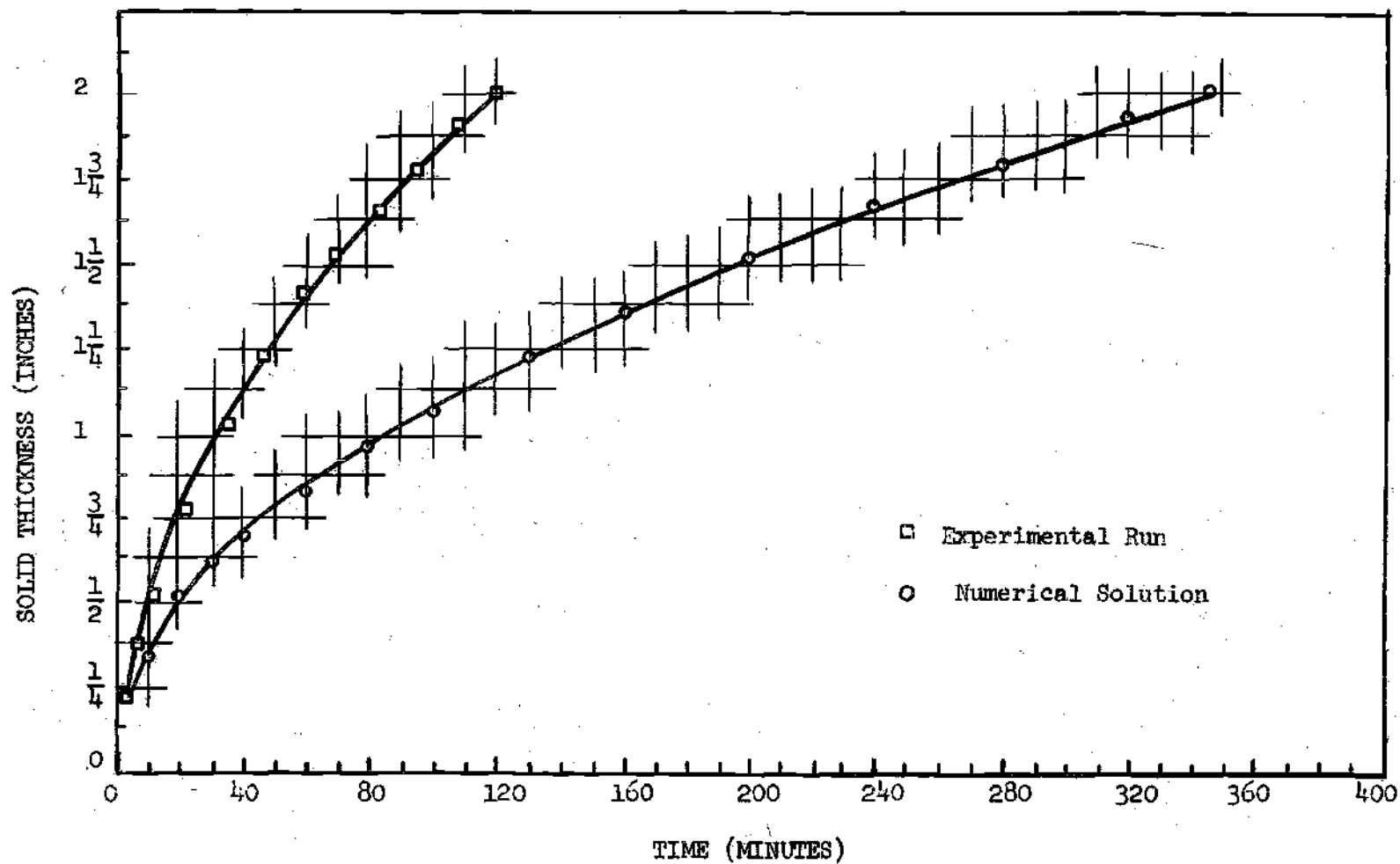


Figure 8. Solidification of N-Octadecane at 100°F.

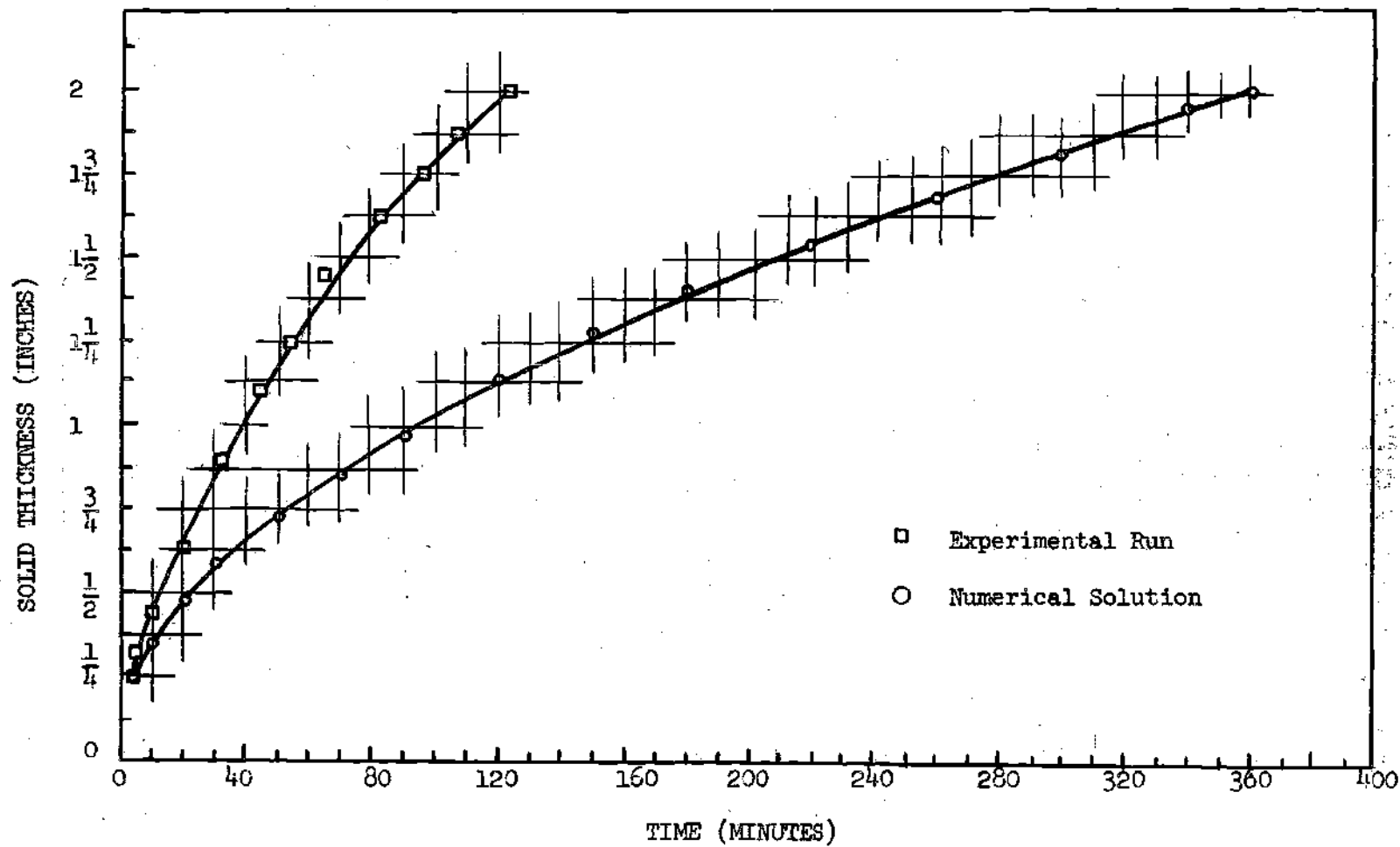


Figure 9. Solidification of N-Octadecane at 120°F.

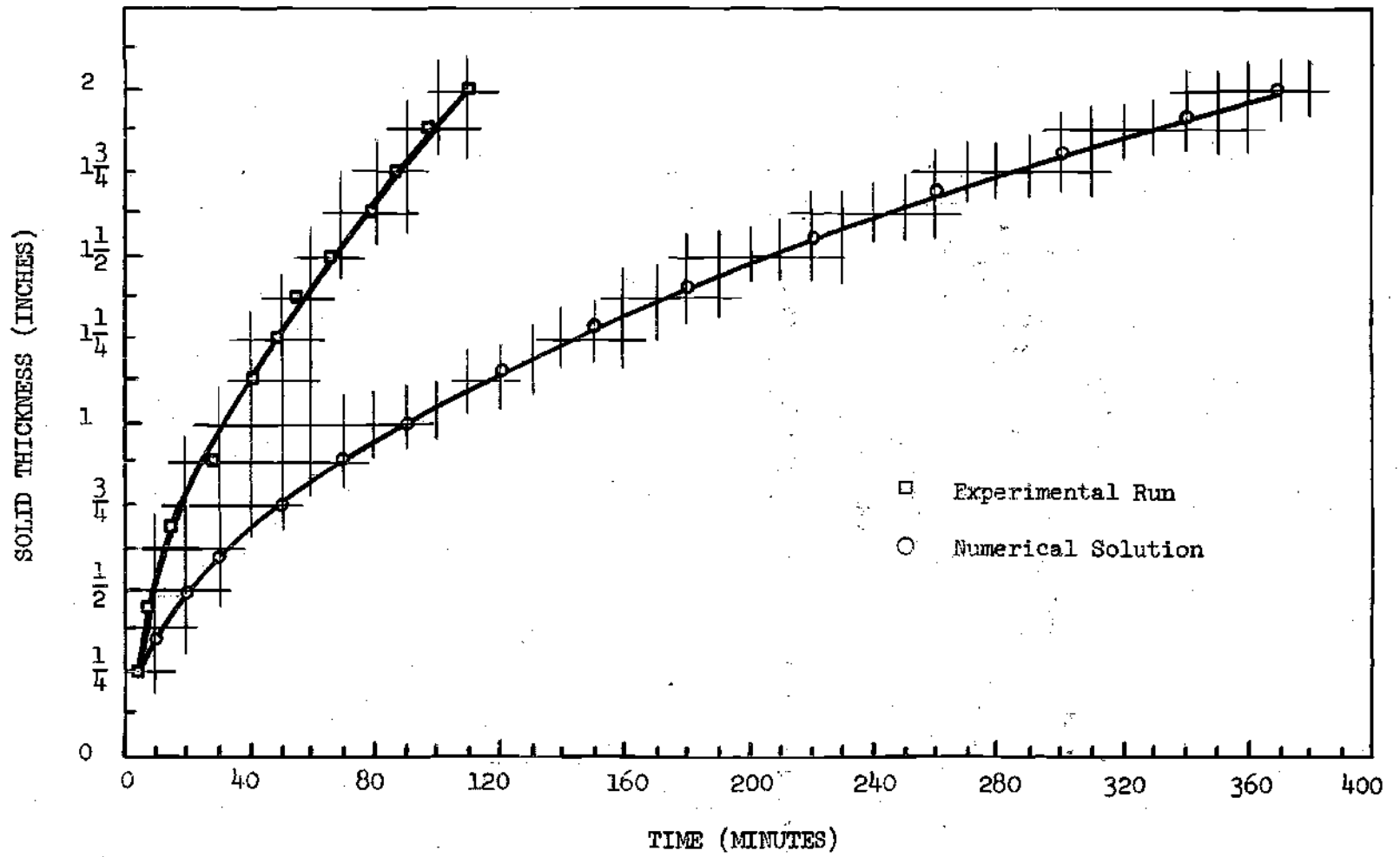


Figure 10. Solidification of N-Hexadecane at 70°F.

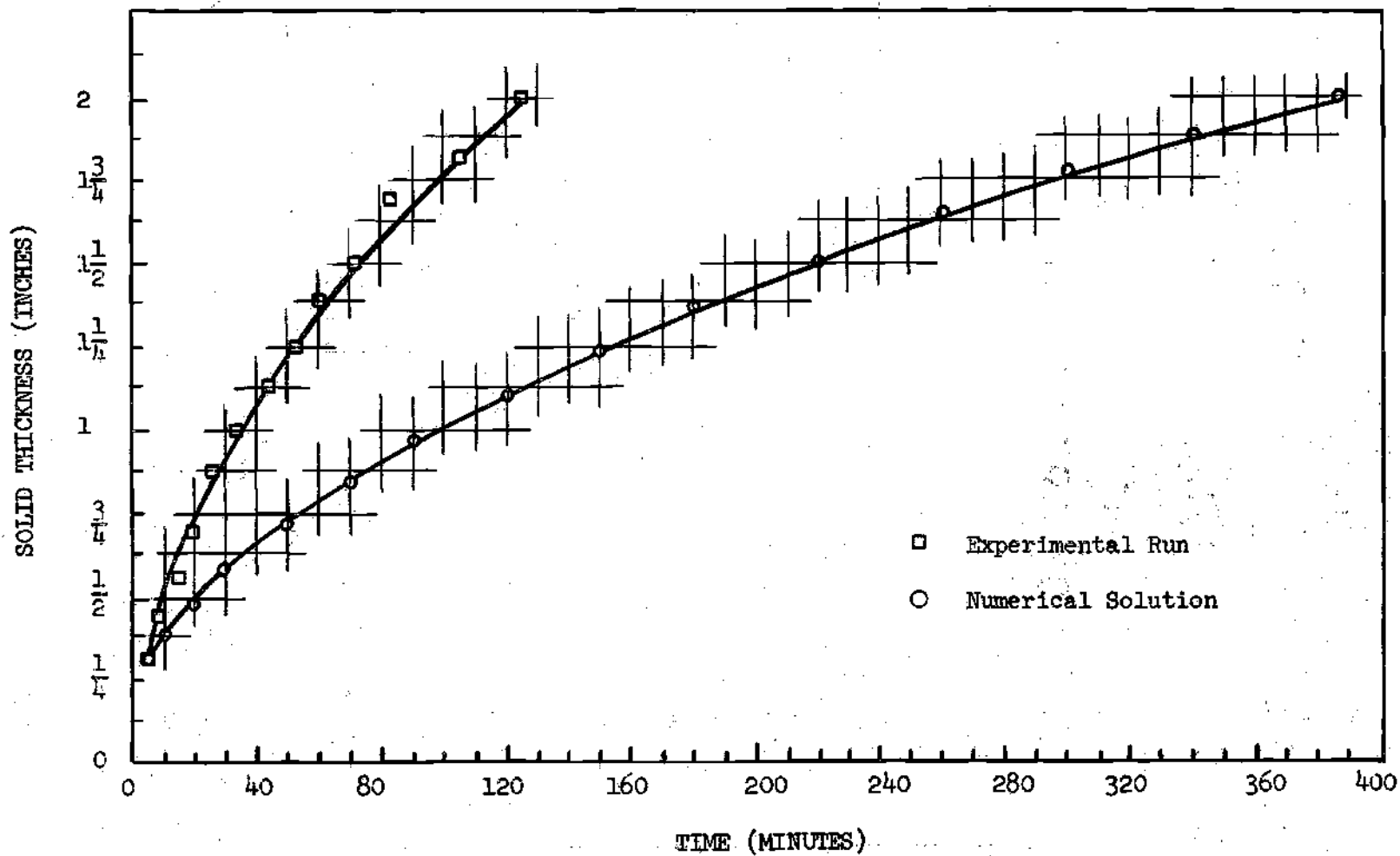


Figure 11. Solidification of N-Hexadecane at 90°F.

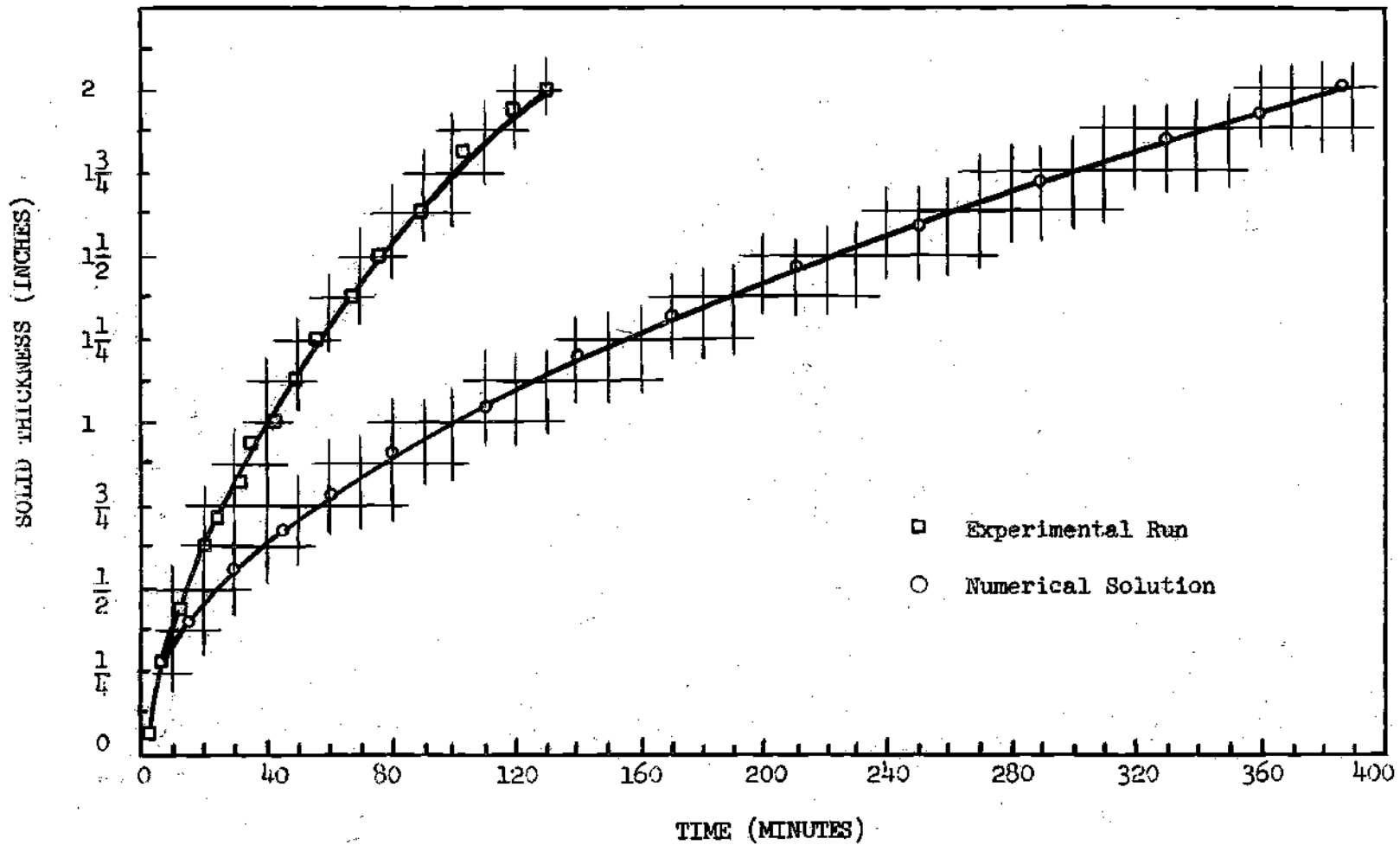


Figure 12. Solidification of N-Hexadecane at 120°F.

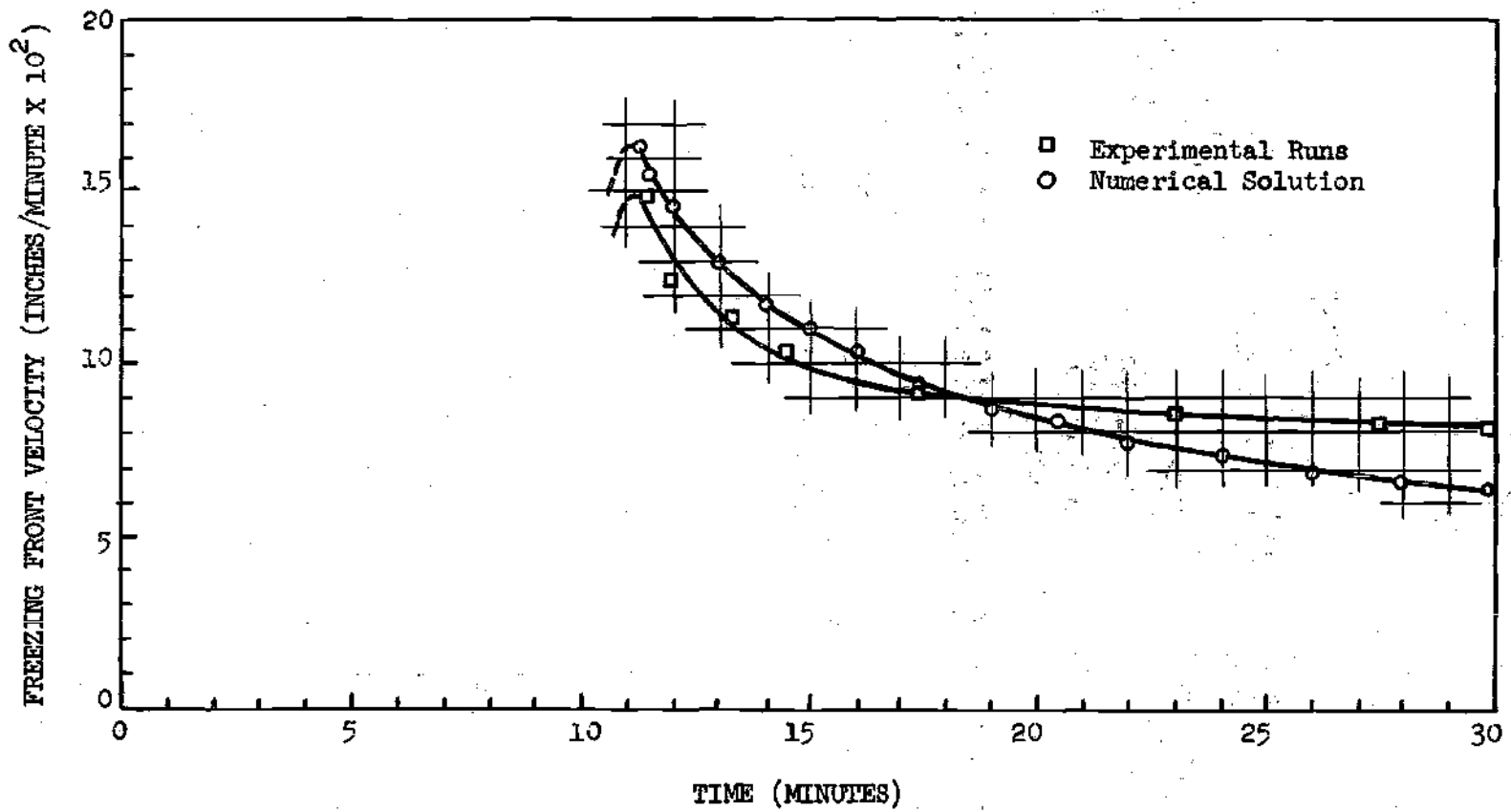


Figure 13. Rate of Solidification for Mercury at 75°F.

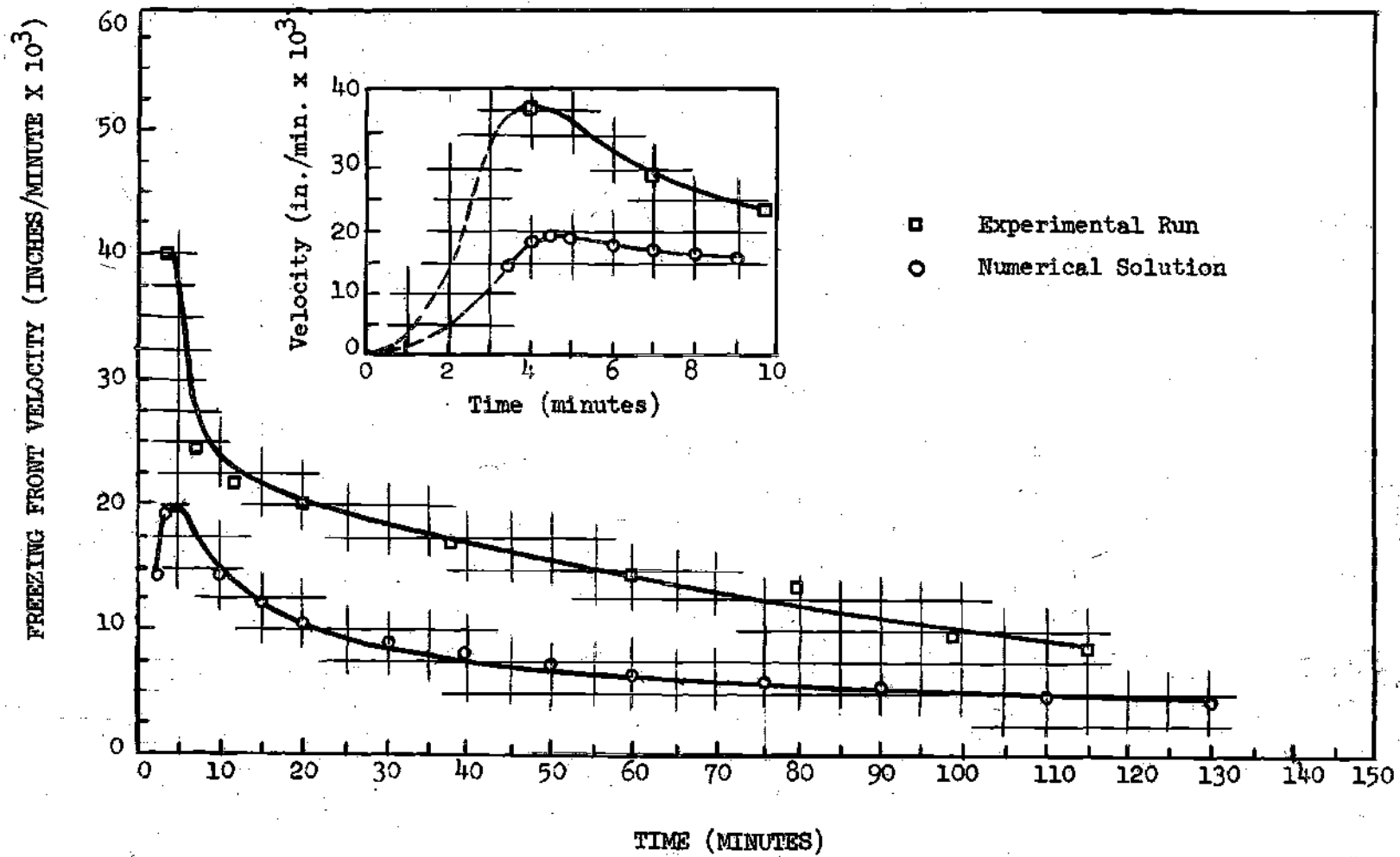


Figure 14. Rate of Solidification for N-Octadecane at 120°F.



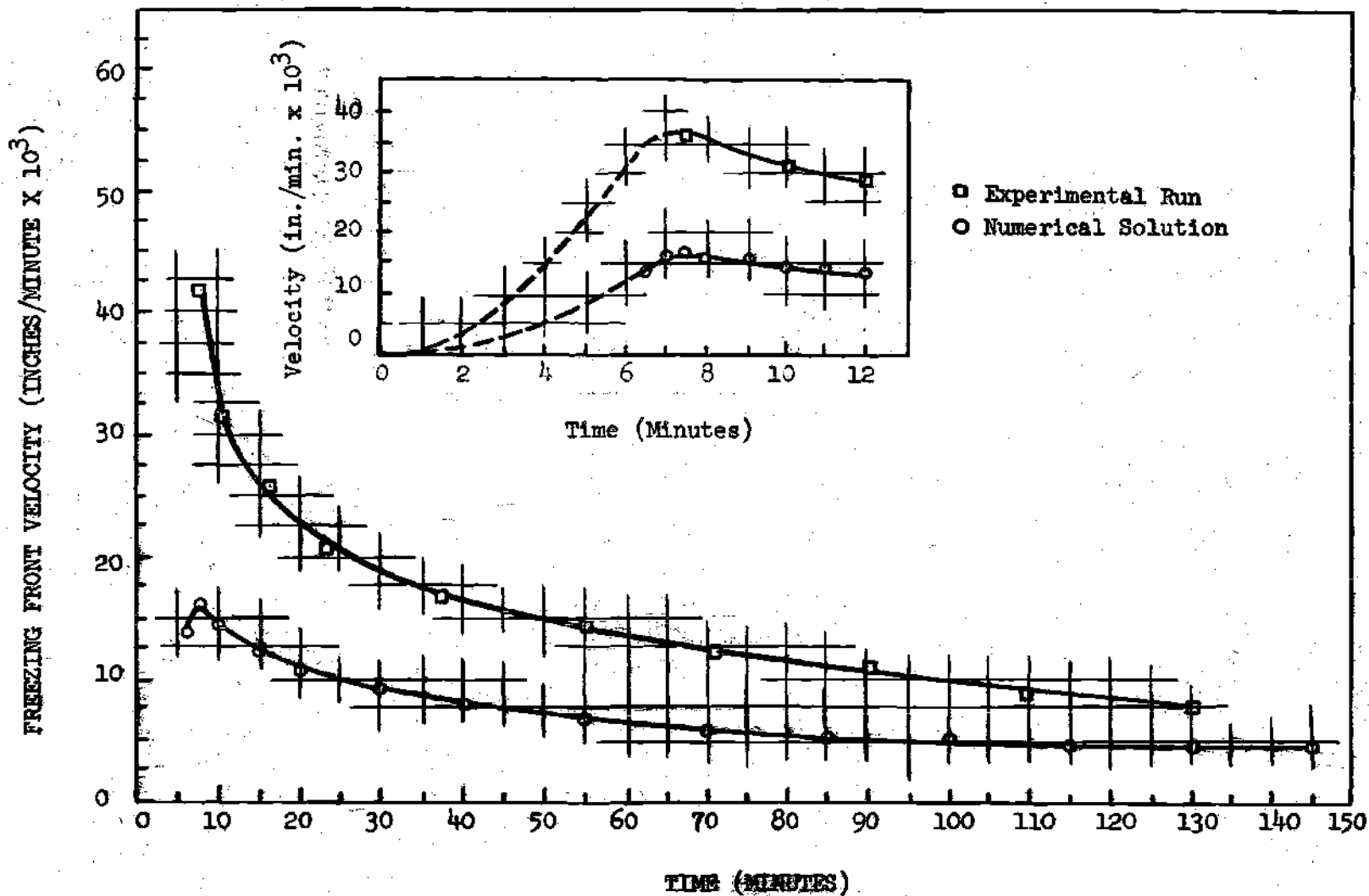


Figure 15. Rate of Solidification for N-Hexadecane at 120°F

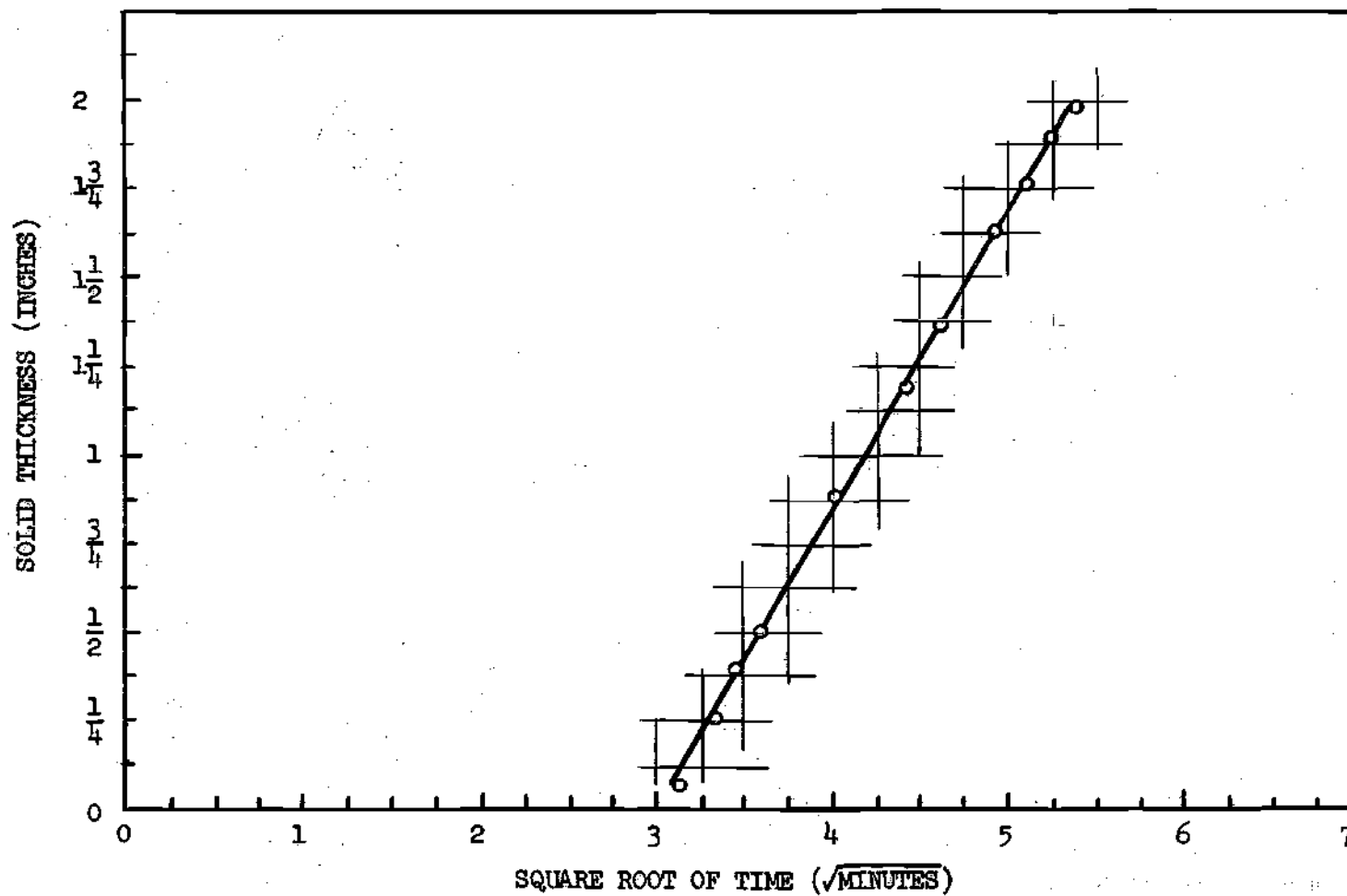


Figure 16. Solid Thickness versus  $\sqrt{\text{Time}}$  for Mercury at 75°F.

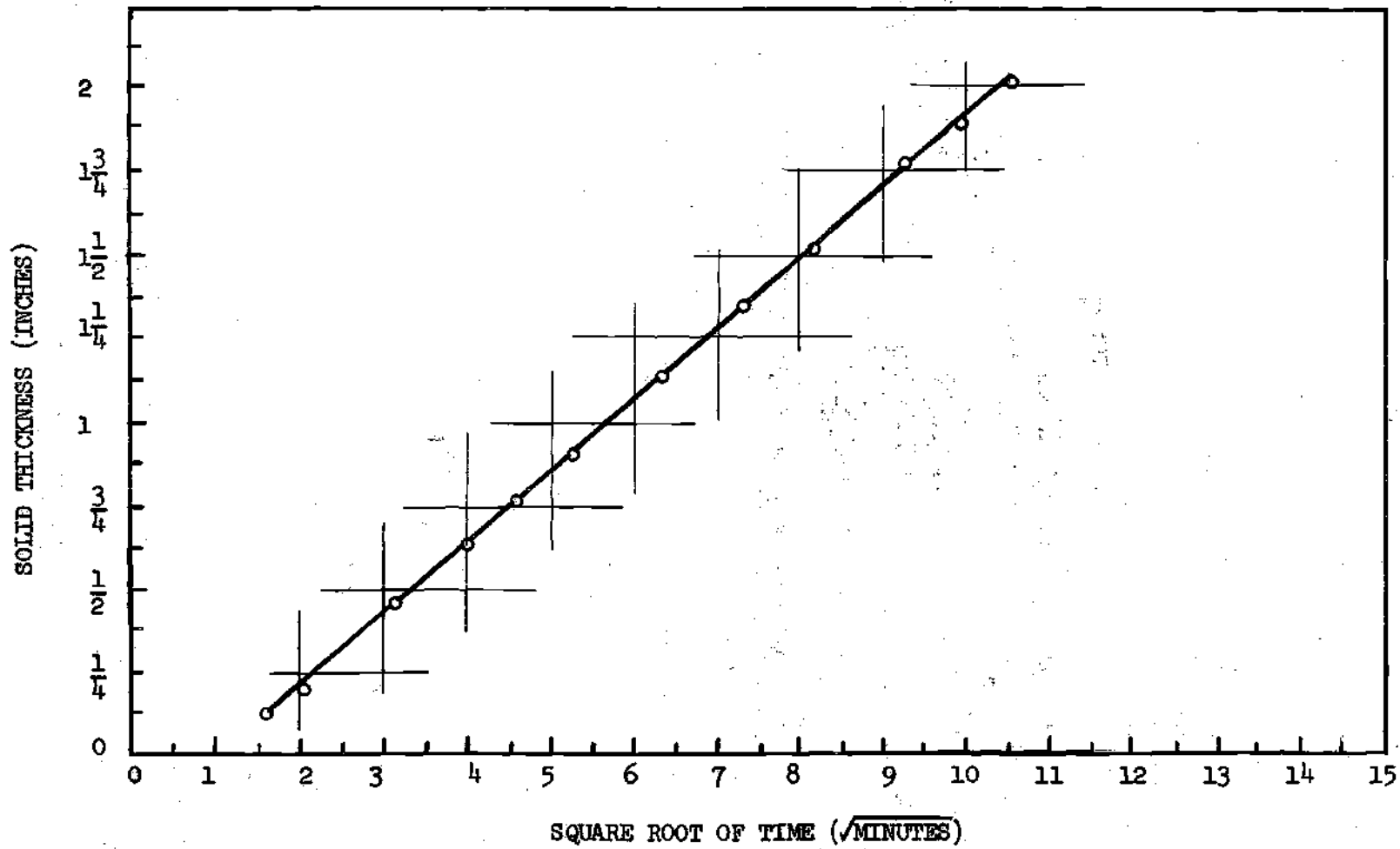


Figure 17. Solid Thickness versus  $\sqrt{\text{Time}}$  for N-Octadecane at 90°F

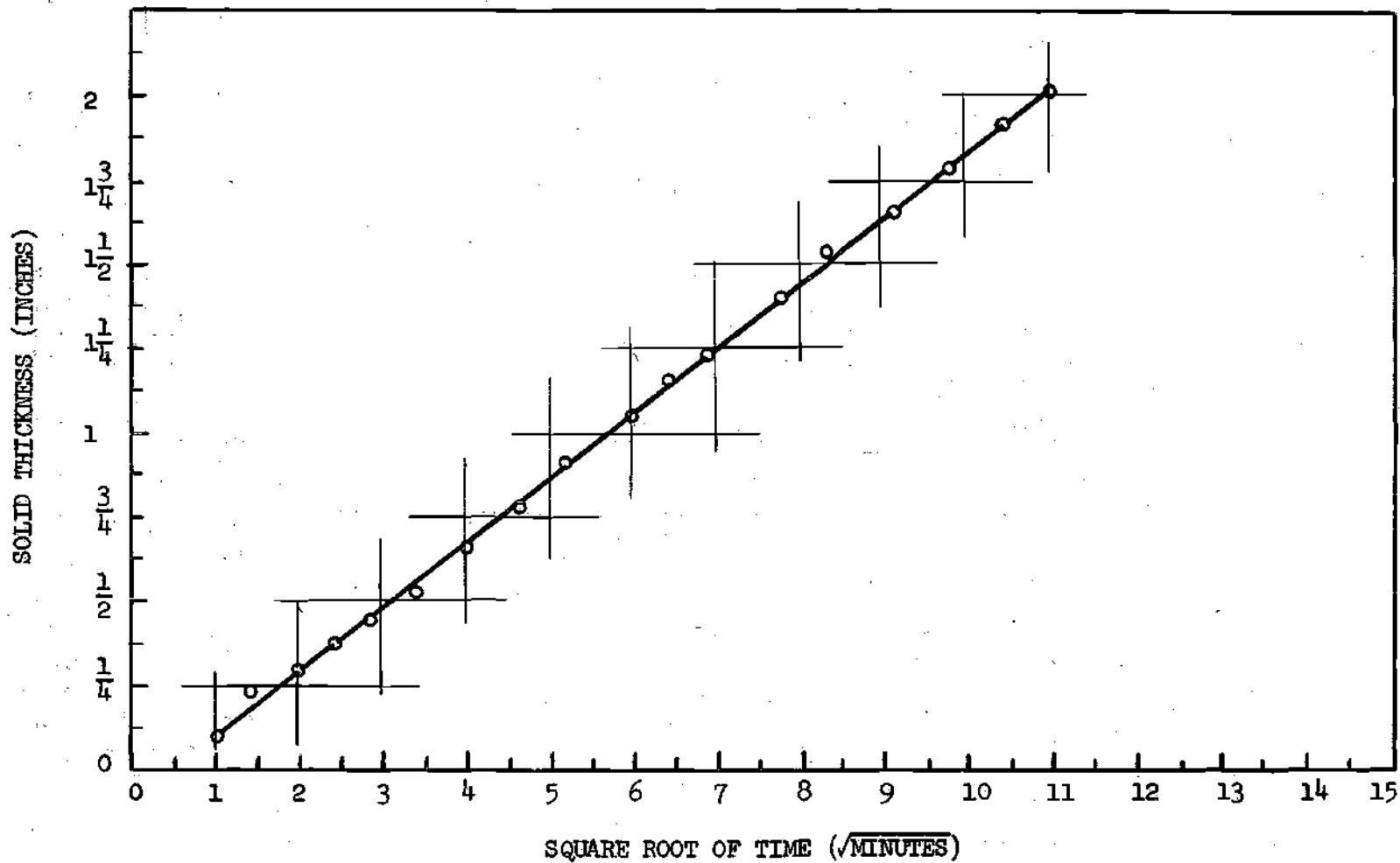


Figure 18. Solid Thickness versus  $\sqrt{\text{Time}}$  for N-Octadecane at 100°F.

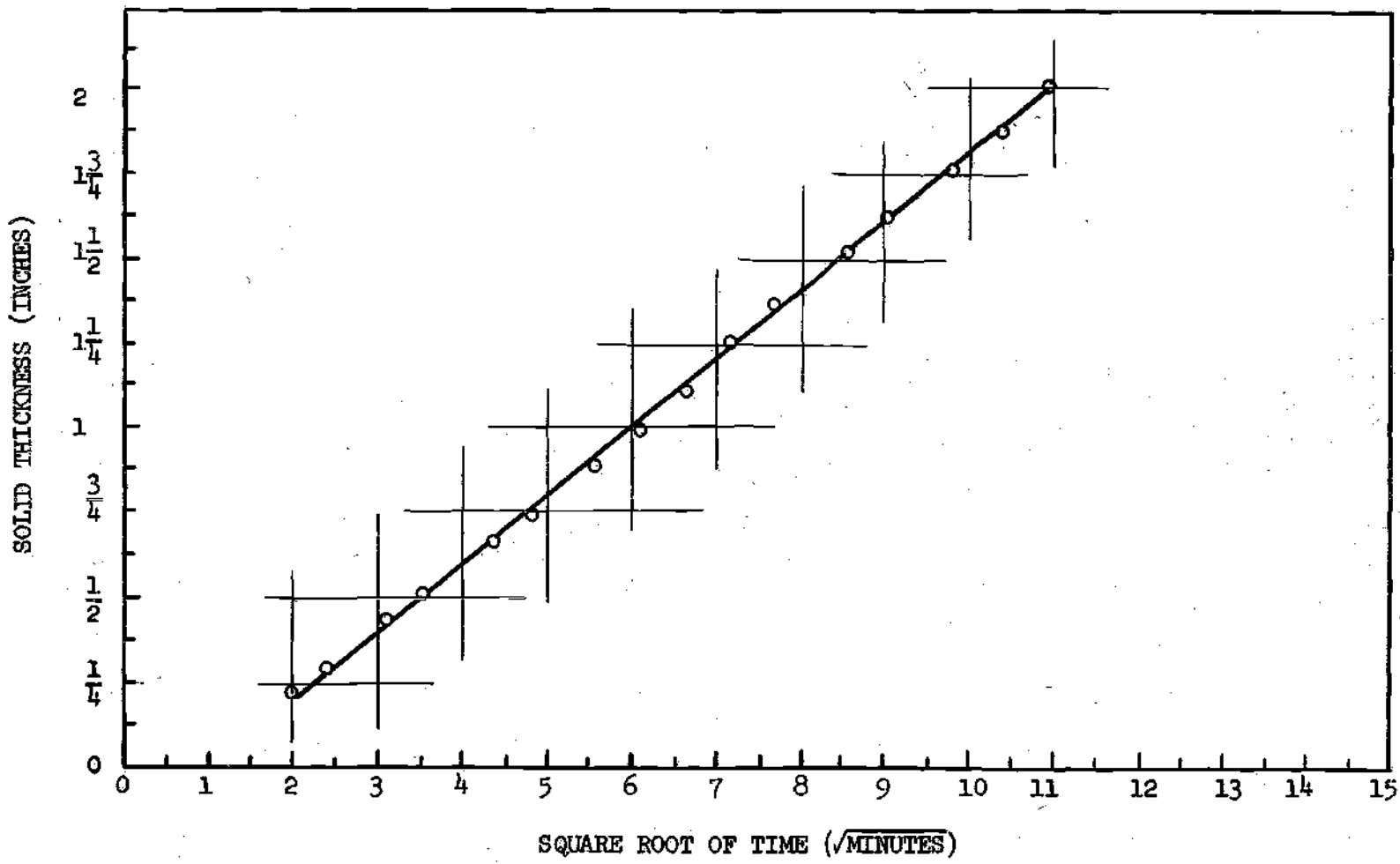


Figure 19. Solid Thickness versus  $\sqrt{\text{Time}}$  for N-Octadecane at 120°F.

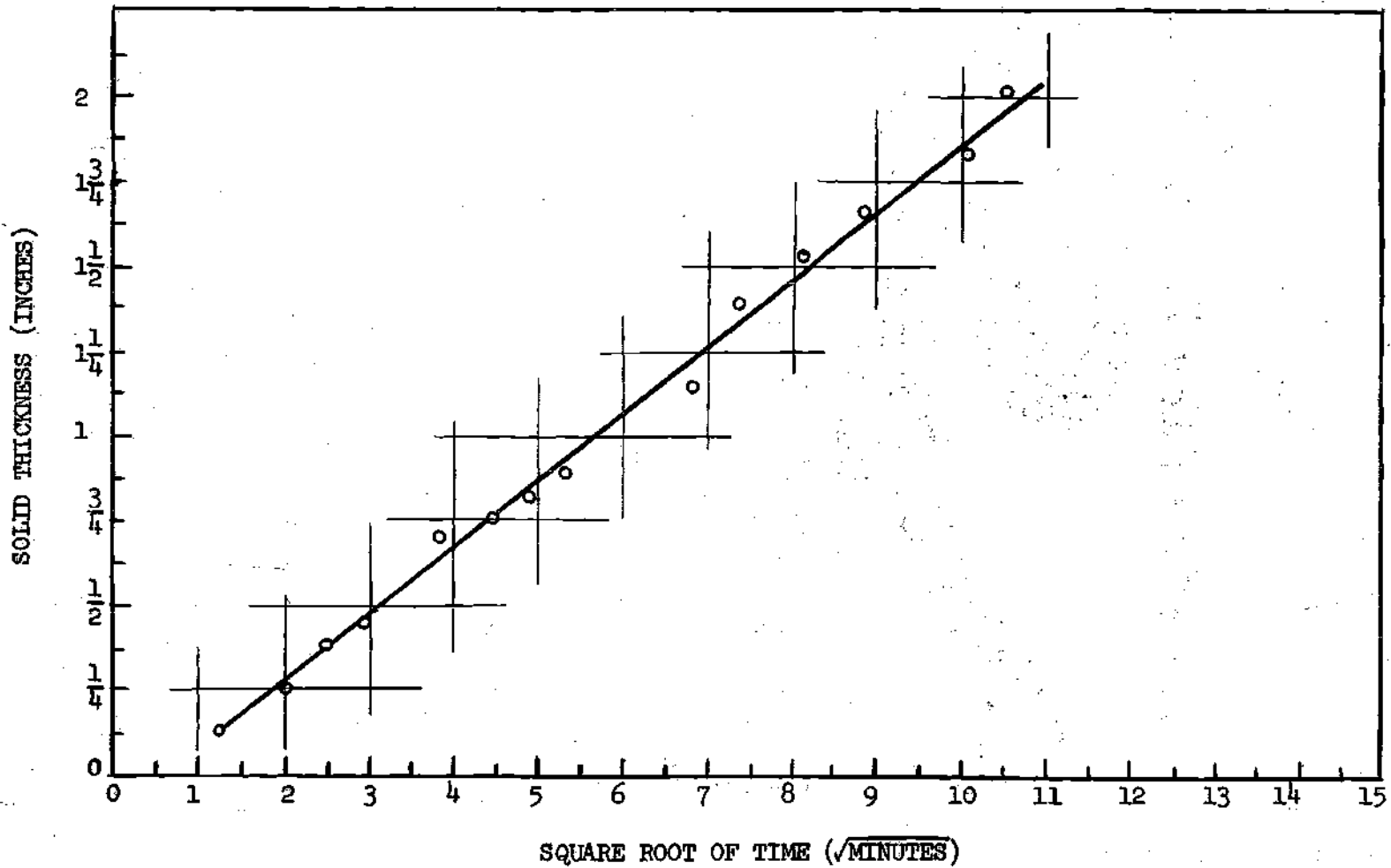


Figure 20. Solid Thickness versus  $\sqrt{\text{Time}}$  for N-Hexadecane at 70°F.

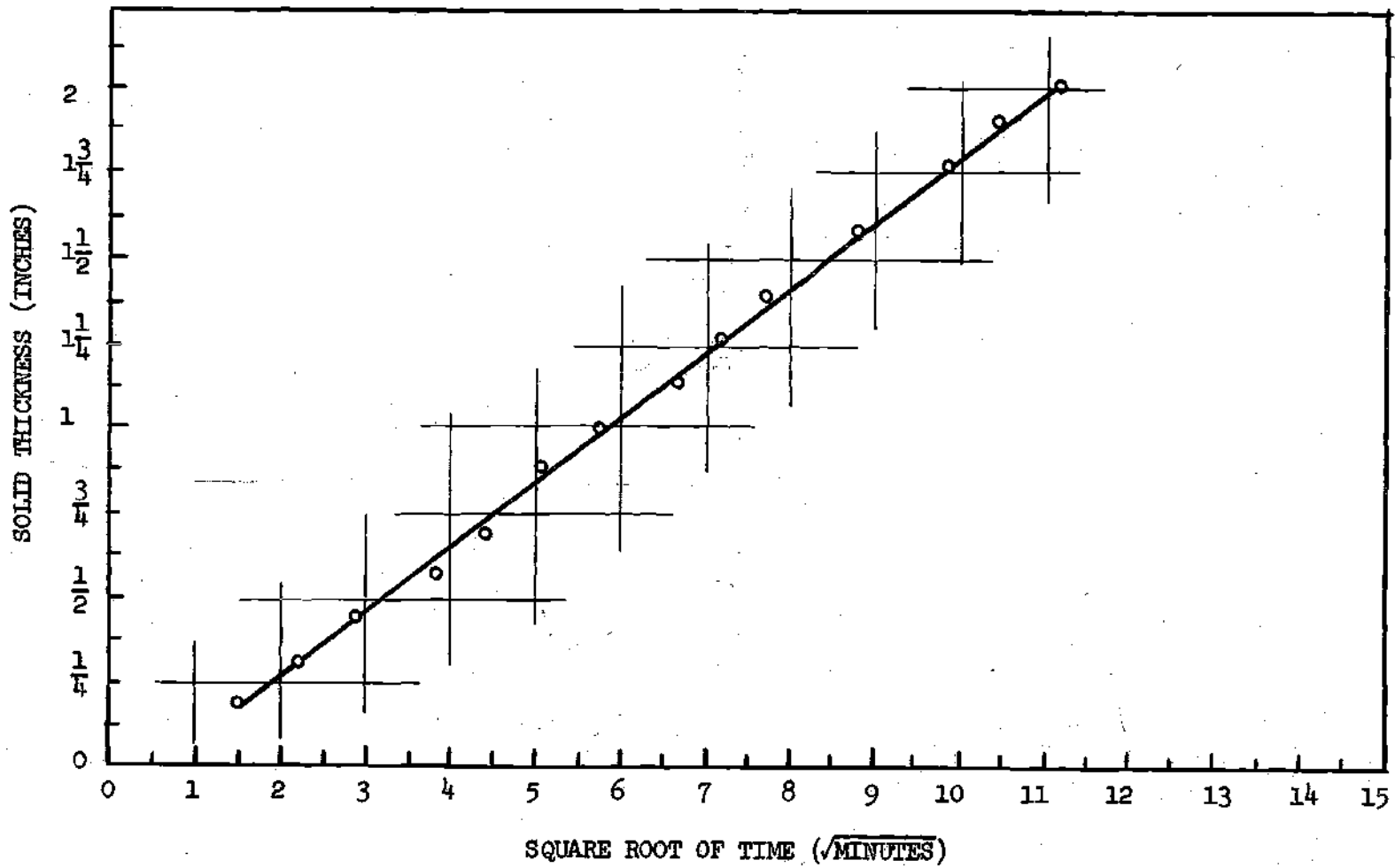


Figure 21. Solid Thickness versus  $\sqrt{\text{Time}}$  for N-Hexadecane at 90°F.

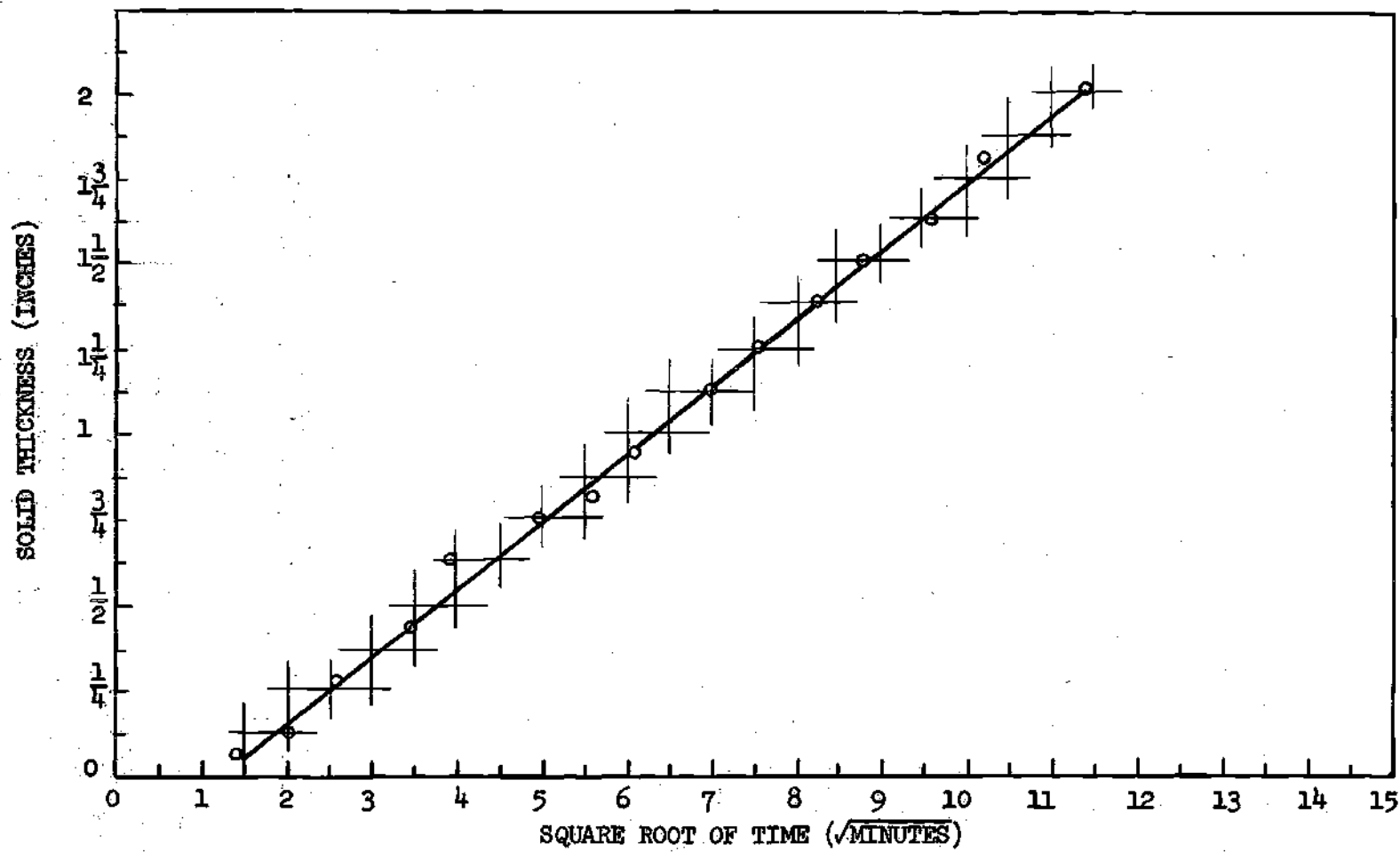


Figure 22 . Solid Thickness versus  $\sqrt{\text{Time}}$  for N-Hexadecane at 120°F.



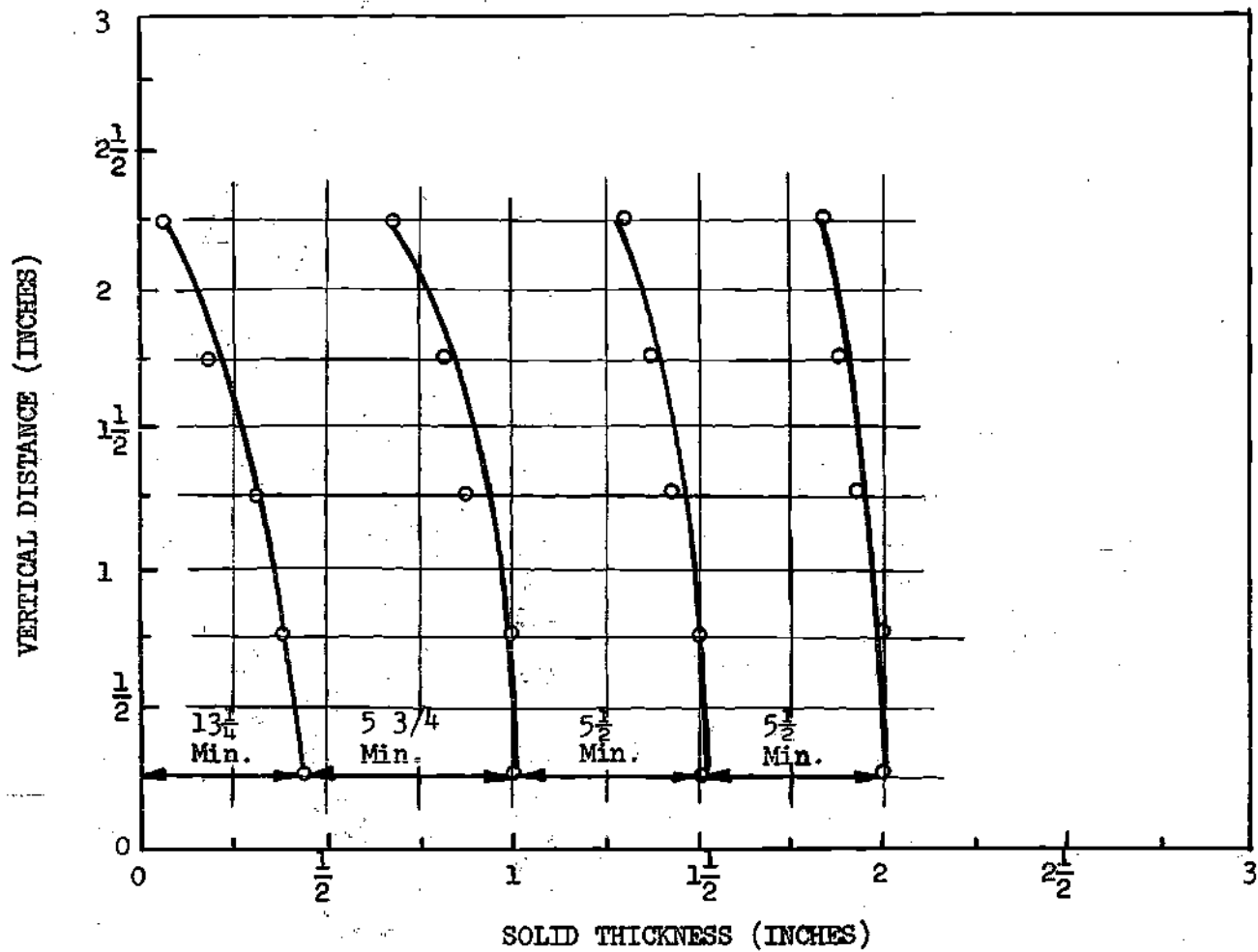


Figure 23. Solidification Front Profile for Mercury at 75°F.

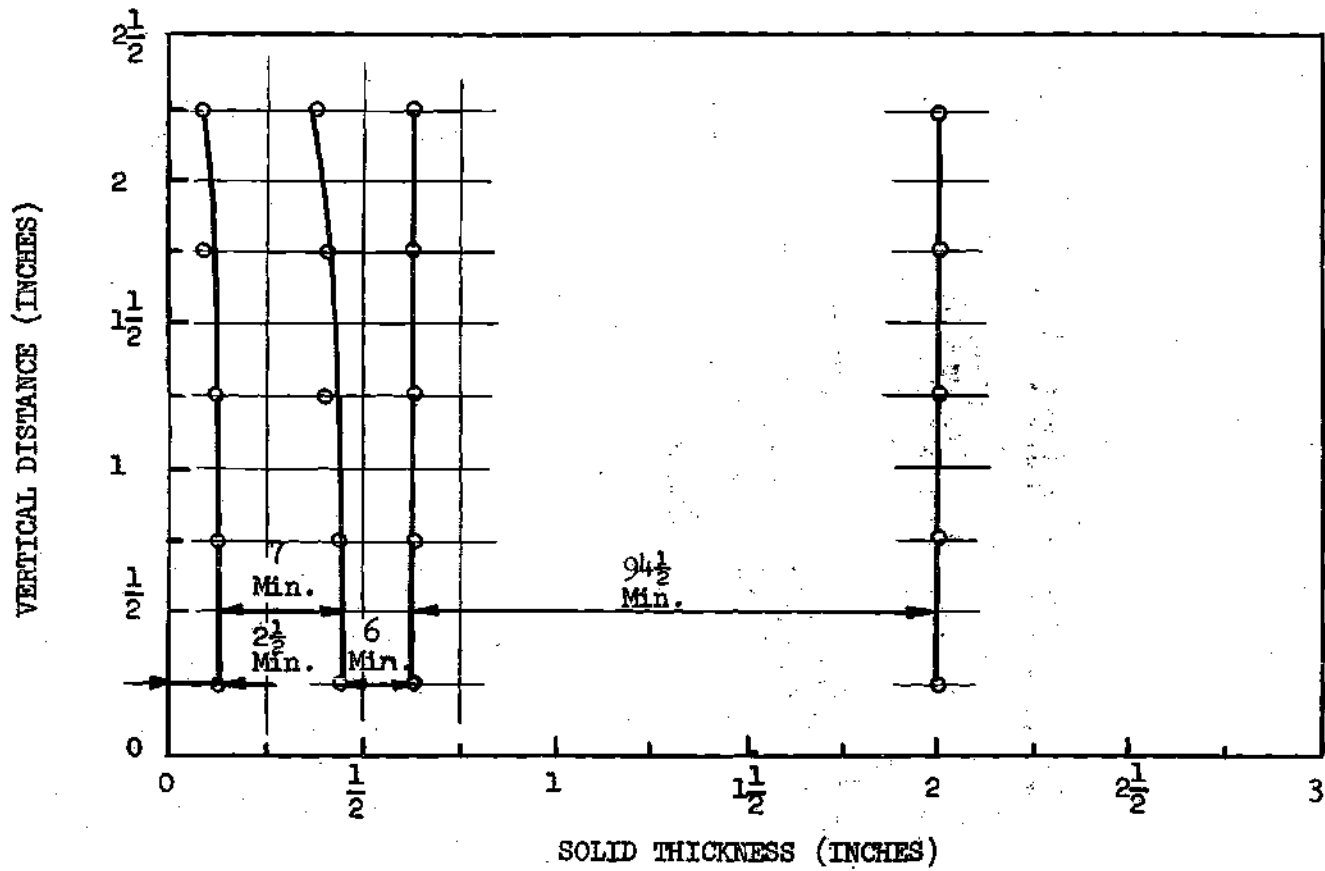


Figure 24. Solidification Front Profile for N-Octadecane at 90°F.

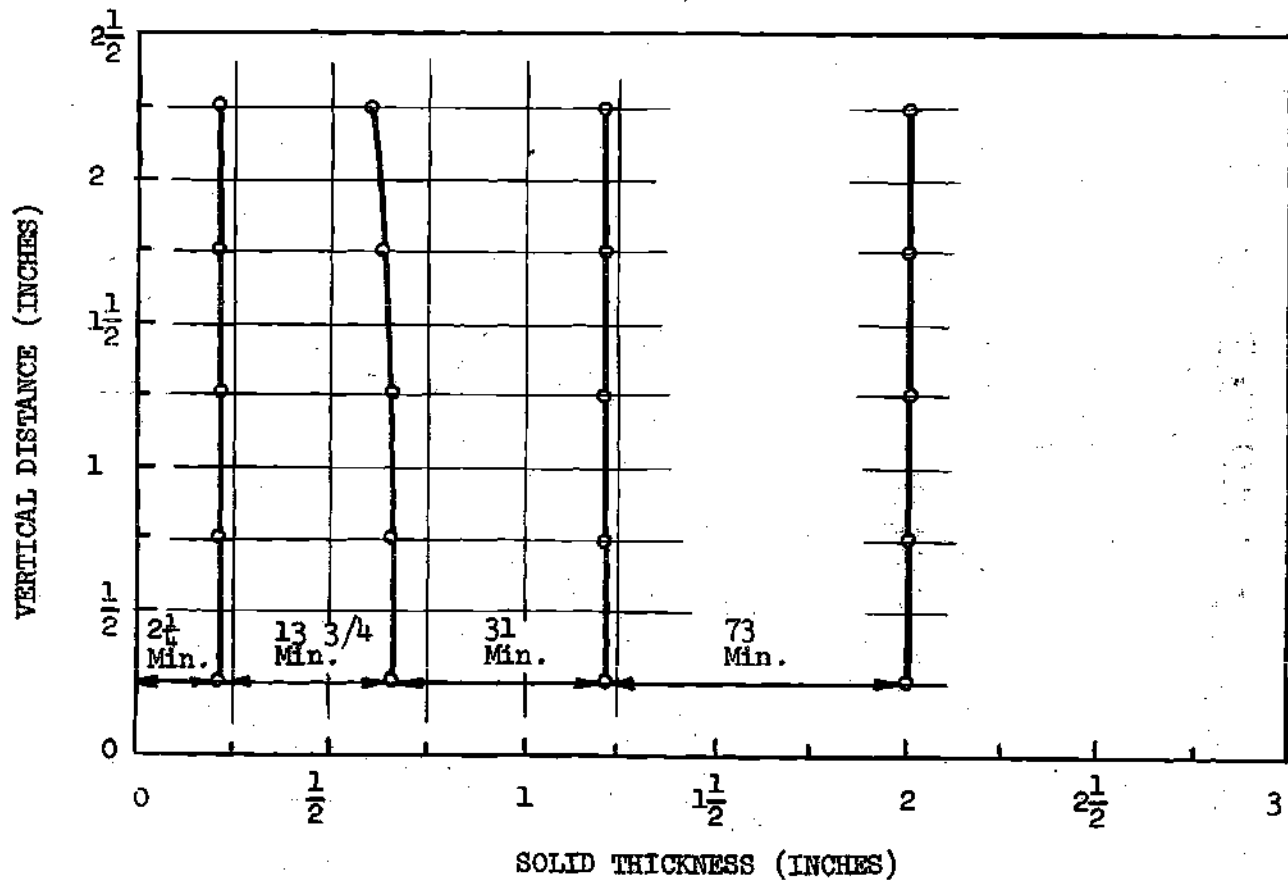


Figure 25. Solidification Front Profile for N-Octadecane at 100°F.

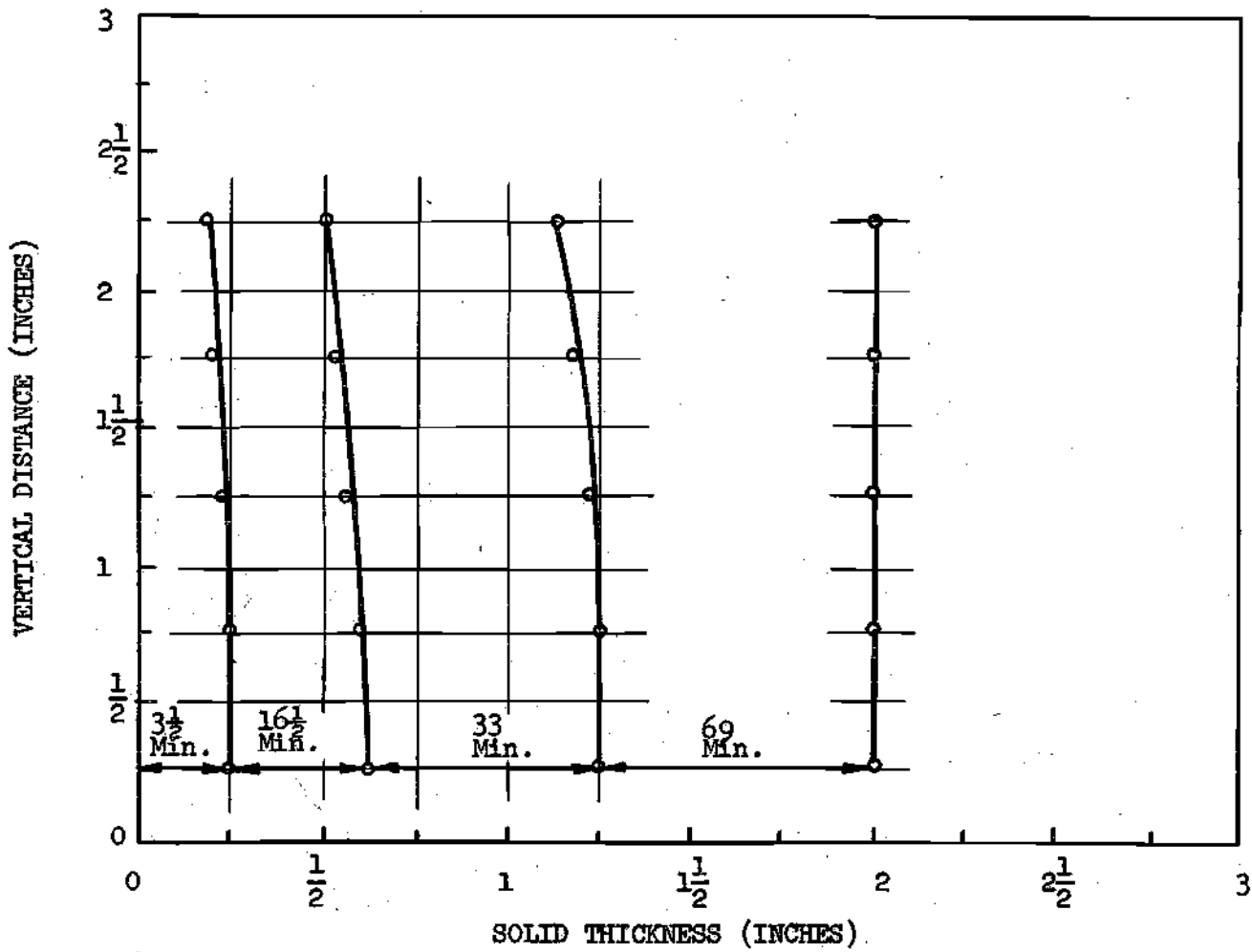


Figure 26. Solidification Front Profile for N-Octadecane at 120°F.

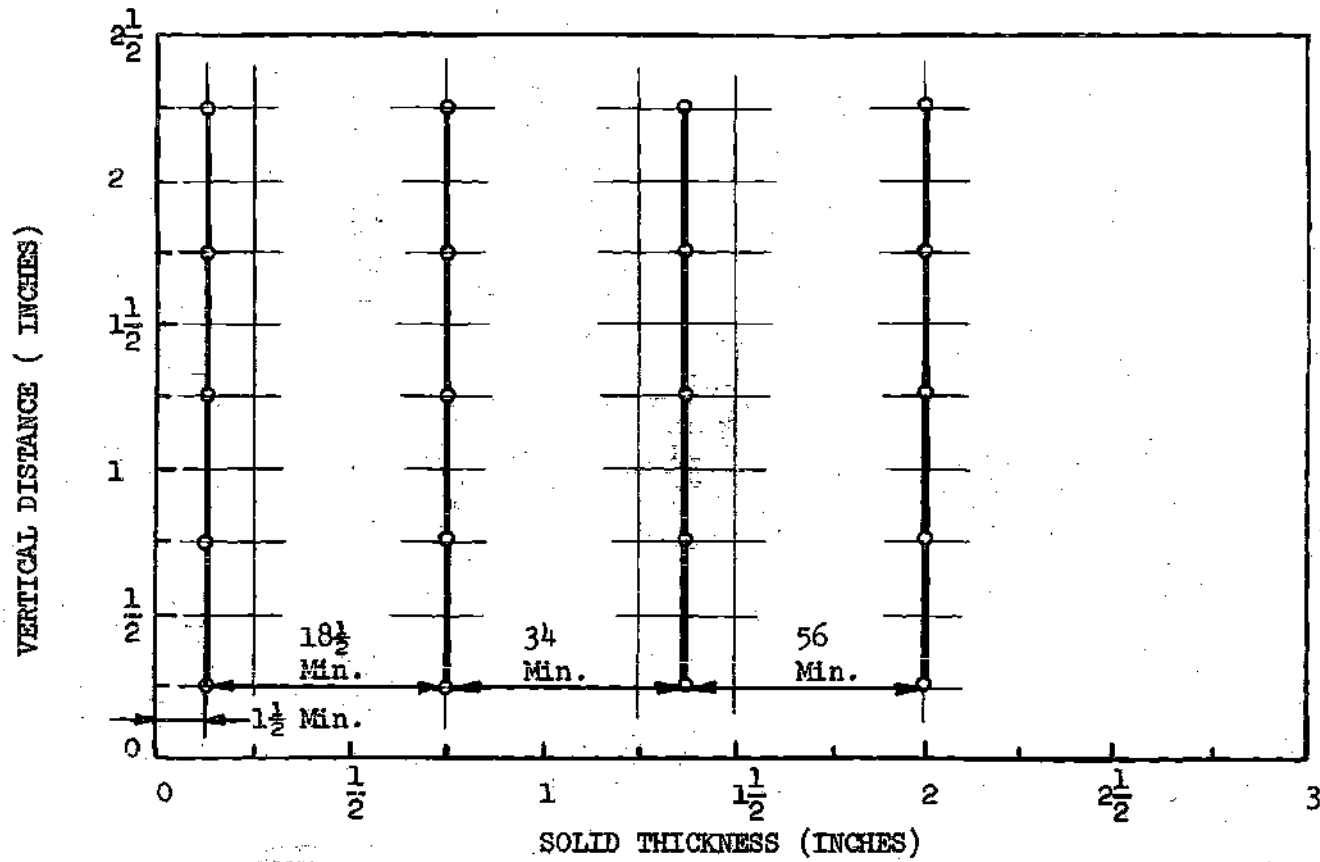


Figure 27. Solidification Front Profile for N-Hexadecane at 70°F.

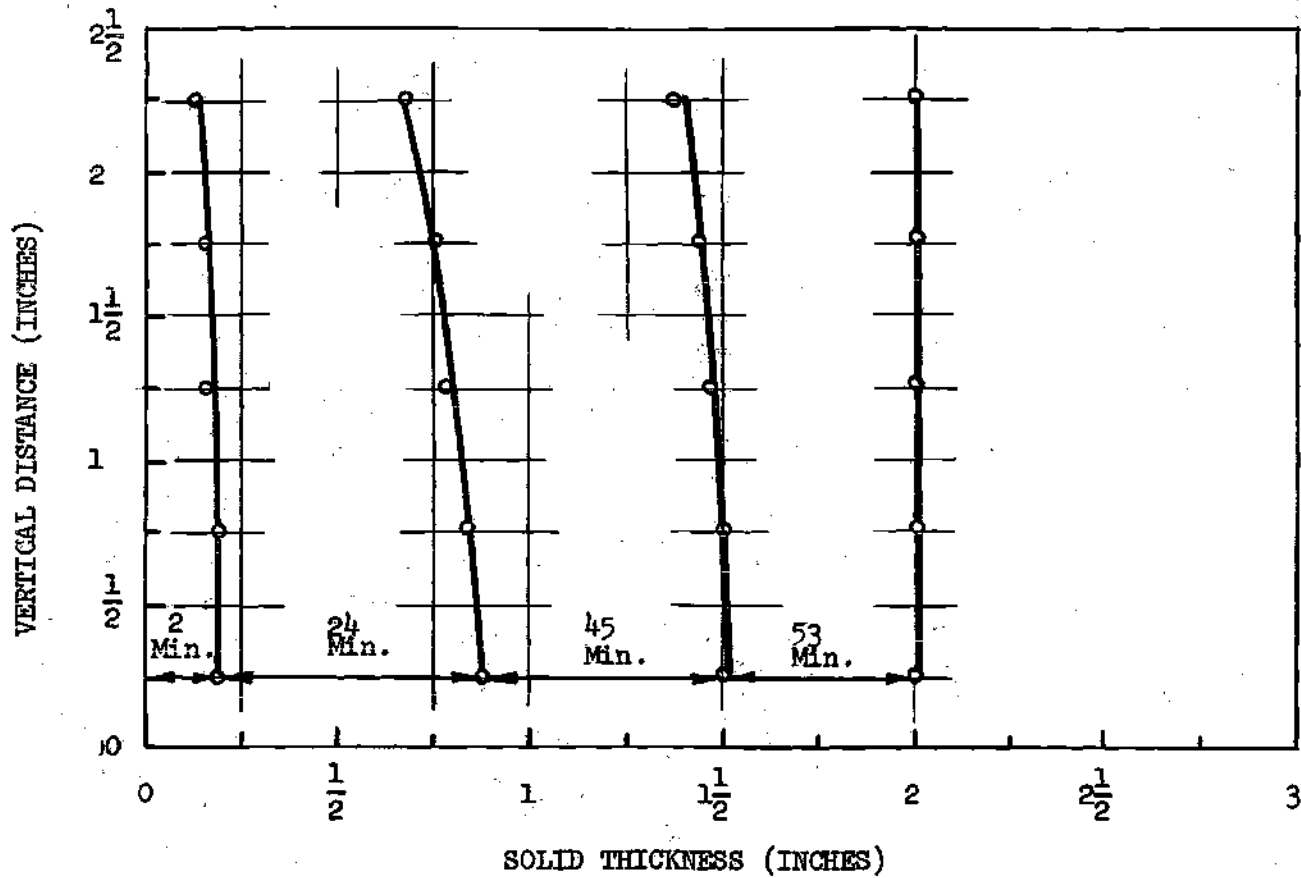


Figure 28. Solidification Front Profile for N-Hexadecane at 90°F.

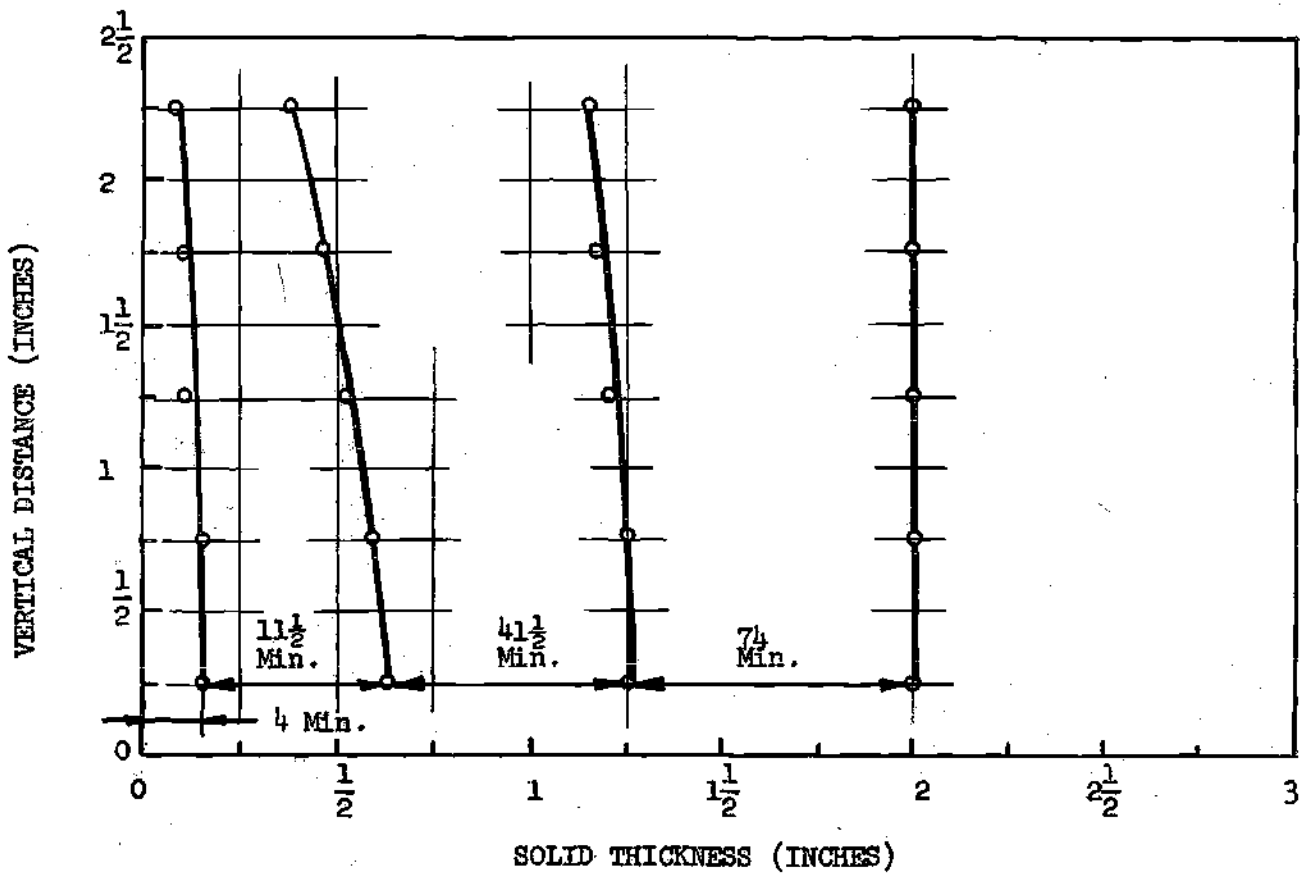


Figure 29. Solidification Front Profile for N-Hexadecane at 120°F.

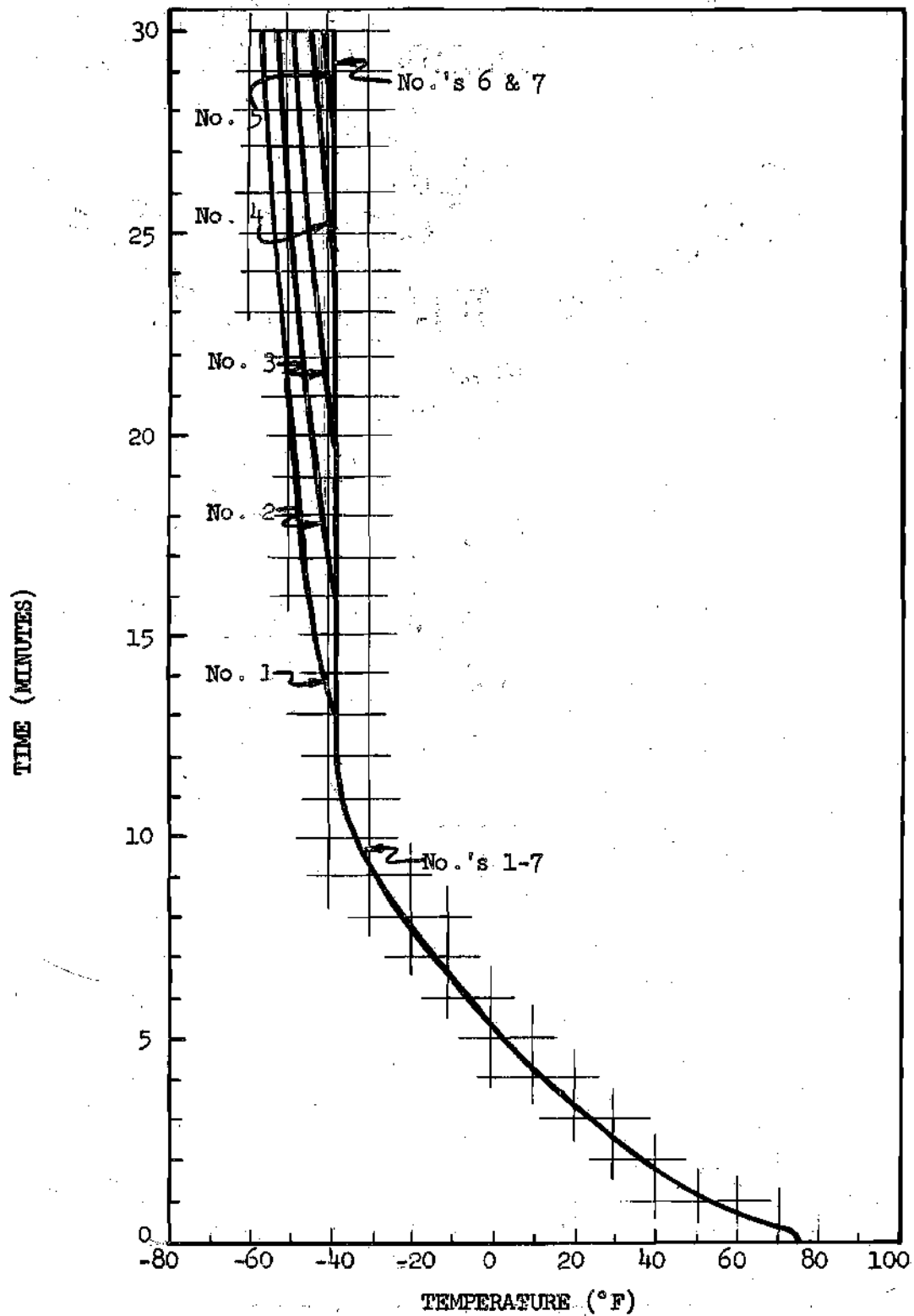


Figure 30. Experimental Temperature Profile.  
Solidification of Mercury at 75°F.



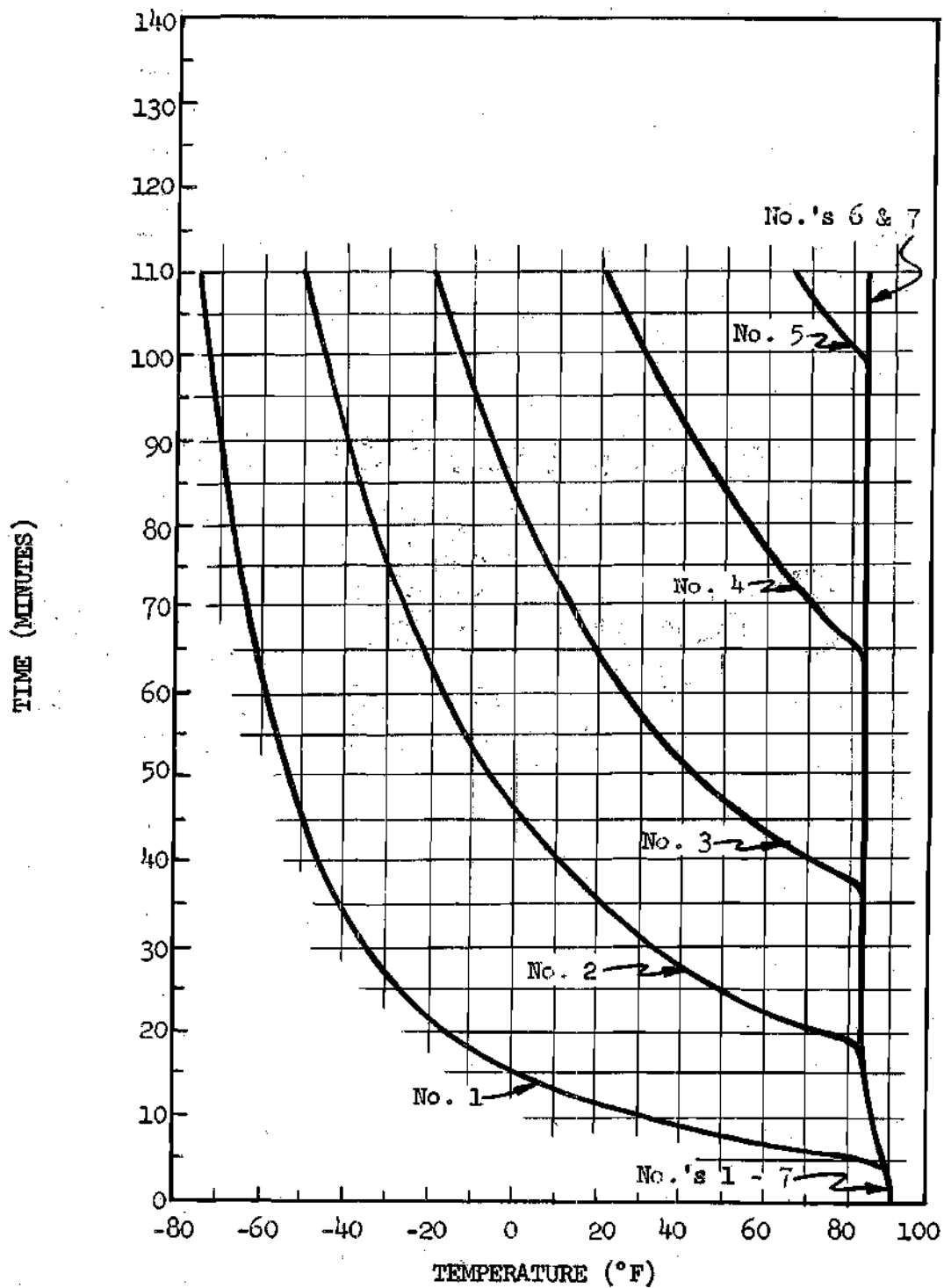


Figure 31. Experimental Temperature Profile.  
Solidification of N-Octadecane at 90°F.

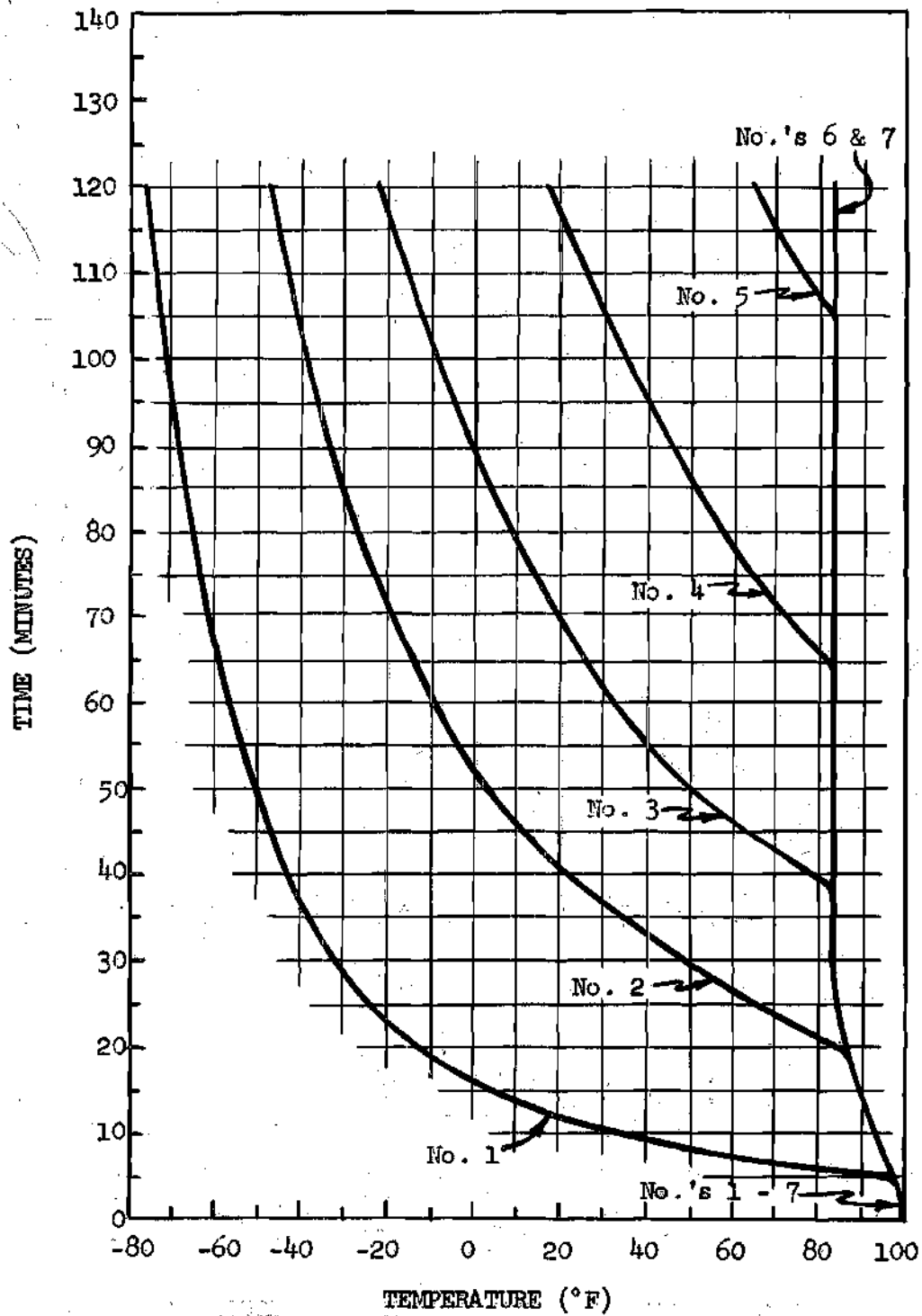


Figure 32. Experimental Temperature Profile.  
Solidification of N-Octadecane at 100°F.

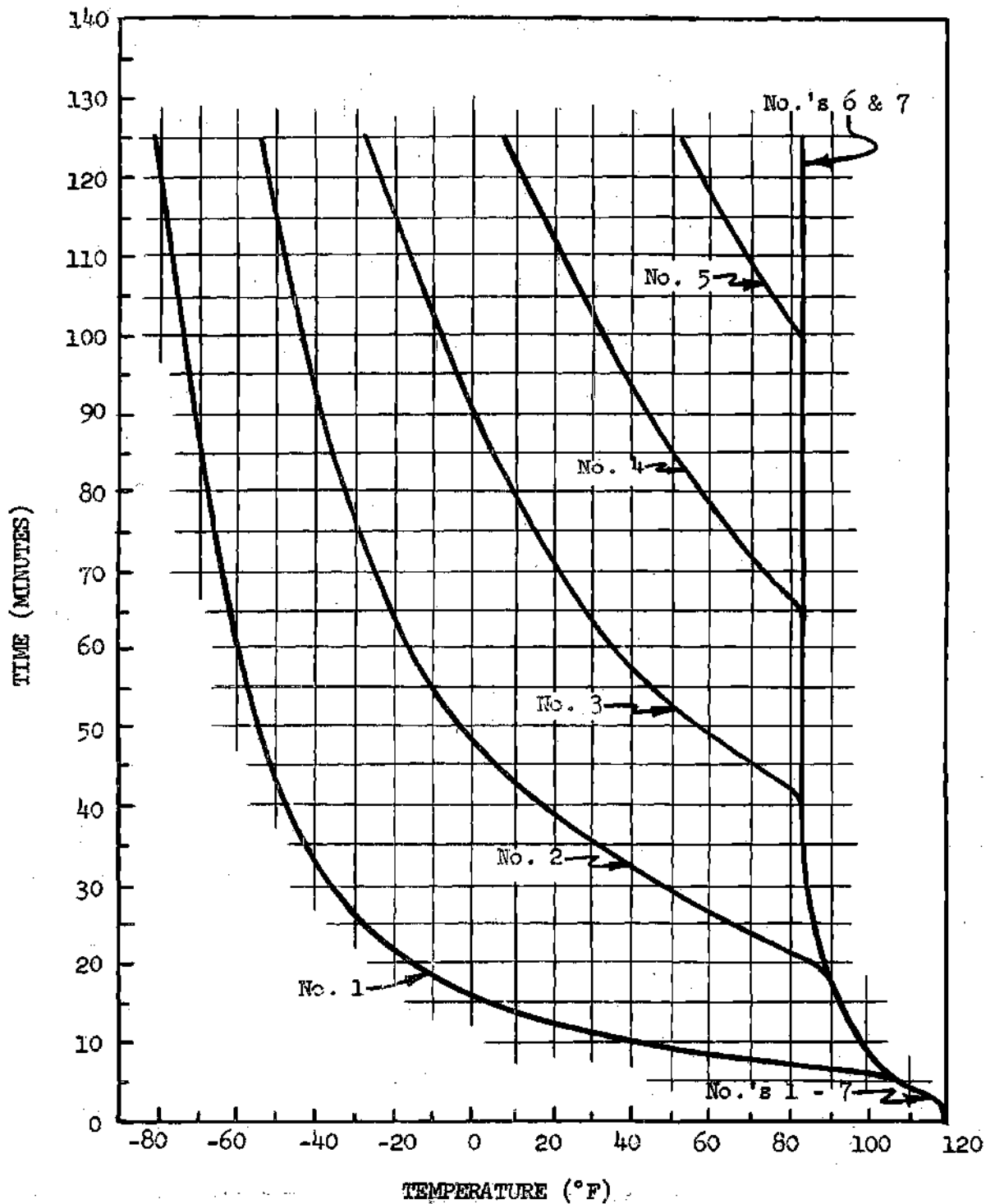


Figure 33. Experimental Temperature Profile.  
Solidification of N-Octadecane at 120°F.

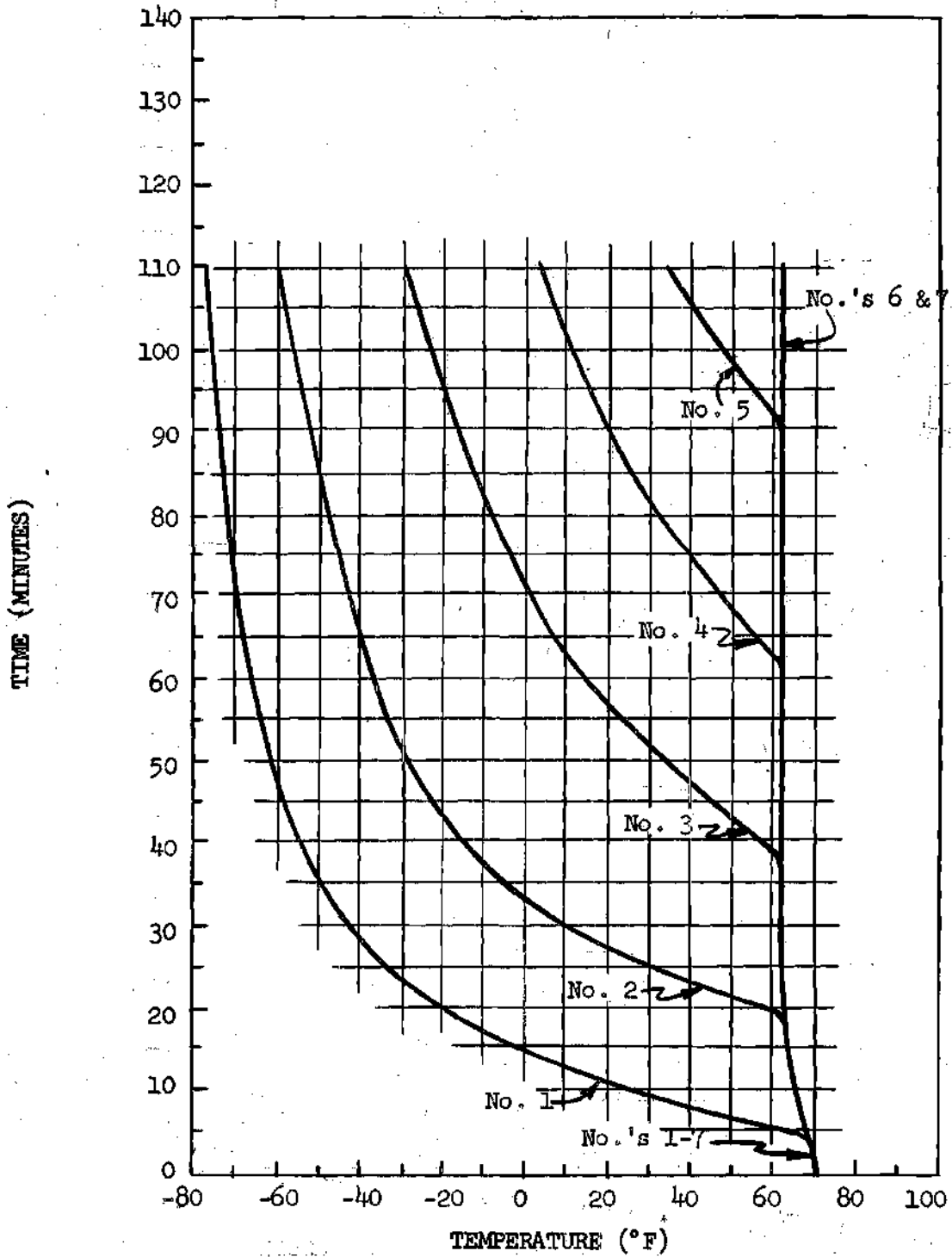


Figure 34. Experimental Temperature Profile.  
Solidification of N-Hexadecane at 70°F.

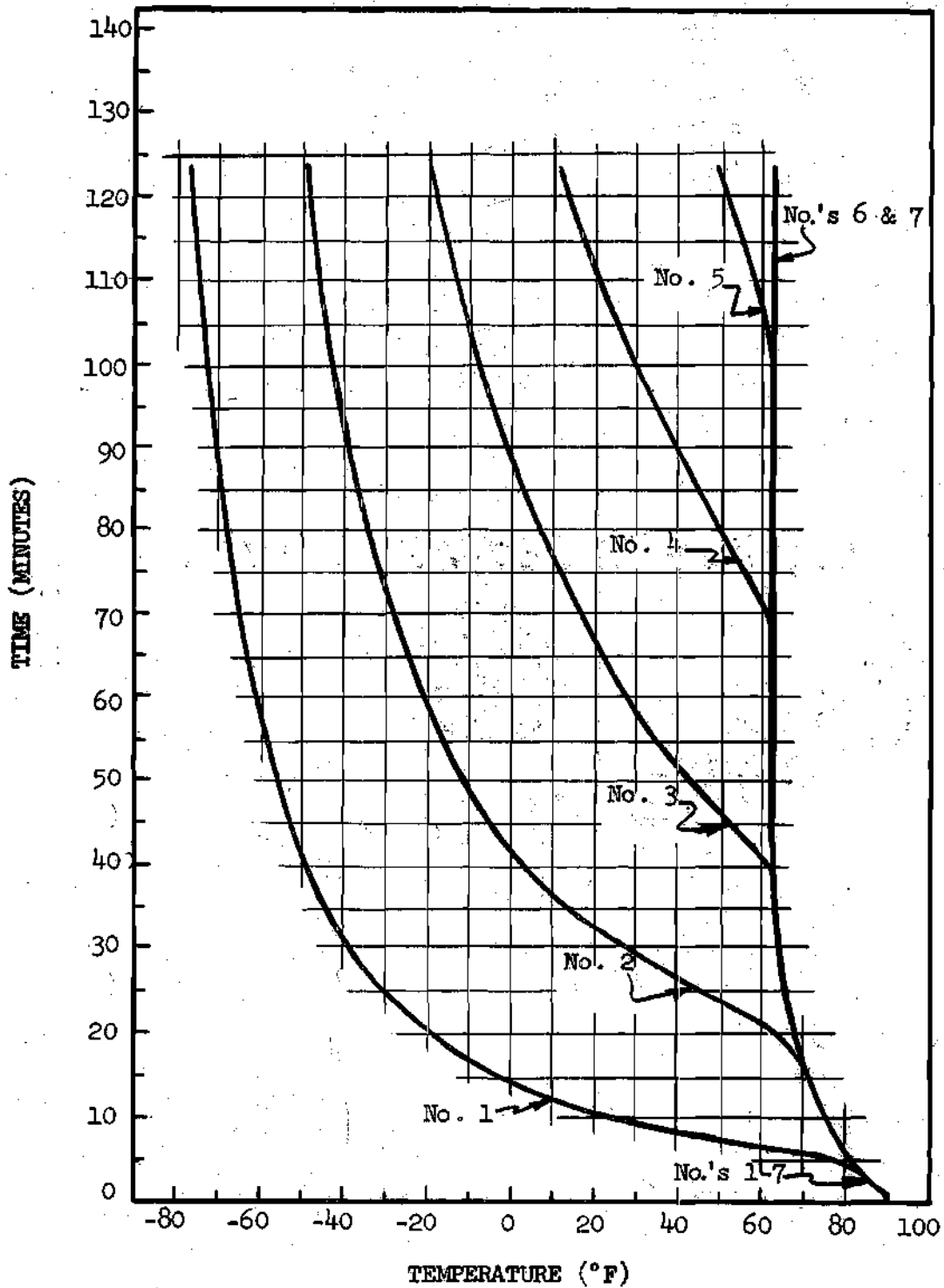


Figure 35. Experimental Temperature Profile.  
Solidification of N-Hexadecane at 90°F.

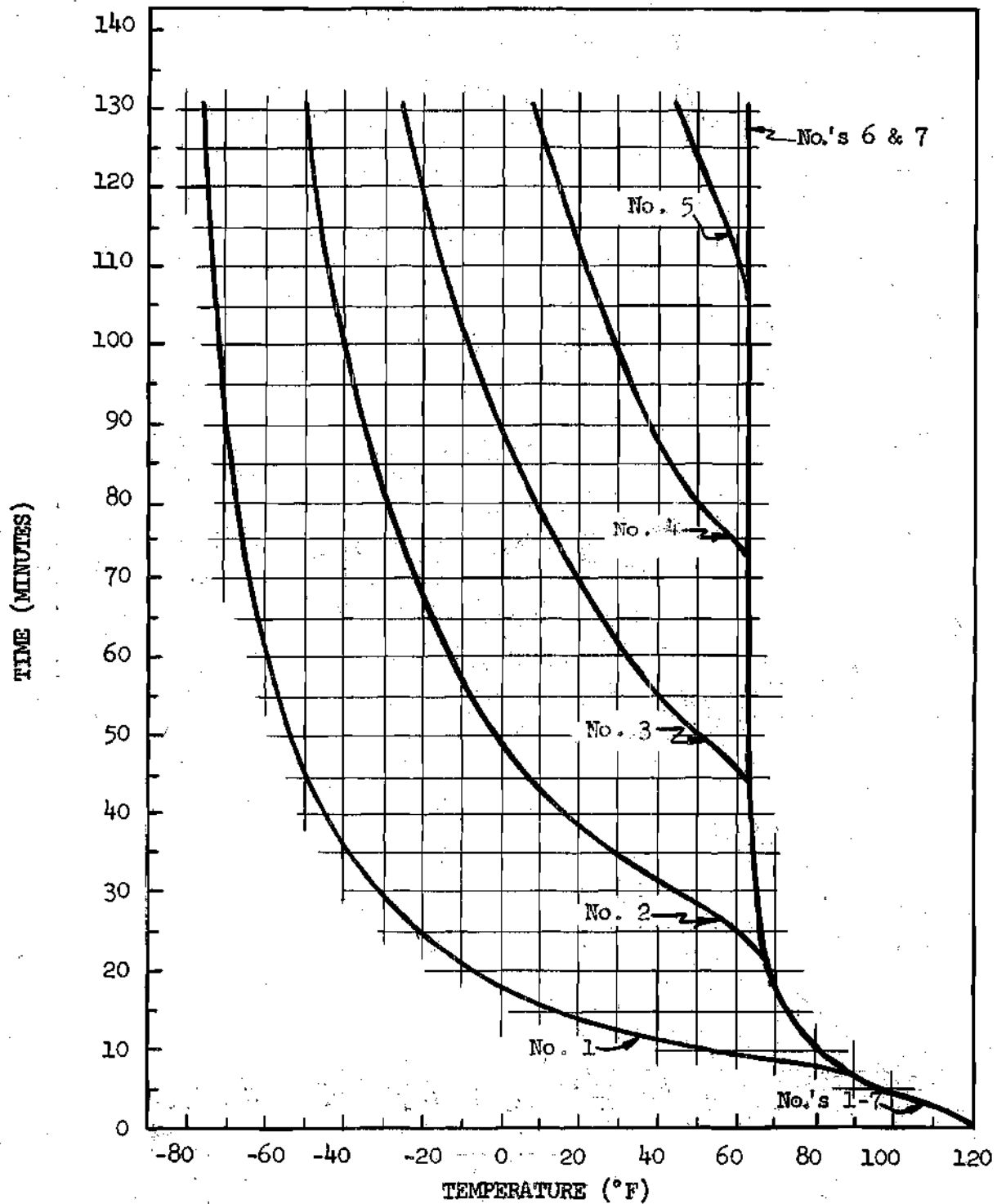


Figure 36. Experimental Temperature Profile.  
Solidification of N-Hexadecane at 120°F.

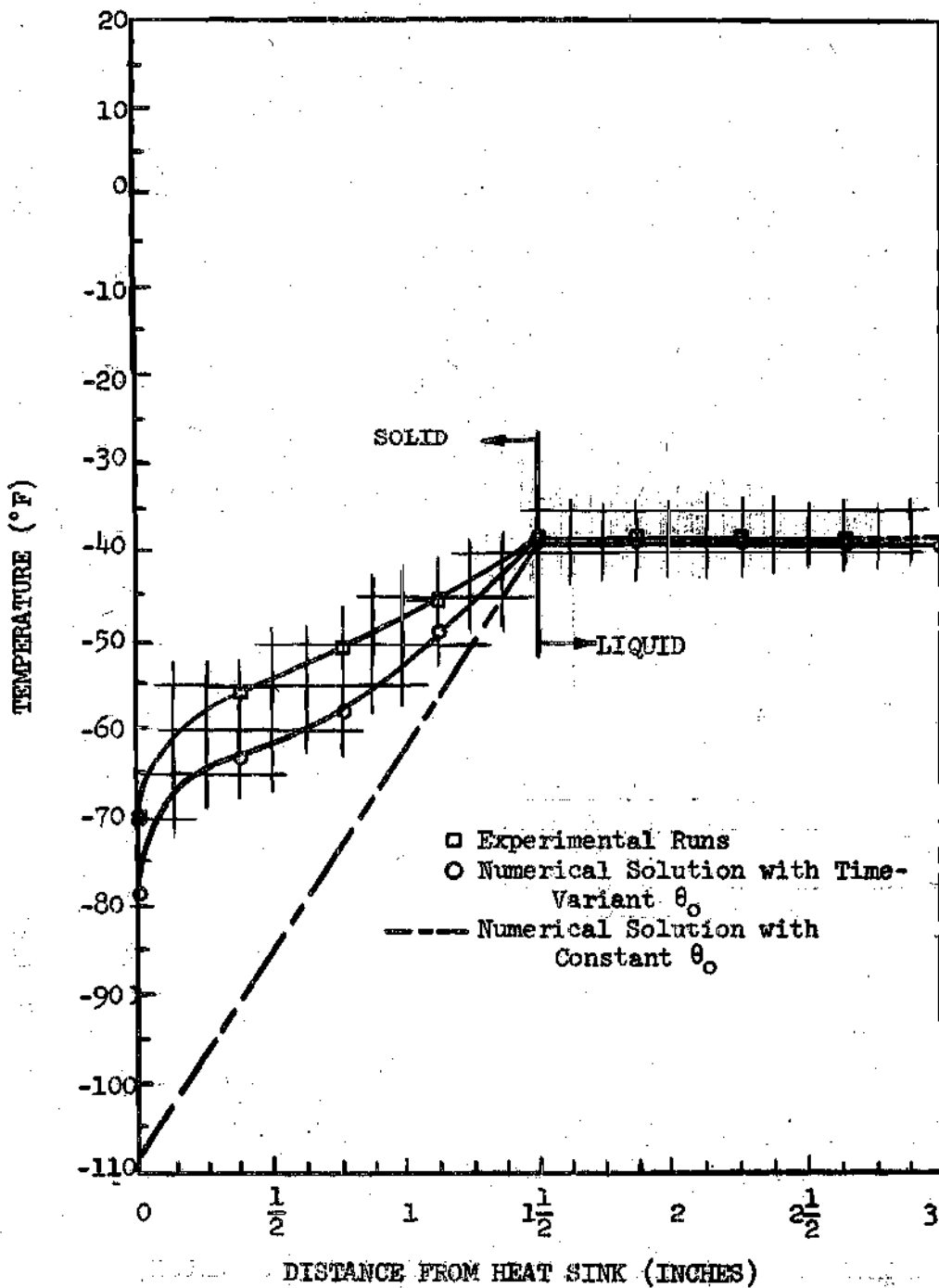


Figure 37. Temperature Distribution at  $D = 1\frac{1}{2}$  inches. Solidification of Mercury at  $75^\circ\text{F}$ .

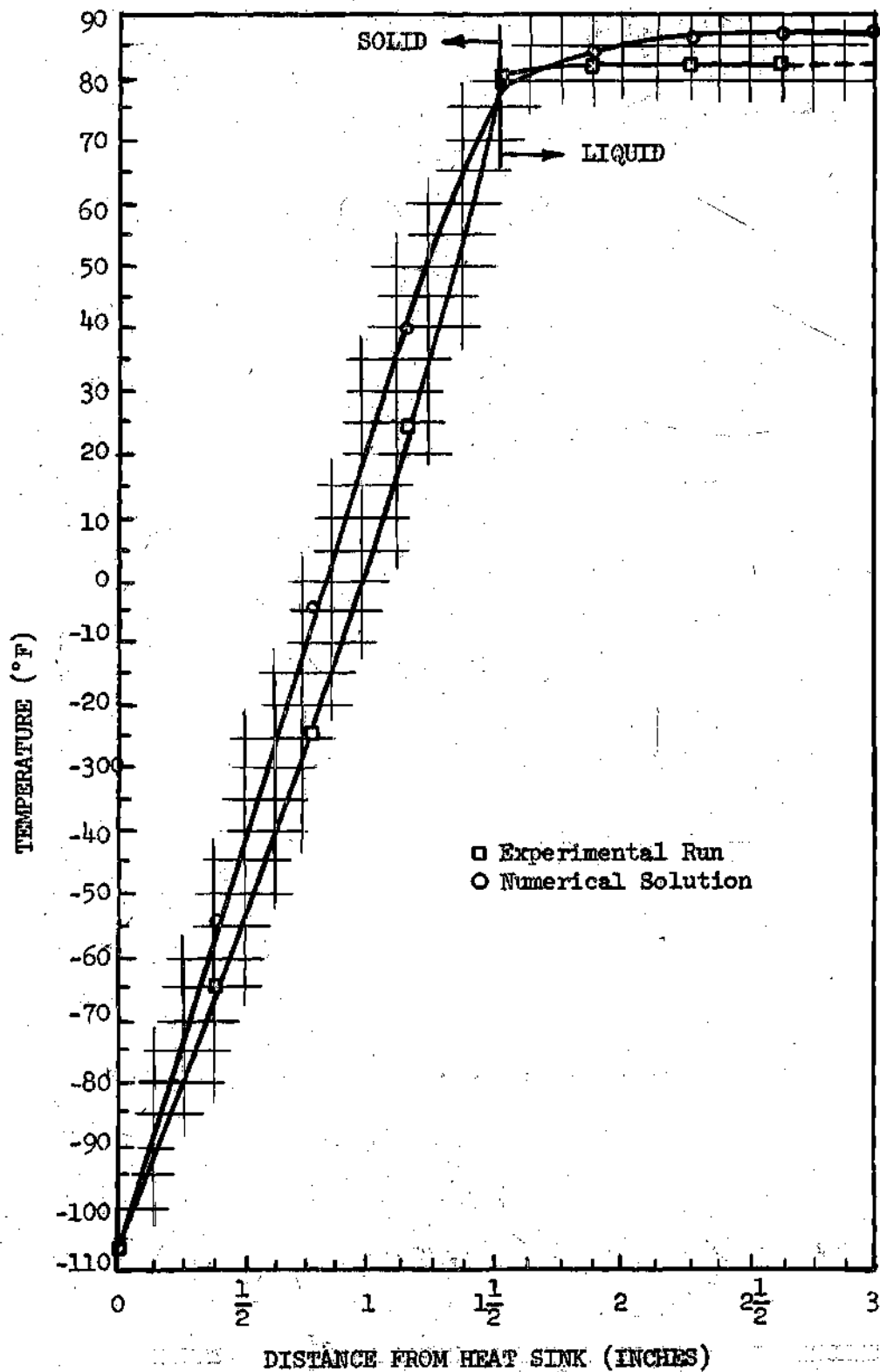


Figure 38. Temperature Distribution at  $D = 1\frac{1}{2}$  inches. Solidification of N-Octadecane at  $120^{\circ}\text{F}$ .



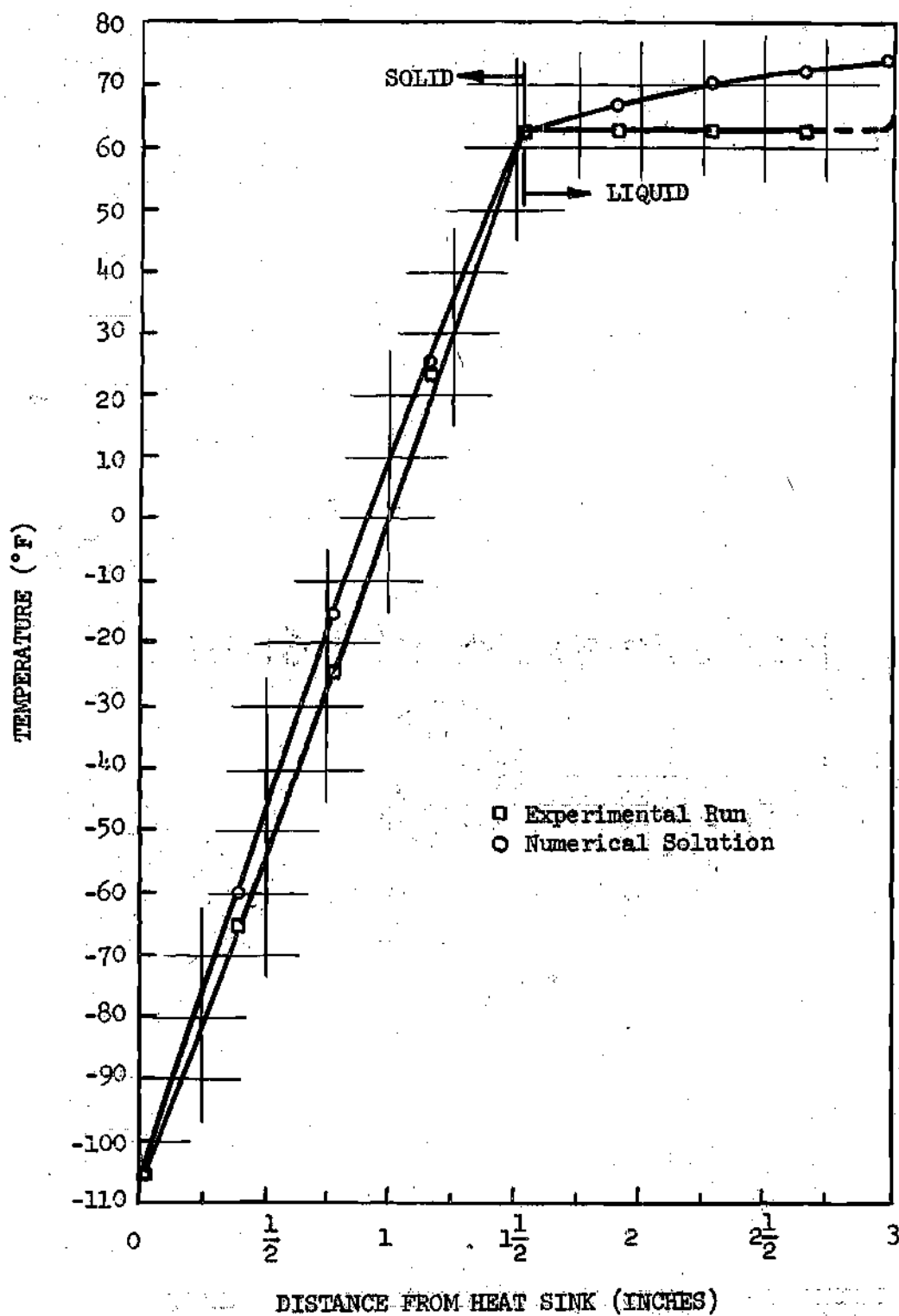


Figure 39. Temperature Distribution at  $D = 1\frac{1}{2}$  inches. Solidification of N-Hexadecane at  $120^{\circ}\text{F}$ .

## CHAPTER VI

## CONCLUSIONS AND RECOMMENDATIONS

From this study of the ultrasonic pulse-echo technique as a means of detecting the motion of the solidification front, the following conclusions may be drawn:

1. The unidirectional motion and the profile configuration of the solidification front can be accurately determined for mercury, n-octadecane and n-hexadecane paraffins by use of the ultrasonic pulse-echo technique.

2. Changes in the temperature of the medium through which sound waves are traveling must be taken into consideration if accurate readings are to be obtained.

3. The tangent plane to the solid-liquid interface at the point of reflection must be nearly perpendicular to the incoming ultrasonic signal, otherwise the reflected sound waves will not be received by the transducer.

4. A low frequency ultrasound is recommended for maximum intensity of the transmitted signal through the medium.

5. The ultrasonic energy, when applied in a non-continuous fashion as in this investigation does not noticeably affect the solidification process, the motion of the freezing front being a function of the physical and thermal properties of the system only.

6. The ultrasonic pulse-echo technique as applied in this work would appear to provide an external means of studying solidification rates

of metals and non-metals without greatly interfering with the solidification process.

The following items are recommended as a logical extension of the work which has been presented in this thesis:

1. A study should follow using pure metals and metal alloys as the solidifying material in one-dimensional and two-dimensional configurations.

2. Methods to use transducers at temperatures higher than their present operating ranges should be studied and developed for use with pure metals and metal alloys having a high freezing temperature.

## APPENDIX A

## SOLIDIFICATION RATE DATA

Table 1. Solidification Rate Data  
for Mercury at 75°F (Run No. 1)

Time Minutes	Ultrasonoscope Readings Inches	Corrected Solid Thickness Inches	Heat Sink Temperature °F
0.00	3 1/16	0	-102
10.00	3	0	-110
13.25	2 9/16	7/16	-110
14.25	2 15/32	17/32	-109
16.50	2 4/16	12/16	-109
19.00	2	1	-109
20.00	1 15/16	1 1/16	-109
21.50	1 13/16	1 3/16	-108
23.50	1 9/16	1 7/16	-109
24.50	1 8/16	1 8/16	-109
25.50	1 7/16	1 9/16	-109
27.50	1 5/16	1 11/16	-109
28.25	1 4/16	1 12/16	-109
30.00	1 3/32	1 29/32	-109
31.00	1	2	-109

Table 2. Solidification Rate Data  
for Mercury at 75° (Run No. 2)

Time Minutes	Ultrasonoscope Readings Inches	Corrected Solid Thickness Inches	Heat Sink Temperature °F
0.00	3 1/16	0	-105
10.00	2 31/32	1/32	-109
11.00	2 12/16	4/16	-109
12.00	2 10/16	6/16	-109
13.00	2 8/16	8/16	-110
17.00	2 2/16	14/16	-109
20.00	1 13/16	1 3/16	-109
21.50	1 21/32	1 11/32	-109
24.50	1 6/16	1 10/16	-108
26.00	1 4/16	1 12/16	-109
26.75	1 3/16	1 13/16	-109
27.75	1 2/16	1 14/16	-109
29.75	1	2	-109

Table 3. Solidification Rate Data  
for N-Hexadecane at 70°F.

Time Minutes	Ultrasonoscope Readings Inches	Corrected Solid Thickness Inches	Heat Sink Temperature °F
0.0	3 1/32	0	-104
1.5	2 14/16	2/16	-105
4.0	2 12/16	4/16	-106
6.0	2 10/16	6/16	-107
8.5	2 9/16	7/16	-107
15.0	2 5/16	11/16	-107
20.0	2 4/16	12/16	-108
24.0	2 3/16	13/16	-108
28.0	2 2/16	14/16	-109
40.0	1 14/16	1 2/16	-108
49.0	1 12/16	1 4/16	-108
54.0	1 10/16	1 6/16	-108
61.0	1 9/16	1 7/16	-109
66.0	1 8/16	1 8/16	-108
71.0	1 7/16	1 9/16	-107
78.0	1 6/16	1 10/16	-108
86.0	1 4/16	1 12/16	-109
92.0	1 3/16	1 13/16	-109
97.0	1 2/16	1 14/16	-109
103.0	1 1/16	1 15/16	-109
110.0	1	2	-109

Table 4. Solidification Rate Data  
for N-Hexadecane at 90°F.

Time Minutes	Ultrasonoscope Reading Inches	Corrected Solid Thickness Inches	Heat Sink Temperature °F
0.0	3 2/16	0	-102
2.0	2 14/16	3/16	-104
5.0	2 12/16	5/16	-106
8.0	2 10/16	7/16	-107
15.0	2 7/16	9/16	-107
20.0	2 5/16	11/16	-107
26.0	2 2/16	14/16	-108
33.0	2	1	-108
40.0	1 15/16	1 1/16	-108
44.0	1 14/16	1 2/16	-108
49.0	1 13/16	1 3/16	-108
52.5	1 12/16	1 4/16	-108
60.0	1 10/16	1 6/16	-108
66.5	1 9/16	1 7/16	-108
71.0	1 8/16	1 8/16	-108
78.0	1 7/16	1 9/16	-108
92.0	1 5/16	1 11/16	-107
96.5	1 4/16	1 12/16	-108
105.0	1 3/16	1 13/16	-108
109.0	1 2/16	1 14/16	-107
116.5	1 1/16	1 15/16	-108
124.0	1	2	-108

Table 5. Solidification Rate Data  
for N-Hexadecane at 120°F.

Time Minutes	Ultrasonoscope Readings Inches	Corrected Solid Thickness Inches	Heat Sink Temperature °F
0.0	3 5/16	0	-100
2.0	3 2/16	1/16	-102
4.0	3	2/16	-104
6.5	2 15/16	9/32	-105
12.0	2 11/16	7/16	-106
15.5	2 15/32	9/16	-106
20.0	2 13/32	10/16	-106
24.0	2 4/16	12/16	-106
31.0	2 3/16	13/16	-104
36.5	2 1/16	15/16	-104
42.0	2		-106
49.0	1 14/16	1 2/16	-108
53.0	1 13/16	1 3/16	-108
57.0	1 12/16	1 4/16	-108
68.0	1 10/16	1 6/16	-108
72.0	1 9/16	1 7/16	-108
77.0	1 8/16	1 8/16	-108
83.0	1 7/16	1 9/16	-109
90.0	1 6/16	1 10/16	-108
95.0	1 5/16	1 11/16	-108
104.0	1 3/16	1 13/16	-108
114.0	1 2/16	1 14/16	-109
120.0	1 1/16	1 15/16	-109
131.0	1	2	-109



Table 6. Solidification Rate Data  
for N-Octadecane at 90°F.

Time Minutes	Ultrasonoscope Readings Inches	Corrected Solid Thickness Inches	Heat Sink Temperature °F
0.0	3 1/32	0	-104
2.5	2 29/32	2/16	-105
4.0	2 27/32	3/16	-106
9.5	2 19/32	7/16	-109
12.0	2 8/16	8/16	-109
15.5	2 6/16	10/16	-109
20.5	2 4/16	12/16	-110
24.0	2 3/16	13/16	-110
27.5	2 2/16	14/16	-110
39.5	1 14/16	1 2/16	-110
47.0	1 13/16	1 3/16	-110
53.0	1 11/16	1 5/16	-110
58.5	1 10/16	1 6/16	-110
65.0	1 8/16	1 8/16	-109
74.0	1 6/16	1 10/16	-109
85.5	1 4/16	1 12/16	-110
97.5	1 2/16	1 14/16	-110
101.5	1 1/16	1 15/16	-110
110.0	1	2	-110

Table 7. Solidification Rate Data  
for N-Octadecane at 100°F.

Time Minutes	Ultrasonoscope Readings Inches	Corrected Solid Thickness Inches	Heat Sink Temperature °F
0.00	3 3/32	0	-104
1.00	2 31/32	3/32	-107
2.25	2 27/32	7/32	-108
4.00	2 25/32	9/32	-108
6.00	2 11/16	12/32	-109
8.00	2 19/32	7/16	-109
12.00	2 15/32	17/32	-109
16.00	2 11/32	21/32	-109
21.00	2 7/32	25/32	-109
27.00	2 3/32	29/32	-109
35.00	1 31/32	1 1/32	-109
41.50	1 27/32	1 5/32	-109
47.00	1 25/32	1 7/32	-109
52.00	1 11/16	1 5/16	-109
59.00	1 19/32	1 13/32	-109
69.50	1 15/32	1 17/32	-109
77.00	1 13/32	1 19/32	-109
83.50	1 11/32	1 21/32	-109
95.00	1 7/32	1 25/32	-109
108.50	1 3/32	1 29/32	-109
117.00	1 1/32	1 31/32	-109
120.00	1	2	-109

Table 8. Solidification Rate Data  
for N-Octadecane at 120°F.

Time Minutes	Ultrasonoscope Readings Inches	Corrected Solid Thickness Inches	Heat Sink Temperature °F
0.0	3 3/16	0	-104
3.5	2 14/16	4/16	-106
5.5	2 25/32	5/16	-108
10.0	2 10/16	7/16	-108
13.0	2 9/16	8/16	-109
20.0	2 13/32	10/16	-109
23.0	2 5/16	11/16	-109
32.0	2 3/32	29/32	-109
38.0	2 1/32	31/32	-109
44.0	1 29/32	1 3/32	-109
53.0	1 12/16	1 4/16	-109
60.0	1 21/32	1 11/32	-109
64.0	1 9/16	1 7/16	-109
74.0	1 8/16	1 8/16	-109
82.5	1 6/16	1 10/16	-109
91.0	1 5/16	1 11/16	-109
96.0	1 4/16	1 12/16	-109
104.0	1 5/32	1 27/32	-109
107.0	1 2/16	1 14/16	-109
116.0	1 1/16	1 15/16	-109
122.0	1	2	-109

## APPENDIX B

## SOLIDIFICATION FRONT PROFILE DATA

Table 9. Solidification Front Profile Data  
for Mercury at 75°F.

Time Minutes	Corrected Solid Thickness for Transducer Positions 1 through 5				
	Inches				
	1	2	3	4	5
10.00	0	0	0	0	0
13.25	7/16	6/16	5/16	3/16	1/16
16.50	12/16	23/32	21/32	8/16	7/16
19.00	1	1	14/16	13/16	11/16
21.50	1 3/16	1 3/16	1 2/16	1 1/16	1
24.50	1 8/16	1 8/16	1 7/16	1 1/16	1 5/16
27.50	1 11/16	1 21/32	1 10/16	1 10/16	1 9/16
31.00	2	2	1 15/16	1 29/32	1 27/32

Table 10. Solidification Front Profile Data  
for N-Hexadecane at 70°F.

Corrected Solid Thickness for Transducer Positions 1 through 5					
Time Minutes	Inches				
	1	2	3	4	5
1.50	2/16	2/16	2/16	2/16	2/16
4.00	4/16	4/16	4/16	4/16	4/16
8.50	7/16	7/16	7/16	7/16	7/16
110.00	2	2	2	2	2

Table 11. Solidification Front Profile Data  
for N-Hexadecane at 90°F.

Time Minutes	Corrected Solid Thickness for Transducer Positions 1 through 5				
	Inches				
	1	2	3	4	5
2.00	3/16	3/16	5/32	5/32	2/16
5.00	5/16	5/16	9/32	4/16	7/32
8.00	7/16	13/32	6/16	11/32	9/32
15.00	9/16	9/16	8/16	15/32	7/16
26.00	14/16	27/32	25/32	12/16	11/16
33.00	1	31/32	15/16	14/16	13/16
53.50	1 9/32	1 4/16	1 7/32	1 5/32	1 3/32
71.00	1 8/16	1 8/16	1 15/32	1 7/16	1 6/16
99.00	1 25/32	1 25/32	1 12/16	1 23/32	1 23/32
124.00	2	2	2	2	2

Table 12. Solidification Front Profile Data  
for N-Hexadecane at 120°F.

Time Minutes	Corrected Solid Thickness for Transducer Positions 1 through 5				
	Inches				
	1	2	3	4	5
2.00	1/16	1/16	1/16	1/32	1/32
4.00	5/32	5/32	3/32	3/32	1/16
6.50	9/32	4/16	3/16	5/32	3/32
15.50	10/16	19/32	17/32	15/32	6/16
24.00	12/16	23/32	21/32	10/16	9/16
36.50	15/16	15/16	29/32	14/16	13/16
57.00	1 4/16	1 4/16	1 7/32	1 3/16	1 5/32
83.00	1 9/16	1 9/16	1 17/32	1 17/32	1 8/16
114.00	1 14/16	1 14/16	1 14/16	1 14/16	1 14/16
131.00	2	2	2	2	2

Table 13. Solidification Front Profile Data for  
N-Octadecane at 90°F.

Time Minutes	Corrected Solid Thickness for Transducer Positions 1 through 5				
	1	2	3	4	5
2.50	2/16	2/16	2/16	3/32	3/32
4.00	3/16	3/16	5/32	5/32	2/16
9.50	7/16	7/16	13/32	13/32	6/16
15.50	10/16	10/16	10/16	10/16	10/16
24.00	13/16	13/16	13/16	13/16	13/16
110.00	2	2	2	2	2



Table 14. Solidification Front Profile Data  
for N-Octadecane at 100°F.

Time Minutes	Corrected Solid Thickness for Transducer Positions 1 through 5				
	Inches				
	1	2	3	4	5
2:25	7/32	7/32	7/32	7/32	7/32
8.00	7/16	7/16	7/16	13/32	13/32
12.00	17/32	17/32	17/32	33/64	8/16
16.00	21/32	21/32	21/32	10/16	19/32
31.50	31/32	31/32	31/32	15/16	15/16
47.00	1 7/32	1 7/32	1 7/32	1 7/32	1 7/32
65.00	1 15/32	1 15/32	1 15/32	1 15/32	1 15/32
83.50	1 21/32	1 21/32	1 21/32	1 21/32	1 21/32
103.00	1 27/32	1 27/32	1 27/32	1 27/32	1 27/32
120.00	2	2	2	2	2

Table 15. Solidification Front Profile Data  
for N-Octadecane at 120°F.

Time Minutes	Corrected Solid Thickness for Transducer Positions 1 through 5				
	1	2	3	4	5
3.50	4/16	4/16	7/32	13/64	3/16
10.00	7/16	13/32	11/32	5/16	9/32
20.00	10/16	19/32	9/16	17/32	8/16
23.00	11/16	21/32	10/16	19/32	9/16
38.00	31/32	31/32	61/64	15/16	29/32
53.00	1 4/16	1 4/16	1 7/32	1 3/16	1 5/32
64.00	1 7/16	1 7/16	1 13/32	1 25/64	1 6/16
82.50	1 10/16	1 10/16	1 39/64	1 39/64	1 19/32
104.00	1 5/32	1 5/32	1 5/32	1 5/32	1 5/32
122.00	2	2	2	2	2

## APPENDIX C

## NUMERICAL SOLUTION OF THE SOLIDIFICATION PROBLEM

The solution to the transient heat conduction problem involving melting or freezing proposed by Murray (41) is based on a variable space network technique. A slab of material of total thickness  $E$  is taken and divided into  $N$  increments. The position of the freezing front is denoted by  $\epsilon$ . The solid region ( $x < \epsilon$ ) is divided into  $r$  equal increments of  $\epsilon/r$  thickness, while the liquid region is divided into  $(N - r)$  equal increment of  $(E - \epsilon)/(N - r)$  thickness. Figure 40 shows how the solid phase increments increase in size as the liquid phase increments decrease during the process of solidification.

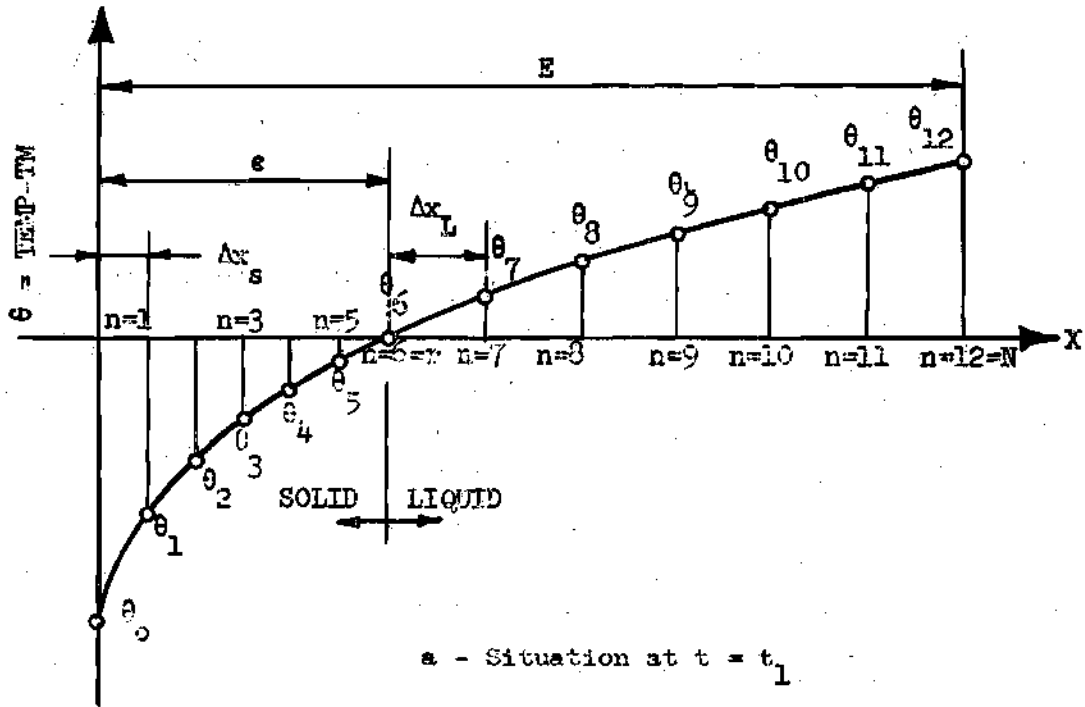
Derivation of Numerical Approximations

The differential equations for one-dimensional heat conduction in the solid and liquid regions respectively of a freezing body are given by:

$$\frac{\partial \theta_s}{\partial t} = \alpha_s \frac{\partial^2 \theta_s}{\partial x^2} \quad (1a)$$

and

$$\frac{\partial \theta_L}{\partial t} = \alpha_L \frac{\partial^2 \theta_L}{\partial x^2} \quad (1b)$$



$$\Delta x_s = \frac{e}{r}$$

$$\Delta x_L = \frac{E - e}{N - r}$$

$$N = 2r = 12$$

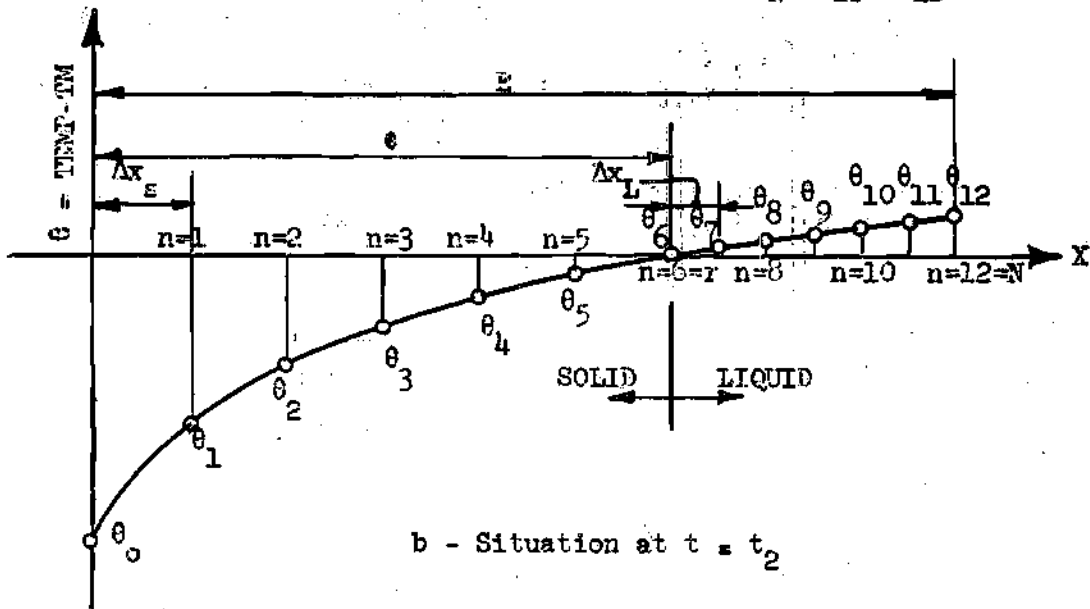


Figure 40. Description of Variables.

The motion of the freezing front in terms of the temperature gradients and thermal properties of the liquid and solid phases is given by the expression:

$$\frac{d\epsilon}{dt} = \frac{1}{\rho L} \left\{ k_s \left. \frac{\partial \theta}{\partial x} \right|_{x=\epsilon} - k_L \left. \frac{\partial \theta}{\partial x} \right|_{x=\epsilon} \right\} \quad (2)$$

The effect of variation of density with temperature is neglected. Thermal properties  $k$  and  $\alpha$ , however, are given for both the solid and liquid phases.

The numerical approximation for  $\left. \frac{\partial \theta}{\partial x} \right|_{x=\epsilon}$  can be represented in several ways. Murray shows that the most accurate expression is given by:

$$\left. \frac{\partial \theta}{\partial x} \right|_{x=\epsilon} = \frac{\theta_{r-2} - 4\theta_{r-1}}{2\Delta x_s} \quad (3a)$$

and

$$\left. \frac{\partial \theta}{\partial x} \right|_{x=\epsilon} = \frac{\theta_{r+2} - 4\theta_{r+1}}{2\Delta x_L} \quad (3b)$$

Also

$$\frac{d\epsilon}{dt} = \frac{\epsilon_{m+1} - \epsilon_m}{\Delta t} \quad (4)$$

Substitution of equations (3) and (4) into equation (2) yields an algebraic expression, applicable to the digital computer, which defines the motion of the freezing front:

$$\frac{\epsilon_{m+1} - \epsilon_m}{\Delta t} = \frac{1}{\rho L} \left\{ k_s \frac{(\theta_{r-2} - \theta_{r-1})}{2\Delta x_s} + k_L \frac{(\theta_{r+2} - \theta_{r+1})}{2\Delta x_L} \right\} \quad (5)$$

The following derivation of the temperature distribution will be restricted to the solid region. The same equations will apply to the liquid region by just changing the pertaining parameters. The derivative with respect to space,  $\partial^2\theta/\partial x^2$ , can be represented by a finite difference approximation as:

$$\frac{\partial^2\theta}{\partial x^2} \approx \frac{\theta_{n+1} - 2\theta_n + \theta_{n-1}}{\Delta x^2} \quad (6a)$$

Similarly:

$$\frac{\partial\theta}{\partial x} \approx \frac{\theta_{n+1} - \theta_{n-1}}{2\Delta x} \quad (6b)$$

Since temperatures are to be described at moving points, the substantial temperature-time derivative must be used to represent the rate of change of temperature. In the solid region the temperature at each point  $x = x_n(t)$ , as described by the substantial derivative is:

$$\frac{d\theta}{dt} = \frac{\partial\theta}{\partial x} \bigg|_t \frac{dx}{dt} \bigg|_{x=x_n} + \frac{\partial\theta}{\partial t} \bigg|_x \quad (7a)$$

$$= \frac{x_n}{\epsilon} \frac{\partial\theta}{\partial x} \bigg|_t \frac{d\epsilon}{dt} + \alpha_s \frac{\partial^2\theta}{\partial x^2} \bigg|_t \quad (7b)$$

since  $dx_n/dt = d\epsilon/\epsilon$  for equally spaced lumps. Substitution of equations

(6a) and (6b) into (7b) yields:

$$\frac{d\theta}{dt} = \frac{n\Delta x_s}{\epsilon} \frac{(\theta_{n+1} - \theta_{n-1})}{2\Delta x_s} \frac{d\epsilon}{dt} + \alpha_s \frac{(\theta_{n+1} - 2\theta_n + \theta_{n-1})}{\Delta x_s^2} \quad (8)$$

since  $x_n = n\Delta x_s$

Also, by further approximations:

$$\frac{d\theta}{dt} \approx \frac{\theta_{n,m+1} - \theta_{n,m}}{\Delta t} \quad (9)$$

where the subscript  $n$  represents a specific location in the material, and the subscript  $m$  represents the corresponding time interval. Substitution of equations (4) and (9) into equation (8) yields an algebraic temperature distribution equation which is applicable for digital computation:

$$\begin{aligned} \frac{\theta_{n,m+1} - \theta_{n,m}}{\Delta t} = & \frac{n\Delta x_s}{\epsilon} \left( \frac{\theta_{n+1,m} - \theta_{n-1,m}}{2\Delta x_s} \right) \left( \frac{\epsilon_{m+1} - \epsilon_m}{\Delta t} \right) \\ & + \alpha_s \left( \frac{\theta_{n+1,m} - 2\theta_{n,m} + \theta_{n-1,m}}{\Delta x_s^2} \right) \end{aligned} \quad (10a)$$

Similarly for the liquid region:

$$\begin{aligned} \frac{\theta_{n,m+1} - \theta_{n,m}}{\Delta t} = & \frac{(N-n)\Delta x_L}{(E-\epsilon)} \left( \frac{\theta_{n+1,m} - \theta_{n-1,m}}{2\Delta x_L} \right) \left( \frac{\epsilon_{m+1} - \epsilon_m}{\Delta t} \right) \\ & + \alpha_L \left( \frac{\theta_{n+1,m} - 2\theta_{n,m} + \theta_{n-1,m}}{\Delta x_L^2} \right) \end{aligned} \quad (10b)$$

In this work a system of  $N = 2r = 12$  network intervals is used. For this case and after some algebraic manipulation equations (10) reduce to:

$$\theta_{n,m+1} = \theta_{n,m} + \frac{36\alpha_s \Delta t}{\epsilon_m^2} \left\{ \frac{n\epsilon_m}{72\alpha_s} (\theta_{n+1,m} - \theta_{n-1,m}) \left( \frac{\epsilon_{m+1} - \epsilon_m}{\Delta t} \right) + \theta_{n+1,m} - 2\theta_n + \theta_{n-1,m} \right\}, \quad n = 1, 2, 3, 4, 5 \quad (11)$$

$$\theta_{n,m+1} = \theta_{n,m} + \frac{36\alpha_s \Delta t}{(E - \epsilon_m)^2} \left\{ \frac{(N-n)(E - \epsilon_m)}{72\alpha_L} (\theta_{n+1,m} - \theta_{n-1,m}) \left( \frac{\epsilon_{m+1} - \epsilon_m}{\Delta t} \right) + \theta_{n+1,m} - 2\theta_{n,m} + \theta_{n-1,m} \right\}, \quad n = 7, 8, 9, 10, 11 \quad (12)$$

where  $\theta_6 = \theta_{\text{fusion}} = 0$

and  $\theta_{13} = \theta_{11}$  by symmetry.

For the motion of the fusion front:

$$\epsilon_{m+1} = \epsilon_m + \frac{3\Delta t}{\rho L} \left\{ k_s \frac{\theta_4 - 4\theta_5}{\epsilon_m} + k_L \frac{\theta_8 - 4\theta_7}{E - \epsilon_m} \right\} \quad (13)$$

#### Boundary Conditions

In addition to the equations for the interior region and for the motion of the freezing front, two conditions at the boundaries of the mold must be prescribed. For n-octadecane and n-hexadecane the boundary condition at  $x = 0$  is given by:



$$\theta_{o,t} = \theta_o \quad (\text{constant for } t > 0)$$

where  $\theta_o$  represents the equilibrium temperature of the acetone and dry ice mixture. For mercury, however, the temperature at the solid-mold interface is always higher than the heat sink temperature as discussed in Chapter V. The boundary condition at  $x = 0$  in this case must be determined by consideration of the heat flux across the glass panel separating the heat sink and mold area:

$$QO = \frac{TS - \theta_o}{\frac{\Delta x_g}{k_g}} \quad (14a)$$

$$= UO(TS - \theta_o) \quad (14b)$$

By a numerical approximation:

$$\frac{d\theta_o}{dt} = \frac{\theta_{o,m+1} - \theta_{o,m}}{\Delta t} \quad (15a)$$

$$= \frac{2\alpha_s}{\Delta x_s} \left\{ \frac{\theta_{1,m} - \theta_{o,m}}{\Delta x_s} + \frac{QO}{k_s} \right\} \quad (15b)$$

Substitution of equation (14b) into equation (15b) yields an expression for  $\theta_o$ :

$$\theta_{o,m+1} = \theta_{o,m} + \frac{12\alpha_s \Delta t}{\epsilon_m} \left\{ \frac{6(\theta_{1,m} - \theta_{o,m})}{\epsilon_m} + \frac{UO}{k_s}(TS - \theta_o) \right\} \quad (16)$$

The boundary condition at  $x = E$  ( $\theta_{12}$ ) is similarly determined by consideration of the heat flux across the front glass panel:

$$QN = \frac{\theta_{12,m} - TR}{\frac{\Delta x}{k} + \frac{1}{h}} \quad (17a)$$

$$= UN(\theta_{12,m} - TR) \quad (17b)$$

By a numerical approximation:

$$\frac{d\theta_{12}}{dt} = \frac{\theta_{12,m+1} - \theta_{12,m}}{\Delta t} \quad (18a)$$

$$= \frac{2\alpha_L}{\Delta x_L} \left\{ \frac{\theta_{11,m} - \theta_{12,m}}{\Delta x_L} - \frac{QN}{k_L} \right\} \quad (18b)$$

Substitution of equation (17b) into equation (18b) yields an expression for  $\theta_{12}$ :

$$\theta_{12,m+1} = \theta_{12,m} + \frac{12\alpha_L \Delta t}{(E - \epsilon_m)} \left\{ \frac{6(\theta_{11,m} - \theta_{12,m})}{(E - \epsilon_m)} - \frac{UN}{k_L} (\theta_{12,m} - TR) \right\} \quad (19)$$

#### Initial Conditions

When  $\epsilon = 0$  it is seen that infinite or indeterminate forms result in some terms of the equations. Thus the problem must be started with an assumed value of  $\epsilon_0$ . In the present work  $\epsilon_0$  and the corresponding time increment are selected from the experimental data. The initial value of  $\theta_0$  for mercury can be obtained by a trial and error calculation or by experimental determination of the temperature at the solid-mold interface. For n-octadecane and n-hexadecane  $\theta_0$  is assumed at the heat sink temperature as previously discussed. Initial values of  $\theta_1$  and  $\theta_5$  are

obtained by extrapolation between  $\theta_0$  and  $\theta_6$ , the fusion temperature. Values of  $\theta_7$  through  $\theta_{12}$  represent the temperature excess above the fusion temperature in the liquid region. These values are obtained by referring to the temperature profiles obtained during experimentation, which show in every case that a constant value of  $\theta$  in the liquid phase is an acceptable assumption.

#### Other Information

In the computer solution the numerical value of the time increment,  $\Delta t$ , must be continually varied in order to maintain a required level of stability. Here  $\Delta t$  is determined from the smallest of:

$$\Delta t = \frac{0.2 \epsilon_m^2}{\alpha_s r^2} \quad (20a)$$

or

$$\Delta t = \frac{0.2 (E - \epsilon_m)^2}{\alpha_L (N - r)^2} \quad (20b)$$

Physical constants for mercury were obtained from the Liquid Metals Handbook (42). Physical constants for n-hexadecane and n-octadecane were obtained from references (43), (44) and (45). All constants used in the numerical solution appear in Appendix D. Symbol changes were necessary to transform the solution into program language. A sample of the computer program appears in Appendix E.

The output of the computer included solid thickness, freezing front velocity and temperature distribution across the mold as a function of time. The freezing front velocity is calculated by the expression:

$$v = \frac{e_{m+1} - e_m}{\Delta t} \quad (21)$$

The temperature distribution across the mold is given by the temperatures at both boundaries and at each of the seven thermocouple positions (see Figure 2). Temperatures at each of the thermocouple positions are calculated by interpolation between the temperatures corresponding to the moving points in the variable space network. A sample of the computer output appears in Appendix F.

## APPENDIX D

## NUMERICAL SOLUTION CONSTANTS

Table 16. Numerical Solution Constants  
for Mercury at 75°F.

<u>Constants</u>	<u>Value</u>	<u>Units</u>
F(1)	-27.0	°F
F(2)	-21.0	°F
F(3)	-16.0	°F
F(4)	-12.0	°F
F(5)	- 7.5	°F
F(6)	- 4.0	°F
F(7)	0.0	°F
F(8)	0.0	°F
F(9)	0.0	°F
F(10)	0.0	°F
F(11)	0.0	°F
F(12)	0.0	°F
F(13)	0.0	°F
E	0.242	ft
G	0.0208	ft <sup>2</sup> /sec
PS	$5.30 \times 10^{-5}$	ft <sup>2</sup> /sec
PL	$4.24 \times 10^{-5}$	ft <sup>2</sup> /sec
L	4.9	Btu/lb
QS	$1.50 \times 10^{-3}$	Btu/sec-ft-°F
QL	$1.12 \times 10^{-3}$	Btu/sec-ft-°F
R	856.0	lb/ft <sup>3</sup>
T	660.0	°F
TEMP	75.0	°F
TM	-38.0	°F
TR	113.0	°F
UN	$5.25 \times 10^{-4}$	Btu/sec-ft <sup>2</sup> -°F
TS	-69.0	°F
UO	$1.99 \times 10^{-2}$	Btu/sec-ft <sup>2</sup> -°F

Table 17. Numerical Solution Constants  
for N-Hexadecane at 70°F.

<u>Constants</u>	<u>Value</u>	<u>Units</u>
F(1)	-169.0	°F
F(2)	-130.0	°F
F(3)	-100.0	°F
F(4)	-70.0	°F
F(5)	-45.0	°F
F(6)	-20.0	°F
F(7)	0.0	°F
F(8)	6.0	°F
F(9)	6.0	°F
F(10)	6.0	°F
F(11)	6.0	°F
F(12)	6.0	°F
F(13)	6.0	°F
E	0.242	ft
G	0.0208	ft
PS	$1.01 \times 10^{-6}$	ft <sup>2</sup> /sec
PL	$8.32 \times 10^{-7}$	ft <sup>2</sup> /sec
L	102.0	Btu/lb
QS	$2.62 \times 10^{-5}$	Btu/sec-ft-°F
QL	$2.00 \times 10^{-5}$	Btu/sec-ft-°F
R	50.0	lb/ft <sup>3</sup>
T	240.0	°F
TEMP	70.0	°F
TM	62.0	°F
TR	13.0	°F
UN	$2.93 \times 10^{-4}$	Btu/sec-ft <sup>2</sup> -°F

Table 18. Numerical Solution Constants  
for N-Hexadecane at 90°F.

<u>Constants</u>	<u>Value</u>	<u>Units</u>
F(1)	-169.0	°F
F(2)	-130.0	°F
F(3)	-100.0	°F
F(4)	- 70.0	°F
F(5)	- 45.0	°F
F(6)	- 20.0	°F
F(7)	0.0	°F
F(8)	26.0	°F
F(9)	26.0	°F
F(10)	26.0	°F
F(11)	26.0	°F
F(12)	26.0	°F
F(13)	26.0	°F
E	0.242	ft
G	0.0260	ft
PS	$1.01 \times 10^{-6}$	ft <sup>2</sup> /sec
PL	$8.32 \times 10^{-7}$	ft <sup>2</sup> /sec
L	102.0	Btu/lb
QS	$2.62 \times 10^{-5}$	Btu/sec-ft-°F
QL	$2.00 \times 10^{-5}$	Btu/sec-ft-°F
R	50.0	lb/ft <sup>3</sup>
T	300.0	°F
TEMP	90.0	°F
TM	62.0	°F
TR	13.0	°F
UN	$2.93 \times 10^{-4}$	Btu/sec-ft <sup>2</sup> -°F

Table 19. Numerical Solution Constants  
for N-Hexadecane at 120°F.

Constants	Value	Units
F(1)	-169.0	°F
F(2)	-130.0	°F
F(3)	-100.0	°F
F(4)	-70.0	°F
F(5)	-45.0	°F
F(6)	-20.0	°F
F(7)	0.0	°F
F(8)	24.0	°F
F(9)	24.0	°F
F(10)	24.0	°F
F(11)	24.0	°F
F(12)	24.0	°F
F(13)	24.0	°F
E	0.242	ft
G	0.0234	ft
PS	$1.01 \times 10^{-6}$	ft <sup>2</sup> /sec
PL	$8.32 \times 10^{-7}$	ft <sup>2</sup> /sec
L	102.0	Btu/lb
QS	$2.62 \times 10^{-5}$	Btu/sec-ft-°F
QL	$2.00 \times 10^{-5}$	Btu/sec-ft-°F
R	50.0	lb/ft <sup>3</sup>
T	390.0	°F
TEMP	120.0	°F
TM	62.0	°F
TR	13.0	°F
UN	$2.93 \times 10^{-4}$	Btu/sec-ft <sup>2</sup> -°F



Table 20. Numerical Solution Constants  
for N-Octadecane at 90°F.

<u>Constants</u>	<u>Value</u>	<u>Units</u>
F(1)	-190.0	°F
F(2)	-140.0	°F
F(3)	-105.0	°F
F(4)	-75.0	°F
F(5)	-45.0	°F
F(6)	-20.0	°F
F(7)	0.0	°F
F(8)	5.0	°F
F(9)	5.0	°F
F(10)	5.0	°F
F(11)	5.0	°F
F(12)	5.0	°F
F(13)	5.0	°F
E	0.242	ft
G	0.026	ft
PS	$9.60 \times 10^{-7}$	ft <sup>2</sup> /sec
PL	$8.41 \times 10^{-7}$	ft <sup>2</sup> /sec
L	105.0	Btu/lb
QS	$2.64 \times 10^{-5}$	Btu/sec-ft-°F
QL	$2.06 \times 10^{-5}$	Btu/sec-ft-°F
R	51.0	lb/ft <sup>3</sup>
T	240.0	°F
TEMP	90.0	°F
TM	83.0	°F
TR	2.0	°F
UN	$2.58 \times 10^{-4}$	Btu/sec-ft <sup>2</sup> -°F

Table 21. Numerical Solution Constants  
for N-Octadecane at 100°F.

<u>Constants</u>	<u>Value</u>	<u>Units</u>
F(1)	-190.0	°F
F(2)	-140.0	°F
F(3)	-105.0	°F
F(4)	- 75.0	°F
F(5)	- 45.0	°F
F(6)	- 20.0	°F
F(7)	0.0	°F
F(8)	14.0	°F
F(9)	14.0	°F
F(10)	14.0	°F
F(11)	14.0	°F
F(12)	14.0	°F
F(13)	14.0	°F
E	0.242	ft
G	0.0234	ft
PS	$9.60 \times 10^{-7}$	ft <sup>2</sup> /sec
PL	$8.41 \times 10^{-7}$	ft <sup>2</sup> /sec
L	105.0	Btu/lb
QS	$2.64 \times 10^{-5}$	Btu/sec-ft-°F
QL	$2.06 \times 10^{-5}$	Btu/sec-ft-°F
R	51.0	lb/ft <sup>3</sup>
T	240.0	°F
TEMP	100.0	°F
TM	83.0	°F
TR	2.0	°F
UN	$2.58 \times 10^{-4}$	Btu/sec-ft <sup>2</sup> -°F

Table 22. Numerical Solution Constants  
for N-Octadecane at 120°F.

<u>Constants</u>	<u>Value</u>	<u>Units</u>
F(1)	-190.0	°F
F(2)	-140.0	°F
F(3)	-105.0	°F
F(4)	- 75.0	°F
F(5)	- 45.0	°F
F(6)	- 20.0	°F
F(7)	0.0	°F
F(8)	29.0	°F
F(9)	29.0	°F
F(10)	29.0	°F
F(11)	29.0	°F
F(12)	29.0	°F
F(13)	29.0	°F
E	0.242	ft
G	0.0208	ft
PS	$9.60 \times 10^{-7}$	ft <sup>2</sup> /sec
PL	$8.41 \times 10^{-7}$	ft <sup>2</sup> /sec
L	105.0	Btu/lb
QS	$2.64 \times 10^{-5}$	Btu/sec-ft-°F
QL	$2.06 \times 10^{-5}$	Btu/sec-ft-°F
R	51.0	lb/ft <sup>3</sup>
T	210.0	°F
TEMP	120.0	°F
TM	83.0	°F
TR	2.0	°F
UN	$2.58 \times 10^{-4}$	Btu/sec-ft <sup>2</sup> -°F

APPENDIX E

SAMPLE COMPUTER PROGRAM

BEGIN

```
INTEGER N,K,M,H
REAL E,G,PS,PL,L,QS,QL,R,T,XX,XT,T1,DT,DX,G1,XS,XL,TEMP,TR,
    P,UN,TR,V,TS,UO
ARRAY F[1:14],O[1:13],THERM[0:8]
LABEL L1,L2,HELL,L3,L4
FILE IN MYDATA(2,10)
FILE OUT ANS 6(2,15)
LIST LT1 (E,G,PS,PL,L,QS,QL,R,T,TEMP,IM,TR,UN,TS,UO),
    LT2(T1,DT,G1,DX,P,FOR M=0 STEP 1 UNTIL 8 DO THERMEM),V)
FORMAT FM1(F7.2,X1,F9.7,X3,F7.4,X1,F9.7,X2,F7.2,X3,9(I4,X1),
    X2,E10.3),
    FM2(X2,"TIME=MINUTES",X6,"SOLID PORTION-IN",X4,"PERCENT",
    X4,"TEMPERATURE PROFILE - DEGREES ",
    "FARENHEIT",X6,"VELOCITY",/,
    X2,"TOTAL",X4,"DT",X8,"TOTAL",X5,"DX",X8,"SOLID",
    X4," TO T1 T2 T3 T4 T5 T6 T7 T8 ",X4,
    "IN/MIN",/),
    FM3(X25,"SOLIDIFICATION RATE STUDIES FOR MERCURY",/
    X25,"INITIAL TEMP = ",I3," DEGREES FARENHEIT",///)
WRITE(ANS(NO))
FILL F[*] WITH -27.0, -21.0, -16.0, -12.0, -7.5, -4.0, 0.0,
0.0, 0.0, 0.0, 0.0, 0.0, 0.0
READ (MYDATA,/,LT1)
CLOSE(MYDATA,RELEASE)
WRITE(ANS,FM3,TEMP)
WRITE(ANS,FM2)
K + 5
L1: IF(0.2*G*2/(36.0*PS) >= 0.2*(E-G)*2/(36.0*PL)) THEN
    XT=0.2*(E-G)*2/(36.0*PL) ELSE
    XT=0.2*G*2/(36.0*PS)
    F[7]+0.0
    F[14]+F[12]
    XX+3.0*XT/(R*L)*(QS/G*(F[5]-4.0*F[6])+QL/(E-G)*(F[9]-4.0*F[8])
    )
    O[1]+F[1]+12.0*PS*XT/G*(6.0*(F[2]-F[1])/G+UO/QS*(TS-F[1]))
    O[7]+0.0
```

```

FOR N+2 STEP 1 UNTIL 6 DO
O[N]+F[N] + 36.0*PS*XT/(G*2)*(N*G/(72.0*PS)*(F[N+1]-F[N-1]))*
XX/XT+F[N+1]-2.0*F[N]+F[N-1])
FOR N+8 STEP 1 UNTIL 12 DO
O[N]+F[N] + 36.0*PL*XT/((E-G)+2)*((12-N)*(E-G)/(72.0*PL)*
(F[N+1]-F[N-1]))*XX/XT+F[N+1]-2.0*F[N]+F[N-1])
O[13]+F[13]+12.0*PL*XT/(E-G)*(6.0*(F[12]-F[13]))/(E-G)
-UN/QL*(F[13]-TR))
FOR N+1 STEP 1 UNTIL 13 DO
BEGIN F[N]+O[N]
O[N]+O[N]+TM END
G+G+XX
T+T+XT
T1+T/60.0
DT+XT/60.0
DX+12.0*XX
G1+12.0*G
V+DX/DT
P+G/0.1667*100.0
IF K= 57 THEN
BEGIN WRITE(ANS[PAGE])
WRITE(ANS,FM2)
K+0 END
K+K+1
XS+G/6.0
XL+(E-G)/6.0
H+1
FOR M+1 STEP 1 UNTIL 7 DO
BEGIN
L2: IF H >6 THEN
BEGIN IF (M+E/8.0>(H-6)*XL+G) THEN
BEGIN H+H+1 ) GO TO L2 END ELSE
BEGIN THERM(H)+O(H)+(M+E/8.0-G-(H-7)*XL)*(O(H+1)-O(H))/XL
GO TO L4 END) END ELSE
IF(M+E/8.0>H*XS) THEN
BEGIN H+H+1 ) GO TO L2 END ELSE
THERM(H)+O(H)+(M+E/8.0-(H-1)*XS)*(O(H+1)-O(H))/XS

```

L4: END;

```
THERM[0]+0[1] ;  
THERM[8]+0[13] ;  
WRITE(ANS,FM1,LT2) ;  
IF G>0.1667 THEN ;  
GO TO HELL ;  
GO TO L1 ;
```

HELL:

END.

DATA MYDATA

0.242, 0.0208, 5.30e-05, 4.24e-05, 4.9, 1.50e-03, 1.12e-03, 856.0,  
660.0, 75.0, -38.0, 113.0, 5.25e-04, -69.0, 1.99e-02.





## APPENDIX G

## NOMENCLATURE

English  
Letters

C	constant
D	shell thickness
E	mold thickness
F	temperature excess above fusion temperature
G	position of fusion front
h	film coefficient
k	thermal conductivity
L	latent heat of fusion
n	increment in space
N	number of space increments
q	constant
R	density
r	number of space increments in the solid region
T	time
t	time
V	freezing front velocity
x	space location
PL	thermal diffusivity in liquid region
PS	thermal diffusivity in solid region
QL	thermal conductivity in liquid region

English  
Letters

QN	heat flux across front glass panel
QS	thermal conductivity in solid region
QO	heat flux across solid-mold interface
TM	melting temperature
TR	room temperature excess above fusion temperature
TS	heat sink temperature excess above fusion temperature
UN	over-all heat transfer coefficient at $x = N$
UO	over-all heat transfer coefficient at $x = 0$

Greek  
Letters

$\alpha$	thermal diffusivity
$\epsilon$	position of fusion front
$\gamma$	classification parameter
$\xi$	dimensionless parameter
$\rho$	density
$\theta$	temperature excess above fusion temperature

Subscripts

g	referring to glass mold
L	referring to liquid phase
m	evaluated at time $m\Delta t$
n	evaluated at $x = n\Delta x$
o	evaluated at $x = 0$
r	number of space increments in the solid region
s	referring to solid phase
t	evaluated at time t

## LITERATURE CITED

1. W. C. Winegard, "Solidification: Past - Present - Future," Australian Institute of Metals - Journal, Vol. 10, No. 3, August, 1965, p. 204.
2. H. Biloni and B. Chalmers, "Predendritic Solidification," Metallurgical Society of AIME-Transactions, Vol. 233, No. 2, February, 1965, p. 373.
3. T. F. Kattamis and M. C. Flemings, "Dendrite Structure and Grain Size of Undercooled Melts," Met. Soc. of AIME-Trans., Vol. 236, No. 11, November, 1966, p. 1523.
4. T. F. Bower, H. D. Brody, and M. C. Flemings, "Measurements of Solute Redistribution in Dendritic Solidification," Met. Soc. of AIME-Trans., Vol. 236, No. 5, May, 1966, p. 624.
5. M. E. Glicksman and R. J. Schaefer, "In Situ Measurements of Dendrite Profiles in Pure Tin," Acta Metallurgica, Vol. 14, No. 9, September, 1966, p. 1126.
6. M. E. Glicksman, "Dynamic Effects Arising from High-Speed Solidification," Acta Metallurgica, Vol. 13, No. 12, December, 1965, p. 1231.
7. J. O. Courtland and R. Elliot, "Dependence of Size of Cellular Interface Structure in Dilute Binary Alloys on Solidification Conditions," Institute of Metals-Journal, Vol. 95, Pt. 1, January, 1967, p. 21.
8. W. A. Tiller, "Liquid Metals and Solidification," American Society for Metals, Cleveland, Ohio, 1958, p. 276.
9. W. C. Winegard, Metals Review, Vol. 34, No. 6, 1961, p. 57.
10. G. A. Chadwick, Progress in Materials Science, Vol. 12, 1963, p. 97.

11. H. W. Kerr and W. C. Winegard, "Solidification of Eutectic Alloys," Journal of Metals, Vol. 18, No. 5, May, 1966, p. 563.
12. V. de L. Davies, "Mechanisms of Crystallization in Binary Eutectic Systems," Institute of Metals-Journal, Vol. 93, Pt. 1, September, 1964, p. 10.
13. S. Gosh, "Contribution of Segregation Zones in Controlled Eutectic Structures," Modern Castings, Vol. 50, No. 1, July, 1966, p. 116.
14. J. D. Hunt and J. P. Chilton, "An Investigation of the Zinc - 3% Magnesium Eutectic," Institute of Metals-Journal, Vol. 94, 1966, p. 146.
15. J. D. Hunt and J. P. Chilton, "Shock Decanting of Eutectics," Institute of Metals-Journal, Vol. 94, Pt. 9, September, 1966, p. 335.
16. H. Biloni, G. F. Bolling and G. S. Cole, "On Origin of Cellular Solidification Substructure," Met. Soc. of AIME-Trans., Vol. 236, No. 6, June, 1966, p. 930.
17. G. A. Chadwick, "Monotectic Solifidication," British Journal of Applied Physics, Vol. 16, No. 8, August, 1965, p. 1095.
18. J. C. Oostdijk, Metalen, Vol. 40, No. 6, June, 1966, p. 211.
19. B. Chalmers, "The Structure of Ingots," Australian Institute of Metals-Journal, Vol. 8, No. 3, August, 1963, p. 255.
20. J. V. Laukonis, "The Influence of Impurities on the Nucleation and Growth of Iron Whiskers," Memoires Scientifiques de la Revue de Metallurgie, Vol. 62, May 15, 1965, p. 179.
21. G. S. Cole and G. F. Bolling, "Augmented Natural Convection and Equiaxed Grain Structure," Met. Soc. of AIME-Trans., Vol. 236, No. 9, September, 1966, p. 1366.

22. K. A. Jackson and J. D. Hunt, "Transparent Compounds that Freeze like Metals," Acta Metallurgica, Vol. 13, 1965, p. 1212.
23. F. C. Frank, Philosophical Magazine, Vol. 41, 1950, p. 200.
24. D. Turnbull and R. L. Cormia, "Kinetics of Crystal Nucleation in Some Normal Alkane Liquids," Journal of Chemical Physics, Vol. 34, 1961, p. 820.
25. K. A. Jackson, J. D. Hunt, D. R. Uhlmann, and T. P. Seward, "On the Origin of the Equiaxed Zone in Castings," Met. Soc. of AIME-Trans., Vol. 236, No. 2, February, 1966, p. 149.
26. J. D. Hunt and K. A. Jackson, "Binary Eutectic Solidification," Met. Soc. of AIME-Trans., Vol. 236, No. 6, June, 1966, p. 853.
27. J. C. Muehlbauer and J. E. Sunderland, "Heat Conduction with Freezing or Melting," Applied Mechanics Review, Vol. 18, No. 12, 1965, p. 951.
28. A. Kohn and Y. Morillon, Revue de Metallurgie, Vol. 62, No. 4, April, 1965, p. 321.
29. J. G. Henzel and J. Keverian, "Theory and Application of the Digital Computer in Predicting Solidification Patterns," Journal of Metals, Vol. 17, No. 5, May, 1965, p. 561.
30. K. A. Jackson and J. D. Hunt, "Lamellar and Rod Eutectic Growth," Met. Soc. of AIME-Trans., Vol. 236, No. 8, August, 1966, p. 1129.
31. R. H. Tien, "Freezing of Semi-Infinite Slab with Time-Dependent Surface Temperature An Extension of Neumann's Solution," Met. Soc. of AIME-Trans., Vol. 233, No. 10, October, 1965, p. 1887.
32. D. R. Uhlmann and B. Chalmers, "The Energetics of Nucleation," Industrial and Engineering Chemistry, Vol. 57, No. 9, September, 1965, p. 18.

33. K. A. Jackson, "Nucleation from the Melt," Industrial and Engineering Chemistry, Vol. 57, No. 12, December, 1965, p. 28.
34. K. A. Jackson, G. A. Chadwick, and A. Klugert, "Lamellar Growth: An Electric Analog," Met. Soc. of AIME-Trans., Vol. 230, No. 7, December, 1964, p. 1547.
35. J. van Beckhoven, Metalen, Vol. 40, No. 9, September, 1966, p. 314.
36. A. P. Kapustin, "The Effects of Ultrasound on the Kinetics of Crystallization," Consultants Bureau, New York, 1963.
37. A. Dula, "Development of an Ultrasonic Technique for Solidification Rate Studies," Master Thesis, Georgia Institute of Technology, Atlanta, Georgia, April, 1966.
38. L. J. Thomas and J. W. Westwater, Chemical Engineering Progress Symposium Series, Vol. 59, No. 41, 1963, p. 155.
39. W. Kurz and B. Lux, "Lokalisierung der Phasengrenze fest-fluessig in Metallen mit Hilfe von Ultraschall", Feit fuer Metallkunde, Vol. 57, No. 1, January, 1966, p. 70.
40. J. E. Hill and A. L. Ruoff, "Velocity of Sound Measurements in Liquid Metals," Review of Scientific Instruments, Vol. 36, No. 10, October, 1965, p. 1465.
41. W. D. Murray, Numerical and Machine Solutions of Problems in Transient Heat Conduction, Ph.D. Thesis, New York University, New York, N. Y., 1958.
42. Liquid Metals Handbook, 2nd ed., Atomic Energy Commission, Department of the Navy, NAVEXOS P-733, January, 1954.

43. E. W. Bentilla, K. F. Sterrett, and L. E. Karre, Research and Development Study on Thermal Control by Use of Fusible Materials, Northrop Corporation, Hawthorne, California, April, 1966.
44. R. W. Powell and A. R. Challoner, "Measurement of Thermal Conductivity of N-Octadecane," Industrial and Engineering Chemistry, Vol. 53, 1961, p. 581.
45. B. C. Sakiadis and J. Coates, "Studies of Thermal Conductivities of Liquids," American Institute of Chemical Engineers Journal, Vol. 3, 1957, p. 121.